THE JOURNAL OF BIOLOGICAL CHEMISTRY
© 2004 by The American Society for Biochemistry and Molecular Biology, Inc.

Vol. 279, No. 11, Issue of March 12, pp. 10730–10737, 2004
Printed in U.S.A.

Munc13-4 Is a GTP-Rab27-binding Protein Regulating Dense Core Granule Secretion in Platelets*

Received for publication, August 25, 2003, and in revised form, December 16, 2003
Published, JBC Papers in Press, December 29, 2003, DOI 10.1074/jbc.M309426200

Ryutaro Shirakawa‡, Tomohito Higashi‡, Arata Tabuchi‡, Akira Yoshioka‡, Hiroaki Nishioka‡‡, Mitsunori Fukuda§, Toru Kita¶, and Hisanori Horiuchi‡‖**

From the Departments of ‡Geriatric Medicine and ¶Cardiovascular Medicine, Graduate School of Medicine, Kyoto University, Kyoto 606-8507, Japan and the §Fukuda Initiative Research Unit, RIKEN, Wako, Saitama 351-0198 Japan

Platelets store self-agonists such as ADP and serotonin in dense core granules. Although exocytosis of these granules is crucial for hemostasis and thrombosis, the underlying mechanism is not fully understood. Here, we show that incubation of permeabilized platelets with unprenylated active mutant Rab27A-Q78L, wild type Rab27A, and Rab27B inhibited the secretion, whereas inactive mutant Rab27A-T23N and other GTPases had no effects. Furthermore, we affinity-purified a GTP-Rab27A-binding protein in platelets and identified it as Munc13-4, a homologue of Munc13-1 known as a priming factor for neurotransmitter release. Recombinant Munc13-4 directly bound to GTP-Rab27A and -Rab27B *in vitro*, but not other GTPases, and enhanced secretion in an *in vitro* assay. The inhibition of secretion by unprenylated Rab27A was rescued by the addition of Munc13-4, suggesting that Munc13-4 mediates the function of GTP-Rab27. Thus, Rab27 regulates the dense core granule secretion in platelets by employing its binding protein, Munc13-4.

Upon stimulation, platelets secrete self-agonists, such as ADP and serotonin, which are stored in dense core granules (1). These secreted agonists contribute to the explosive activation of platelets in the processes of hemostasis and thrombus formation by a positive feedback mechanism (1). Despite this biological significance (1), the molecular mechanisms underlying this regulated exocytosis remain largely unclear.

Rab GTPases are essential regulatory molecules in vesicle transport (2, 3) and to date more than 60 members have been identified in mammals. Rab GTPases are localized to specific organelles and regulate several steps of vesicle transport including vesicle movement along cytoskeletal tracks and vesicle tethering to the target membrane by employing effector molecules that interact with GTP-bound Rab proteins (2, 3).

Recently, the *ashen* phenotype in mice has been demonstrated to be caused by a mutation in Rab27A (4). *Ashen* mice exhibit impaired coat color because of defective melanosome distribution, where Rab27A links a motor protein myosin Va and actin to melanosomes through its effector, melanophilin/Slac2-a (5–10). In addition, in cytotoxic T lymphocytes and natural killer cells in *ashen* mice, lytic granule secretion is impaired presumably at the docking/fusion step (11, 12). Interestingly, it has been demonstrated that the bleeding time of *ashen* mice is prolonged because of platelet dysfunction caused by a lack of intact platelet dense core granules (4, 13). However, it is important to note that platelets also contain Rab27B, a homologue of Rab27A with 71% identity in the amino acid level, which may compensate for the defect of Rab27A in platelets in *ashen* mice (14). These studies emphasize the requirement of further investigation into the mechanisms by which Rab27 may control the biogenesis and exocytosis of dense core granules in platelets.

The final step of vesicle transport is docking and fusion with the target membrane, which is mediated by *trans*-SNARE[1] complex between the vesicle SNARE and the target membrane SNARE (15). Accumulating evidence has revealed that Rab GTPases function upstream of SNARE pairing (2, 3). In addition to Rab GTPases, SNARE complex formation is directly regulated by several factors such as Munc18 and Munc13-1. In neuronal cells, Munc18 is thought to bind to the closed conformation of syntaxin1, a target membrane SNARE, to inhibit the *trans*-SNARE complex formation (16, 17). In contrast, Munc13-1 acts as a priming factor in neuronal secretion (18). Munc13-1 is suggested to promote formation of an open conformation of syntaxin1 and induce the assembly of *trans*-SNARE complexes. This is supported by the fact that transmission defects of *unc-13* mutants in *Caenorhabditis elegans* could be rescued by expression of open form of syntaxin (19). Munc13-1 and its homologues, Munc13-2 and Munc13-3, are expressed exclusively in brain, except for ubMunc13-2, a splicing variant of Munc13-2 (20, 21). In brain, each Munc13 isoform expression pattern is spatially restricted, although there is some overlap between isoforms. Munc13-1-deficient mice exhibit partial defects in glutamatergic neuron neurotransmitter release (22), whereas Munc13-1/Munc13-2 double knockout mice have complete loss of synaptic transmission in not only glutamatergic neurons but also GABAergic neurons (23). These studies in mice have revealed the essential and general roles of Munc13s in neurotransmitter release. Recently, the fourth Munc13 homologue, Munc13-4, was identified (24). In contrast to Munc13-1–3, Munc13-4 is expressed in non-neuronal tissues (24), and its biological function remains to be elucidated.

Here, we demonstrate that Rab27 regulates the Ca^{2+}-induced dense core granule secretion in platelets by showing that the addition of unprenylated Rab27 in an *in vitro* assay with permeabilized platelets inhibited the secretion. Furthermore, we identified a novel GTP-Rab27-binding protein in platelets as Munc13-4 and demonstrate that Munc13-4 mediates the function of GTP-Rab27 to promote the secretion.

* This work was supported by Ministry of Education, Culture, Sports, Science, and Technology Research Grants 11680629 and 15081101 (to H. H.) and 12CE2006, 09281104, and 13307034 (to T. K.), by Health and Labour Sciences Research Grant H14-Tyouju-012 from the Ministry of Health Labour and Welfare (to T. K. and H. H.), and in part by grants from the Takeda Science Foundation, Suzuken Memorial Foundation, the Study Group of Molecular Cardiology, and the Novartis Foundation for Gerontrogical Research (to H. H.). The costs of publication of this article were defrayed in part by the payment of page charges. This article must therefore be hereby marked "*advertisement*" in accordance with 18 U.S.C. Section 1734 solely to indicate this fact.

‖ To whom correspondence should be addressed. Tel.: 81-75-751-3464; Fax: 81-75-751-3574; E-mail: horiuchi@kuhp.kyoto-u.ac.jp.

** Present address: Department of Internal Medicine, Mitsubishi Kyoto Hospital, Kyoto, 615-8087 Japan.

‡‡ Present address: Sir William Dunn School of Pathology, University of Oxford, South Parks Rd., Oxford OX1 3RE, United Kingdom.

[1] The abbreviations used are: SNARE, soluble *N*-ethylmaleimide-sensitive factor attachment protein receptor; PKC, protein kinase C; SLO, streptolysin-O; GST, glutathione *S*-transferase; GTPγS, guanosine 5′-3-*O*-(thio)triphosphate; TOF-MS, time-of-flight mass spectrometry.

EXPERIMENTAL PROCEDURES

Antibodies, Constructs, Materials, and Others—Anti-Na,K-ATPase rabbit polyclonal antibody (25) was a kind gift from Dr. K. Omori (Kansai Medical University, Kadoma, Japan). Anti-His_6 and anti-PKCα monoclonal antibodies were purchased from Qiagen and Santa Cruz Biotechnology, respectively. Horseradish peroxidase-labeled anti-mouse and anti-rabbit IgG polyclonal antibodies were from Amersham Biosciences and were used as secondary antibodies for Western blot analysis visualized by enhanced chemiluminescence method (Amersham Biosciences). Unless otherwise specified, all of the other chemicals were purchased from Sigma, except for SLO, which was from Dr. S. Bhakdi (Mainz University, Mainz, Germany) (26).

The protein concentrations were determined by the Bradford method (Bio-Rad) or from the intensities of the bands in Coomassie Blue-stained SDS-PAGE gels using bovine serum albumin as a standard. cDNA encoding Rab27A was kindly provided by Dr. Y. Nozawa (Gifu International Institute of Biotechnology, Gifu, Japan) (27), and mutants Rab27A-Q78L and Rab27A-T23N were generated by PCR mutagenesis. cDNAs encoding Rap1B (28) and Rab3B (29) were from Dr. Y. Takai (Osaka University, Osaka, Japan), and Rab4B (30) and Rab5A (30) were from Dr. M. Zerial (Max Plank Institute, Dresden, Germany). Human Rab27B cDNA was isolated from the Marathon-Ready human bone marrow cDNA (Clontech) by PCR. All of these cDNAs were subcloned into the prokaryotic expression vector pDEST17 (Invitrogen) for His_6-tagged recombinant protein production. GST fusion proteins of Rab3B, Rab4B, Rab5A, Rab27A, and Rab27B were produced by subcloning the cDNAs into pGEX-2T (Amersham Biosciences). These His_6-tagged and GST fusion proteins were produced in *Escherichia coli* strain BL21 and purified on nickel-nitrilotriacetic acid-agarose (Qiagen) and glutathione-Sepharose (Amersham Biosciences), respectively. For full-length Munc13-4 recombinant protein production, the cDNA of Munc13-4 was subcloned into pDEST10 (Invitrogen), and a baculovirus encoding the full-length Munc13-4 was produced using the Bac-to-Bac system (Invitrogen). His_6-tagged Munc13-4 recombinant protein was produced in Sf9 insect cells upon infection with the virus and purified on nickel-nitrilotriacetic acid-agarose, followed by further purification with MonoQ anion exchange chromatography (Amersham Biosciences). All of the purified recombinant proteins were extensively dialyzed against buffer A (50 mM Hepes/KOH, pH 7.2, 78 mM KCl, 4 mM $MgCl_2$, 0.2 mM $CaCl_2$, 2 mM EGTA, 1 mM dithiothreitol) and stored at −80 °C until use. All of the sequences of the PCR products were confirmed by sequencing using a 3100 Genetic Analyzer (Applied Biosystems).

The Assay for Secretion of Dense Core Granules—The standard assay method for the Ca^{2+}-induced dense core granule secretion was essentially as described previously (31) except that human platelet cytosol was used (32) instead of rat brain cytosol. Unless otherwise specified, the standard assay was following: Freshly obtained washed platelets (1×10^8 platelets/assay, counted with the Coulter Counter) were incubated with [^{3}H]serotonin (~20,000 cpm/assay) (Amersham Biosciences) to allow uptake into dense core granules. After washing the platelets, the platelet plasma membrane was permeabilized with SLO in Buffer A, where the calculated free calcium ion concentration was ~20 nM (33). The permeabilized platelets were incubated with an ATP regeneration system, human platelet cytosol at 1.5 mg of proteins/ml (for Fig. 1) or 0.8 mg of proteins/ml (for Fig. 6), and tested materials at 4 °C for 30 min followed by further incubation at 30 °C for 2 min. Finally, the platelets were stimulated with 20 μM Ca^{2+} (33) at 30 °C for 1 min, and the reaction was stopped by the addition of ice-cold Buffer A containing 10 mM EGTA. After removing platelets by centrifugation, [^{3}H]serotonin released in the supernatant was measured by a liquid scintillation counter (Beckman). The secretion levels of [^{3}H]serotonin were expressed as percentages of the total [^{3}H]serotonin in the permeabilized platelets before the final incubation.

GST-Rab27A Affinity Column Chromatography—Human platelet pellets were provided by Kyoto Red Cross Blood Center and resuspended in Buffer A. After disruption of the platelets by sonication, the sample was centrifuged at 100,000 × *g* at 4 °C for 1 h. The supernatant was dialyzed against Buffer A and stored as human platelet cytosol at −80 °C until use. For the affinity chromatography, GTPγS- or GDP-bound GST-Rab27A was prepared by incubation of 30 μg of GST-Rab27A with 1 mM GTPγS or GDP in Buffer A containing 10 mM EDTA at 30 °C for 30 min, and the reaction was stopped by the addition of 15 mM $MgCl_2$ (34). Then the GST- or GST-Rab27A-coated beads were

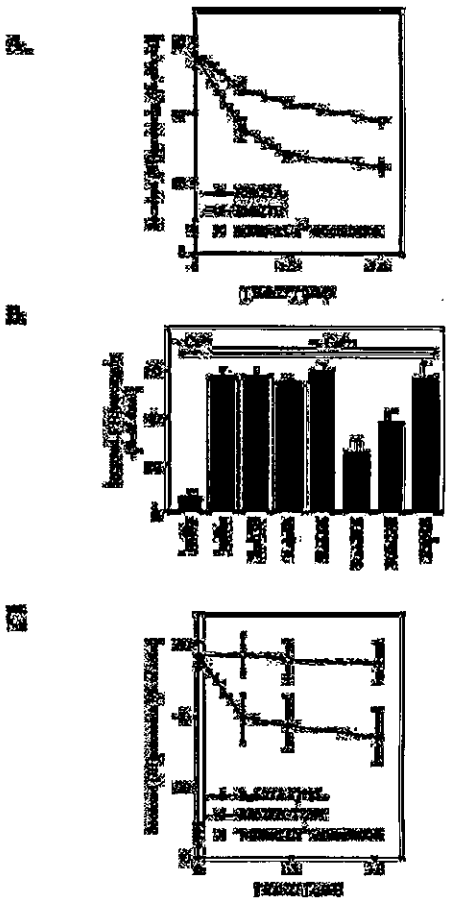

FIG. 1. **Unprenylated Rab27 inhibits Ca^{2+}-induced dense core granule secretion.** Permeabilized platelets were first incubated at 4 °C for 30 min with unprenylated His_6-Rab27A (*closed circles*) and His_6-Rab27B (*open circles*) purified from *E. coli* at various concentrations (*A*), with unprenylated His_6-Rab3B, -Rab4B, -Rab5A, -Rab27A, and -Rab27B and Rap1B at 3 μM (*B*), and with various concentrations of unprenylated mutant Rab27A-Q78L (*closed circles*) and Rab27A-T23N (*open circles*) (*C*). Then the Ca^{2+}-induced secretion of dense core granules was analyzed by measuring secreted [^{3}H]serotonin preloaded in dense core granules as described under "Experimental Procedures." The secretion without Ca^{2+} stimulation is also shown in *A* and *C* (×). The results shown are expressed as the means ± S.E. of three independent experiments.

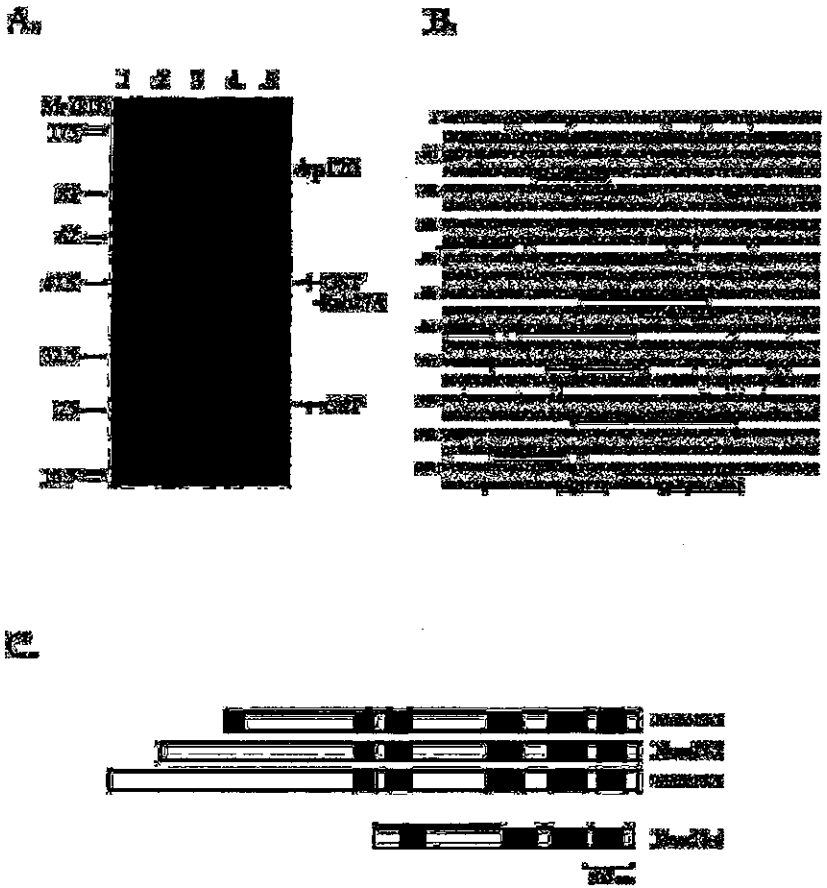

FIG. 2. **Identification of a GTP-Rab27A-binding protein in platelet cytosol as Munc13-4.** *A*, GST-loaded (*lane 3*) and GTPγS-bound (*lane 4*) and GDP-bound (*lane 5*) GST-Rab27A-loaded glutathione beads were incubated with platelet cytosol at 4 °C for 1 h. GST-loaded (*lane 1*) and GST-Rab27A-loaded (*lane 2*) beads were also treated in the same way without the cytosol. After washing the beads, the bead-associated proteins were analyzed in a Coomassie Blue-stained SDS-PAGE gel as described under "Experimental Procedures." A protein band at 120 kDa (*asterisk*) was specifically detected in *lane 4*. *B*, the 120-kDa protein was analyzed by TOF-MS and identified as human Munc13-4 as described under "Experimental Procedures." *Underlining* indicates the peptides whose masses were matched with peptide masses detected by the TOF-MS analysis. *C*, the domain structures of Munc13-1–3 and Munc13-4 are shown.

prepared by incubation of glutathione-Sepharose beads with GST or pretreated GST-Rab27A at 4 °C for 1 h, followed by washing the beads with Buffer A three times. The coated beads were incubated with the platelet cytosol (30 mg of proteins) at 4 °C for 1 h, followed by washing the beads with Buffer A three times, and the bead-associated proteins were extracted by the SDS sample buffer. The samples were analyzed in a Coomassie Blue-stained SDS-PAGE gel (4–20% gradient gel; Daiichi Chemical).

Cloning of Munc13-4—The TOF-MS analysis of the GTPγS-Rab27A-binding protein at 120 kDa was performed by Kyoto Science Co. (Kyoto, Japan). The report first showed that a candidate protein could be FLJ00067, which contained an incomplete sequence with possible introns and C-terminal deletion. We reconstituted the full-length sequence with several expressed sequence tags overlapping with FLJ00067 and identified it as a human homologue of rat Munc13-4 (24). Using the sequences, we designed primers and amplified the full-length cDNA by PCR using the Marathon-Ready human bone marrow cDNA (Clontech). The PCR product was cloned into pENTR (Invitrogen) and verified by sequencing using a 3100 Genetic Analyzer.

Anti-Munc13-4 and -Rab27 Antibodies—cDNA encoding the N-terminal region of Munc13-4 (residues 1–262) was obtained by PCR and subcloned into pDEST17 (Invitrogen). The His_6-Munc13-4 (1–262) protein was produced and purified as described above. Anti-Munc13-4 and anti-Rab27A rabbit polyclonal antibodies were generated using His_6-Munc13-4 (1–262) and His_6-Rab27A as antigens, respectively. The anti-Rab27A antibody recognized both Rab27A and Rab27B. For transient expression of Munc13-4, HeLa cells were transfected with pcDNA (Invitrogen) containing full-length Munc13-4 using LipofectAMINE (Invitrogen).

Assay Analyzing Direct Interaction of Munc13-4 with Rab27—Binding of Munc13-4 with small GTPases was carried out by affinity chromatography. Glutathione-Sepharose beads coated with GTPγS- or GDP-bound Rab GTPases (each 1 μg) were prepared by incubation for 1 h at 4 °C in Buffer A. Then the prepared beads were incubated with purified 0.5 μg of His_6-Munc13-4 for 1 h at 4 °C in Buffer A and washed three times with Buffer A at 4 °C. Bead-associated His_6-Munc13-4 was analyzed by immunoblotting with anti-Munc13-4 antibody.

Density Gradient Separation of Platelet Organelles—We first loaded [^{3}H]serotonin into dense core granules of platelets from 50 ml of freshly obtained blood and permeabilized the platelets with SLO. Then, after centrifugation to remove most of cytosol and resuspension in 1 ml of Buffer A containing the ATP regeneration system, the platelets were disrupted by sonication and centrifuged at 600 × *g* for 5 min to remove unbroken platelets. The supernatant was layered on the top of metrizamide stepwise gradient (each 1.0-ml layer at 1.30–1.00 g/ml in density decreasing by each 0.03 g/ml from the bottom) in Buffer A containing the ATP regeneration system and centrifuged at 28,000 rpm with Beckman Rotor SW40 for 2 h at 4 °C as described (31). Aliquots of the fractions were analyzed by Western blot with indicated antibodies and counting radioactivity of [^{3}H]serotonin. The separation of the membrane and cytosolic fraction was performed by centrifugation at 300,000 × *g* for 30 min at 4 °C after disrupting platelets by sonication or at 600 × *g* for 5 min after the SLO permeabilization of platelets.

RESULTS

Unprenylated Rab27 Inhibits the Ca^{2+}-induced Dense Core Granule Secretion—In the present study, we used a previously established *in vitro* assay system using SLO-permeabilized platelets by monitoring secreted [^{3}H]serotonin preloaded into dense core granules (31, 32, 35). Agonists promote granule secretions by increasing intracellular calcium ion concentrations in platelets (36). Upon permeabilization of platelets the intracellular and extracellular concentrations of calcium are equal; therefore we used calcium chloride as a stimulus. In the assay, the secretion of the granules was reconstituted by the addition of ATP and exogenous platelet cytosol, and the response observed was equivalent to intact platelets in the time course and the Ca^{2+} sensitivity (31, 32, 35).

Small GTPases produced in *E. coli* are not modified by the addition of prenyl groups at their C termini (37), which is essential for the correct localization and activity (2, 3, 38). Incubation of permeabilized platelets with Rab27A and Rab27B purified from *E. coli* inhibited the Ca^{2+}-induced dense core granule secretion in a concentration-dependent manner (Fig. 1*A*). Incubation of permeabilized platelets with other small GTPases such as Rab3B, Rab4B, Rab5A, or Rap1B, a Ras family small GTPase whose GTP-bound form has been shown to be increased upon platelet activation (39), had no effect (Fig. 1*B*), indicating that the effect of Rab27 is specific. We prepared and purified mutant Rab27A-T23N, which preferentially binds GDP, and Rab27A-Q78L, which lacks GTPase activity (40). Incubation of permeabilized platelets with Rab27A-Q78L, but not Rab27A-T23N, inhibited the secretion in a concentration-dependent manner (Fig. 1*C*). Inhibition by unprenylated Rab27A-Q78L, wild type Rab27A, and Rab27B could be due to sequestration of putative Rab27 effector molecules from endogenous membrane-associated GTP-Rab27 by forming nonfunctional complexes with effector proteins. These data demonstrate that Rab27 is involved in the regulation of dense core granule secretion in platelets.

Identification of Munc13-4 as a GTP-Rab27-binding Protein in Platelet Cytosol—To elucidate the mechanism of action of Rab27, we attempted to identify GTP-Rab27-binding proteins that might mediate the function of Rab27 in the granule secretion, from platelet cytosol by affinity chromatography. As shown in Fig. 2*A*, we detected one major protein migrating at ~120 kDa on GTPγS-GST-Rab27A beads (*lane 4*) but not on GDP-GST-Rab27A- (lane 5) or GST beads (*lane 3*). TOF-MS analysis of the protein and a data base search revealed that the 120-kDa protein was the human homologue of rat Munc13-4 (24) because most of the peptide masses obtained by the TOF-MS analysis were detected all over the human Munc13-4 molecule (Fig. 2*B*). Human Munc13-4 consists of 1,090 amino acids, and the primary structure is 88% identical to that of rat Munc13-4. As is the case with Munc13-1–3, Munc13-4 contains two calcium-binding C2 domains and Munc13 homology do-

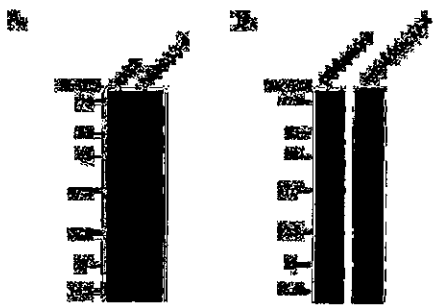

FIG. 3. **Anti-Munc13-4 antibody recognizes a single band at 120 kDa in platelet lysate.** *A*, Munc13-4- and mock-transfected HeLa cell lysates were immunoblotted with the anti-Munc13-4 antibody as described under "Experimental Procedures." *B*, platelet lysates were immunoblotted with preimmune serum and the anti-Munc13-4 antibody as described under "Experimental Procedures." The data shown are the representative of three independent experiments with similar results.

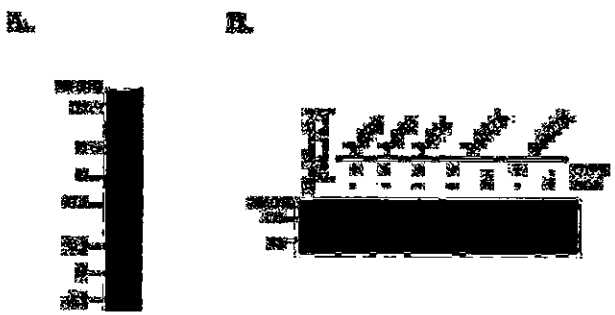

FIG. 4. **Direct interaction of recombinant Munc13-4 with GTPγS-Rab27 *in vitro*.** *A*, recombinant His_6-Munc13-4 was produced and purified from the over-expressing Sf9 cells and analyzed by SDS-PAGE gel stained by Coomassie Blue as described under "Experimental Procedures." *B*, glutathione beads coated with GTPγS- or GDP-bound various GST-Rab GTPases (each 1 μg) were incubated with His_6-Munc13-4 (0.5 μg) *in vitro*, and the bead-associated His_6-Munc13-4 was detected by Western blotting with anti-His_6 antibody as described under "Experimental Procedures." Purified Munc13-4 used for the affinity analysis is also shown (10% of load). The data shown are representative of three independent experiments with similar results.

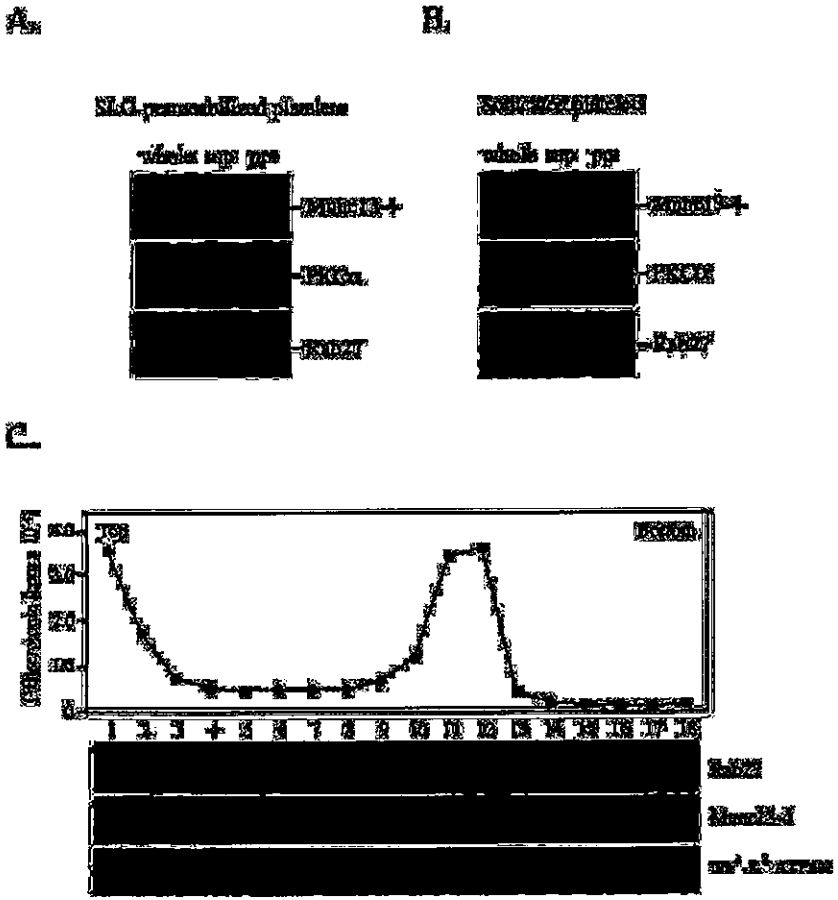

FIG. 5. **Localization of Munc13-4 in platelet organelles.** *A* and *B*, after centrifugation of isolated platelets permeabilized with SLO for 30 min (*A*) or sonicated directly (*B*), comparable amounts of the supernatant (*sup*) and pellets (*ppt*) were analyzed by immunoblotting with anti-Munc13-4, anti-PKCα, and anti-Rab27 antibodies as described under "Experimental Procedures." The data shown are the representative of three independent experiments with similar results. *C*, after separation of organelles of [^{3}H]serotonin-loaded permeabilized platelets by density gradient, [^{3}H]serotonin was measured by a liquid scintillation counter and Munc13-4, Rab27, and Na,K-ATPase were detected by immunoblotting in each fraction as described under "Experimental Procedures." The data shown are the representative of three independent experiments with similar results.

mains, whereas Munc13-4 lacks the long N-terminal region containing a phorbol ester-binding C1 domain present in Munc13-1–3 (21, 24) (Fig. 2*C*).

We generated an antibody against the N-terminal region of human Munc13-4 (residues 1–262). The antibody recognized a 120-kDa protein in HeLa cells transfected with Munc13-4 but not in mock transfected cells (Fig. 3*A*). The antibody recognized a single band at 120 kDa in platelet lysate (Fig. 3*B*) and also the 120-kDa protein eluted from the GTPγS-GST-Rab27A-loaded affinity chromatography column (data not shown), confirming that the 120-kDa protein that we identified is indeed Munc13-4.

To examine whether the interaction of Munc13-4 with Rab27 is direct, we produced and purified full-length His_6-Munc13-4 using the baculovirus expression system in Sf9 insect cells (Fig. 4*A*). As shown in Fig. 4*B*, recombinant Munc13-4 could bind directly to GTPγS-Rab27A but only slightly to GDP-Rab27A *in vitro*. Furthermore, Munc13-4 demonstrated a weaker interaction with GTPγS-Rab27B, compared with GTPγS-Rab27A. Importantly, Munc13-4 did not bind to GTPγS-Rab3B, -Rab4B, or -Rab5A (Fig. 4*B*). Thus, the interaction of Munc13-4 with Rab27 is direct, GTP-dependent, and specific.

Localization of Munc13-4—Munc13-1 has been demonstrated to localize specifically to the presynaptic plasma membrane, although it does not contain a membrane-spanning region (20). Munc13-4 also lacks a transmembrane region. We examined the subcellular localization of Munc13-4 in platelets. As shown in Fig. 5*A*, Munc13-4 was equally distributed between the cytosolic and membrane fractions in SLO-permeabilized platelets, whereas Rab27 was exclusively membrane-associated. As expected, PKCα was found predominantly in the soluble supernatant fraction (Fig. 5*A*). When isolated platelets were directly sonicated and centrifuged at 300,000 × *g*, localization of Munc13-4, Rab27, and PKCα was similar to the results in the SLO-permeabilized platelets (Fig. 5*B*). Namely, ~50% of Munc13-4, most of Rab27, and a small part of PKCα were recovered in the pellet after the high speed centrifugation (Fig. 5*B*), suggesting a strong affinity of Munc13-4 to the membrane.

Next, we biochemically examined the localization of Rab27 and membrane-associated Munc13-4 in platelet organelles. We first loaded [^{3}H]serotonin into dense core granules of platelets and permeabilized the platelets with SLO. Then, after centrifugation to remove cytosol, the cytosol-depleted platelets were disrupted by sonication, and the low speed supernatant containing platelet organelles was separated by a density gradient method (31). As shown in Fig. 5*C*, [^{3}H]serotonin was recovered in two peaks. The lighter peak is presumably due to [^{3}H]serotonin leaking from the dense core granules. The heavier fractions of [^{3}H]serotonin indicate the presence of dense core granules. The majority of Rab27 was recovered together with fractions of dense core granules containing [^{3}H]serotonin, whereas some Rab27 was detected in the low density fractions where a plasma membrane marker Na,K-ATPase was recovered (Fig. 5*C*). Under these conditions, Munc13-4 was recovered in the lighter fractions together with Na,K-ATPase but not in the vesicle fractions (Fig. 5*C*), suggesting that Munc13-4 is on the plasma membrane but not on the dense core granules in platelets.

Involvement of Munc13-4 in the Regulation of Dense Core Granule Secretion—We finally examined whether Munc13-4 regulates dense core granule secretion in platelets using the semi-intact secretion assay. In basal conditions, SLO-permeabilized platelets retained a residual amount of membrane-associated Munc13-4 (Fig. 5*A*), and exogenously added platelet cytosol contained 80 nM Munc13-4. Under these conditions, the addition of purified Munc13-4 (Fig. 4*A*) enhanced the Ca^{2+}-induced secretion of dense core granules in a concentration-dependent manner (Fig. 6*A*). The activity of Munc13-4 was abolished when Munc13-4 was denatured (Fig. 6*A*), suggesting that the activity was not due to a nonspecific effect of the buffer. The dense core granule secretion was time-dependent, and the addition of Munc13-4 not only accelerated the kinetics but also increased the amounts of the secretion (Fig. 6*B*). Importantly, the inhibition of secretion by unprenylated Rab27A was rescued by the addition of recombinant Munc13-4 in a concentration-dependent manner (Fig. 6*C*).

DISCUSSION

Here we have demonstrated that Rab27 regulates the Ca^{2+}-induced dense core granule secretion in platelets by showing that the addition of unprenylated dominant active Rab27A, wild type Rab27A, and Rab27B but not other GTPases inhibited the secretion in permeabilized platelets. In addition, we identified Munc13-4 as a novel GTP-Rab27-binding protein. We further demonstrated that Munc13-4 mediates the function of GTP-Rab27 in the regulation of the secretion by showing that the addition of Munc13-4 enhanced the secretion and rescued the inhibition of secretion by unprenylated Rab27.

We have shown that the addition of unprenylated Rab27 purified from *E. coli* inhibited the Ca^{2+}-induced dense core granule secretion. In the secretion assay, added unprenylated Rab27 is theoretically unable to localize to the membrane and therefore would sequester Rab27 effector molecules by forming

FIG. 6. **Munc13-4 enhances the dense core granule secretion and rescues the inhibition by unprenylated Rab27A.** *A*, permeabilized platelets were first incubated with the indicated concentrations of Munc13-4, and the Ca^{2+}-induced secretion of dense core granules for 1 min was analyzed in the standard assay condition by measuring secreted [^{3}H]serotonin preloaded in dense core granules as described under "Experimental Procedures." *B*, permeabilized platelets were first incubated in the absence (*open circles*) or the presence (*closed circles*) of 0.2 μM Munc13-4 and then incubated with Ca^{2+} at 20 nM (*broken lines*) or 20 μM (*solid lines*) for the indicated periods. The Ca^{2+}-induced secretion of dense core granules for indicated periods was analyzed as described under "Experimental Procedures." *C*, permeabilized platelets were first incubated in the absence or presence of unprenylated Rab27A at 2.0 μM with various concentrations of Munc13-4. The Ca^{2+}-induced secretion of dense core granules for 1 min was analyzed as described under "Experimental Procedures." The results shown are expressed as the means ± S.E. of three independent experiments.

nonfunctional complexes. Unprenylated Rab27A-T23N with preferential GDP binding would act as a dominant negative protein when expressed in cells (41). However, here we observed almost no effect of Rab27A-T23N on the dense core granule secretion in our semi-intact system (Fig. 1*C*). On the other hand, unprenylated GTPase-deficient mutant Rab27A-Q78L inhibited the secretion to a similar extent as wild type Rab27A and Rab27B. This could depend upon the ability of association with effector molecules of Rab27. The mechanism might be similar to that seen in the inhibition of the insulin signaling in adipocytes by overexpression of prenylation-deficient Rab4 (42). Thus, GTP-Rab27 is essential for dense core granule secretion in platelets once the granules are normally generated, although there is controversy concerning the role of Rab27 in dense core granule biogenesis (4, 13, 14).

To identify specific GTP-Rab27-binding protein(s) that may function in dense core granule secretion in platelets, we performed Rab27 affinity chromatography using platelet cytosol as the source for interacting proteins. We detected a GTPγS-Rab27A-binding protein at 120 kDa and identified it as the human homologue of rat Munc13-4 (24) by TOF-MS analysis and a data base search. Recombinant Munc13-4 bound to purified Rab27A and Rab27B in their GTPγS-bound forms *in vitro*, indicating that their interaction is direct and nucleotide-dependent.

So far, eight proteins have been identified as GTP-Rab27A-binding molecules (43, 44). Five of them contain the C-terminal tandem calcium-binding C2 domains (45) and are designated as synaptotagmin-like proteins (Slp 1–5) (43, 44). The other three are homologous to Slps but lack the C2 domains and are designated as Slp-lacking C2 domains (Slac2-a–c) (43). All of these molecules contain the Slp homology domain at their N-terminal ends, through which these molecules interact directly with GTP-Rab27 (43). Munc13-4 does not contain this Slp homology domain motif (43, 44). Therefore, we conclude that Munc13-4 is a novel type of GTP-Rab27-binding molecule.

We have demonstrated that the addition of recombinant Munc13-4 in the secretion assay accelerated the kinetics and increased secretion, indicating that Munc13-4 positively regulates dense core granule secretion in platelets. Importantly, the inhibitory effect of unprenylated Rab27A was rescued by the addition of recombinant Munc13-4. Exogenously added unprenylated Rab27A is presumed to form nonfunctional complexes with putative Rab27 effectors, thereby inhibiting secretion. Because exogenously added Munc13-4 overcomes inhibition by unprenylated Rab27, it is most likely that Munc13-4 mediates the function of GTP-Rab27 in the dense core granule secretion in platelets. Interestingly, the inhibitory effect of unprenylated Rab27A on the secretion was stronger than that of unprenylated Rab27B (Fig. 1*A*), which may reflect distinct roles of each isoform within the regulation of dense core granule secretion in platelets. Our data suggest that this difference is due to the stronger affinity of Rab27A to Munc13-4 than that of Rab27B (Fig. 4*B*).

Because SNAREs and Rab GTPases are key molecules in the regulation of vesicle transport, elucidation of the molecular mechanism of their cooperation could provide a clue for further understanding of vesicle docking/fusion. There have been several examples of Rab effector proteins interacting with the components of the SNARE machinery. For example, the Rab5 effector Rabenosyn-5 interacts directly with Vps45, a member of the Munc18/Sec1 family, in the regulation of endocytic membrane traffic (46). Similarly, the Ypt7 effector complex that controls vacuolar fusion in yeast interacts directly with Vps33, which is also a Munc18/Sec1 family protein (47). Thus, a group of Rab effectors appear to regulate SNARE pairing through Munc18/Sec1 family proteins. Another group of Rab effectors has been shown to bind SNAREs directly, as shown for the Rab5 effector EEA1 interacting with syntaxin6 (48) and syntaxin13 (49).

It has also been demonstrated that Munc13-1 could be a direct regulator of syntaxin1 (50, 51) and that a GTP-Rab3A-binding protein, RIM1, which is a cytomatrix protein at the active zone in synapses, interacts with Munc13-1 (52). Thus, Rab3A might regulate Munc13-1 indirectly through interaction with RIM1. On the other hand, we here report the first direct link between Rab GTPases and a member of the Munc13 family, which may provide a novel mechanism for the control of SNARE activity by regulatory Rab GTPases. It will now be essential to explore the mechanisms of how Munc13-4 regulates the SNARE pairs that function in dense core granule secretion. In platelets, it has been shown that syntaxin2 mediates dense core granule secretion (53), suggesting that Munc13-4 might regulate syntaxin2.

We detected Munc13-4 in both cytosolic and membrane fractions, whereas Rab27 is exclusively in the membrane fraction (Fig. 5, *A* and *B*). Furthermore, by a density gradient separation, Munc13-4 was recovered in the plasma membrane fraction, whereas a major part of Rab27 was recovered in the granule fraction (Fig. 5*C*). Thus, the localization of Rab27 and Munc13-4 is not overlapping to a great extent. Munc13-4 on the plasma membrane may mark the target site for the dense core granule docking by interacting directly with activated Rab27 on the vesicle membrane. Because Rab3A is present on the synaptic vesicles (54) and its effector RIM1 and RIM1's partner Munc13-1 are on the presynaptic membrane in neurons (20), there might be a common regulatory mechanism used by the Rab GTPase-Munc13 system.

Taken together, the work presented here demonstrates that Rab27 regulates dense core granule secretion in platelets by employing the GTP-Rab27-binding protein, Munc13-4. Our current findings could provide a novel mechanism by which a Rab GTPase controls the regulated exocytosis through direct interaction with a Munc13 family protein. To contribute to further understanding of the regulation of vesicle transport, it is essential to elucidate the molecular mechanism of how the Rab27-Munc13-4 system promotes regulated exocytosis.

Acknowledgments—We are grateful to Dr. M. Zerial for providing plasmids containing Rab4 and Rab5, Dr. Y. Nozawa for a plasmid containing Rab27A, Dr. Y. Takai for a plasmid containing Rap1B and Rab3B, and Dr. K. Omori for providing an anti-Na,K-ATPase antibody. We are also grateful to the Kyoto Red Cross Blood Center for providing platelet pellets. We thank Dr. H. McBride (Ottawa, Canada) and Dr. C. Murphy (Ioannina, Greece) for critical reading of the manuscript and T. Matsubara for excellent technical assistance.

Note Added in Proof—Feldmann *et al.* (Feldmann, J., Callebaut, I., Raposo, G., Certain, S., Bacq, D., Dumont, C., Lambert, N., Ouachee-Chardin, M., Chedeville, G., Tamary, H., Minard-Colin, V., Vilmer, E., Blache, S., Le Deist, F., Fisher, A., and de Saint Basile, G. (2003) *Cell* **115**, 461–473) have published that mutation in Munc13-4 causes familial hemophagocytic lymphohistiocytosis (FHL3) where cytolytic granule fusion to the plasma membrane in cytotoxic T lymphocytes is impaired similar to mutation in Rab27A (11, 12), suggesting that the Rab27-Munc13-4 regulatory system may also function in regulated secretion in the cells.

REFERENCES

1. Brass, L. F. (2000) in *Hematology: Basic Principles and Practice* (Hoffman, R. S., Benz, E. J., Furie, B., Cohen, H., and Silberstein, L. E., ed) 3rd Ed., pp. 1753–1770, Churchill Livingston, New York
2. Takai, Y., Sasaki, T., and Matozaki, T. (2001) *Physiol. Rev.* **81**, 153–208
3. Zerial, M., and McBride, H. (2001) *Nat. Rev. Mol. Cell Biol.* **2**, 107–117
4. Wilson, S. M., Yip, R., Swing, D. A., O'Sullivan, T. N., Zhang, Y., Novak, E. K., Swank, R. T., Russell, L. B., Copeland, N. G., and Jenkins, N. A. (2000) *Proc. Natl. Acad. Sci. U. S. A.* **97**, 7933–7938
5. Wu, X. S., Rao, K., Zhang, H., Wang, F., Sellers, J. R., Matesic, L. E., Copeland, N. G., Jenkins, N. A., and Hammer, J. A., III (2002) *Nat. Cell Biol.* **4**, 271–278
6. Hume, A. N., Collinson, L. M., Hopkins, C. R., Strom, M., Barral, D. C., Bossi, G., Griffiths, G. M., and Seabra, M. C. (2002) *Traffic* **3**, 193–202
7. Provance, D. W., James, T. L., and Mercer, J. A. (2002) *Traffic* **3**, 124–132
8. Fukuda, M., Kuroda, T. S., and Mikoshiba, K. (2002) *J. Biol. Chem.* **277**, 12432–12436
9. Nagashima, K., Torii, S., Yi, Z., Igarashi, M., Okamoto, K., Takeuchi, T., and Izumi, T. (2002) *FEBS Lett.* **517**, 233–238
10. Kuroda, T. S., Ariga, H., and Fukuda, M. (2003) *Mol. Cell Biol.* **23**, 5245–5255
11. Stinchcombe, J. C., Bossi, G., Booth, S., and Griffiths, G. M. (2001) *Immunity* **15**, 751–761
12. Haddad, E. K., Wu, X., Hammer, J. A., III, and Henkart, P. A. (2001) *J. Cell Biol.* **153**, 835–842
13. Novak, E. K., Gautam, R., Reddington, M., Collinson, L. M., Copeland, N. G., Jenkins, N. A., McGarry, M. P., and Swank, R. T. (2002) *Blood* **100**, 128–135
14. Barral, D. C., Ramalho, J. S., Anders, R., Hume, A. N., Knapton, H. J., Tolmachova, T., Collinson, L. M., Goulding, D., Authi, K. S., and Seabra, M. C. (2002) *J. Clin. Invest.* **110**, 247–257
15. Chen, Y. A., and Scheller, R. H. (2001) *Nat. Rev. Mol. Cell Biol.* **2**, 98–106
16. Dulubova, I., Sugita, S., Hill, S., Hosaka, M., Fernandez, I., Sudhof, T. C., and Rizo, J. (1999) *EMBO J.* **18**, 4372–4382
17. Yang, B., Steegmaier, M., Gonzalez, L. C., Jr., and Scheller, R. H. (2000) *J. Cell Biol.* **148**, 247–252
18. Ashery, U., Varoqueaux, F., Voets, T., Betz, A., Thakur, P., Koch, H., Neher, E., Brose, N., and Rettig, J. (2000) *EMBO J.* **19**, 3586–3596
19. Richmond, J. E., Weimer, R. M., and Jorgensen, E. M. (2001) *Nature* **412**, 338–341
20. Brose, N., Hofmann, K., Hata, Y., and Sudhof, T. C. (1995) *J. Biol. Chem.* **270**, 25273–25280
21. Augustin, I., Betz, A., Herrmann, C., Jo, T., and Brose, N. (1999) *Biochem. J.* **337**, 363–371
22. Augustin, I., Rosenmund, C., Sudhof, T. C., and Brose, N. (1999) *Nature* **400**, 457–461
23. Varoqueaux, F., Sigler, A., Rhee, J. S., Brose, N., Enk, C., Reim, K., and Rosenmund, C. (2002) *Proc. Natl. Acad. Sci. U. S. A.* **99**, 9037–9042
24. Koch, H., Hofmann, K., and Brose, N. (2000) *Biochem. J.* **349**, 247–253
25. Akayama, M., Nakada, H., Omori, K., Masaki, R., Taketani, S., and Tashiro, Y. (1986) *Cell Struct. Funct.* **11**, 259–271
26. Palmer, M., Harris, R., Freytag, C., Kehoe, M., Tranum-Jensen, J., and Bhakdi, S. (1996) *EMBO J.* **17**, 1598–1606
27. Nagata, K., Satoh, T., Itoh, H., Kozasa, T., Okano, Y., Doi, T., Kaziro, Y., and Nozawa, Y. (1990) *FEBS Lett.* **275**, 29–32
28. Matsui, Y., Kikuchi, A., Kawata, M., Kondo, J., Teranishi, Y., and Takai, Y. (1990) *Biochem. Biophys. Res. Commun.* **166**, 1010–1016
29. Matsui, Y., Kikuchi, A., Kondo, J., Hishida, T., Teranishi, Y., and Takai, Y. (1988) *J. Biol. Chem.* **263**, 11071–11074
30. Chavrier, P., Vingron, M., Sander, C., Simons, K., and Zerial, M. (1990) *Mol. Cell Biol.* **10**, 6578–6585
31. Shirakawa, R., Yoshioka, A., Horiuchi, H., Nishioka, H., Tabuchi, A., and Kita, T. (2000) *J. Biol. Chem.* **275**, 33844–33849
32. Yoshioka, A., Shirakawa, R., Nishioka, H., Tabuchi, A., Higashi, T., Ozaki, H., Yamamoto, A., Kita, T., and Horiuchi, H. (2001) *J. Biol. Chem.* **276**, 39379–39386
33. Fabiato, A., and Fabiato, F. (1979) *J. Physiol. (Paris)* **75**, 463–505
34. Christoforidis, S., McBride, H. M., Burgoyne, R. D., and Zerial, M. (1999) *Nature* **397**, 621–625
35. Yoshioka, A., Horiuchi, H., Shirakawa, R., Nishioka, H., Tabuchi, A., Higashi, T., Yamamoto, A., and Kita, T. (2001) *Ann. N. Y. Acad. Sci.* **947**, 403–406
36. Knight, D. E., and Scrutton, M. C. (1980) *Thromb. Res.* **20**, 437–446
37. Nuoffer, C., Peter, F., and Balch, W. E. (1995) *Methods Enzymol.* **257**, 3–9
38. Pereira-Leal, J. B., Hume, A. N., and Seabra, M. C. (2001) *FEBS Lett.* **498**, 197–200
39. Franke, B., Akkerman, J. W., and Bos, J. L. (1997) *EMBO J.* **16**, 252–259
40. Menasche, G., Feldmann, J., Houdusse, A., Desnymard, C., Fischer, A., Goud, B., and de Saint Basile, G. (2003) *Blood* **101**, 2736–2742
41. Hume, A. N., Collinson, L. M., Rapak, A., Gomes, A. Q., Hopkins, C. R., and Seabra, M. C. (2001) *J. Cell Biol.* **152**, 795–808
42. Knight, J. B., Cao, K. T., Gibson, G. V., and Olson, A. L. (2000) *Endocrinology* **141**, 208–218
43. Kuroda, T. S., Fukuda, M., Ariga, H., and Mikoshiba, K. (2002) *J. Biol. Chem.* **277**, 9212–9218
44. Kuroda, T. S., Fukuda, M., Ariga, H., and Mikoshiba, K. (2002) *Biochem. Biophys. Res. Commun.* **293**, 899–906
45. Newton, A. C., and Johnson, J. E. (1998) *Biochim. Biophys. Acta* **1376**, 155–172
46. Nielsen, E., Christoforidis, S., Uttenweiler-Joseph, S., Miaczynska, M., Dewitte, F., Wilm, M., Hoflack, B., and Zerial, M. (2000) *J. Cell Biol.* **151**, 601–612
47. Price, A., Seals, D., Wickner, W., and Ungermann, C. (2000) *J. Cell Biol.* **148**, 1231–1238
48. Simonsen, A., Gaullier, J. M., D'Arrigo, A., and Stenmark, H. (1999) *J. Biol. Chem.* **274**, 28857–28860
49. McBride, H. M., Rybin, V., Murphy, C., Giner, A., Teasdale, R., and Zerial, M. (1999) *Cell* **98**, 377–386
50. Sassa, T., Harada, S., Ogawa, H., Rand, J. B., Maruyama, I. N., and Hosono, R. (1999) *J. Neurosci.* **19**, 4772–4777
51. Brose, N., Rosenmund, C., and Rettig, J. (2000) *Curr. Opin. Neurobiol.* **10**, 303–311
52. Schoch, S., Castillo, P. E., Jo, T., Mukherjee, K., Geppert, M., Wang, Y., Schmitz, F., Malenka, R. C., and Sudhof, T. C. (2002) *Nature* **415**, 321–326
53. Chen, D., Bernstein, A. M., Lemons, P. P., and Whiteheart, S. W. (2000) *Blood* **95**, 921–929
54. Matteoli, M., Takei, K., Cameron, R., Hurlbut, P., Johnston, P. A., Sudhof, T. C., Jahn, R., and De Camilli, P. (1991) *J. Cell Biol.* **115**, 625–633

Role of Bone Marrow–Derived Progenitor Cells in Cuff-Induced Vascular Injury in Mice

Yang Xu, Hidenori Arai, Xin Zhuge, Hideto Sano, Toshinori Murayama, Momoko Yoshimoto, Toshio Heike, Tatsutoshi Nakahata, Shin-ichi Nishikawa, Toru Kita, Masayuki Yokode

Objectives—Arterial injury results in vascular remodeling associated with proliferation and migration of smooth muscle cells (SMCs) and the development of intimal hyperplasia, which is a critical component of restenosis after angioplasty of human coronary arteries and an important feature of atherosclerotic lesions. However, the origin of SMCs and other cells in the development of vascular remodeling is not yet fully understood.

Methods and Results—We utilized a cuff-induced vascular injury model after transplantation of the bone marrow (BM) from green fluorescent protein (GFP)-transgenic mice. We found that macrophages were major cells recruited to the adventitia of the vascular injury lesion along with SMCs and endothelial cells (ECs). While investigating whether those cells are derived from the donor, we found that most of the macrophages were GFP-positive, and some of the SMCs and ECs were also GFP-positive. Administration of the anti–c-*fms* antibody resulted in a marked decrease in macrophages and a relative increase of SMCs, while administration of antibodies against the platelet-derived growth factor receptor-β caused a prominent decrease in SMCs and a relative increase in macrophages.

Conclusions—The current study indicates that BM-derived cells play an important role in vascular injury, and that differentiation of macrophages and SMCs might be dependent on each other. (***Arterioscler Thromb Vasc Biol.* 2004; 24:477-482.**)

Key Words: macrophage ■ smooth muscle cell ■ endothelial cell ■ vascular injury ■ bone marrow

Arterial injury results in proliferation and migration of smooth muscle cells (SMCs) and the development of intimal hyperplasia, a critical component of restenosis after angioplasty of human coronary arteries and an important feature of atherosclerotic lesions. However, the origin of SMCs, which engage in the development of neointimal thickening during vascular disease, is not yet fully understood. One possibility is that medial SMCs are phenotypically modified and migrate into the intima, where they proliferate and secrete extracellular matrix components.[1] It has also been proposed that adventitial fibroblasts move into the neointima and give rise to cells with smooth-muscle–like properties.[2]

Recently, several groups have reported that cells of recipient origin take part in the formation of neointimal SMCs during the development of transplant vasculopathy.[3–5] These results agree with the notion that adult bone marrow (BM) contains multipotent cells that can develop into various lineages.[6] It has also been shown that endothelial progenitor cells (EPCs) can transdifferentiate into SMCs.[7] Thus, the origin of SMCs in atherosclerotic lesions is a source of controversy, and it is important to understand the contribution of BM-derived cells to neointimal formation in vascular pathology.

In vascular injury or remodeling, it is not clear whether one specific type of multipotent precursor cell can differentiate into endothelial cells (ECs), SMCs, or macrophages, or whether there are different precursor cells for each cell lineage. We have reported that administration of anti–c-*fms* antibody can prevent early atherosclerosis in apolipoprotein E-deficient (apoE$^{-/-}$) mice.[8] We have also shown that administration of antibodies against the platelet-derived growth factor receptor-β (anti–PDGFR-β) can prevent the recruitment of SMCs, but not of macrophages in the atherosclerotic lesions in apoE$^{-/-}$ mice.[9] These results indicate the important role of macrophages in the initiation of the lesion and recruitment of SMCs in hyperlipidemia-induced atherosclerosis. However, it is not known whether the recruitment of macrophages is critical for the migration of SMCs in vascular injury.

Therefore, we have two goals in this study. One is to explore the contribution of BM-derived cells to the development of vascular remodeling. The other is to examine whether blocking the cell differentiation by a specific antibody can affect the lesion formation in vascular injury. For this purpose we have utilized an inflammation-dependent vascular disease model induced by polyethylene cuff placement around the femoral artery after BM transplantation (BMT) from green fluorescent protein (GFP)-transgenic mice.

Received November 16, 2003; revision accepted January 5, 2004.

From the Departments of Geriatric Medicine (H.S.), Pediatrics (M. Yoshimoto, T.H., T.N.), and Cardiovascular Medicine (T.K.), Kyoto University Graduate School of Medicine, Japan; the Translational Research Center (Y.X., X.Z., T.M., M. Yokode), Kyoto University Hospital, Kyoto, Japan; and the RIKEN Center for Developmental Biology (S.N.), Kobe, Japan

Correspondence to Hidenori Arai, MD, PhD, Department of Geriatric Medicine, Kyoto University Graduate School of Medicine, 54 Kawahara-cho, Shogoin, Sakyo-ku, Kyoto, 606-8507, Japan. E-mail harai@kuhp.kyoto-u.ac.jp

Arterioscler Thromb Vasc Biol. is available at http://www.atvbaha.org

DOI: 10.1161/01.ATV.0000118016.94368.35

Methods

Mice

All experimental protocols were performed in accordance with the guidelines of Kyoto University, Japan. GFP-transgenic mice with C57BL/6 background were a generous gift from Dr. M. Okabe[10] (Osaka University, Japan). The mice were kept in a temperature-controlled facility on a 14-hour light/10-hour dark cycle, with free access to food and water. Mice were fed a normal chow diet containing 8.7% (wt/wt) fat and 0.063% (wt/wt) cholesterol (Oriental Yeast, Chiba, Japan) for the entire period of the experiment.

Bone Marrow Transplantation

Femurs of male or female, 8- to 12-week-old GFP-transgenic mice were dissected, and surrounding muscle tissue was removed by microscissors. Bones were then left in Dulbecco's modified Eagle's medium (DMEM). Both ends of the bones were cut with scissors, and the marrow was flushed with DMEM using a syringe with a 21-gauge needle. The marrow clusters were disaggregated by vigorous pipetting. BM cells were washed, resuspended in PBS, and counted. Eight-week-old female C57BL/6 mice were subjected to a lethal dose of total body irradiation (9 Gy) using the Gammacell 40 Exactor Irradiator (Nordion International). Each irradiated recipient received 5×10^5 BM cells extracted from GFP-transgenic mice in 0.5 mL PBS by tail vein injection. Mice used for BMT experiments were housed in sterilized cages and fed sterilized normal chow diet. Drinking water was supplied with 0.1% hydrochloric acid. Four weeks after BMT, the recipient mice were phlebotomized, and the circulating leukocytes were then checked for the expression of GFP by flow cytometry. Cuff placement was performed at least 4 weeks after BMT.

Cuff Placement

Mice were anesthetized with barbiturate complex [propylene glycol 17.9% (v/v), ethanol 8.9% (v/v), sodium 5-ethyl-5-(1-methylbutyl) barbiturate 10.7% (v/v)]. The right femoral artery was dissected from its surroundings. A nonconstrictive polyethylene cuff (PE50, 0.58 mm inner diameter, 0.965 mm outer diameter, 2 mm length; Becton Dickinson) was placed loosely around the right femoral artery.

Antibody Administration

AFS98, a rat monoclonal anti-murine *c-fms* antibody, which inhibits colony formation dependent on macrophage-colony stimulating factor (M-CSF) and cell growth by blocking the binding of M-CSF to its receptor *c-fms*, was previously described as an anti–*c-fms* antibody.[9] APB5, a rat monoclonal anti-murine PDGFR-β antibody, which blocks the PDGFR-β–mediated signaling pathway, was also described.[9] Four C57BL/6 mice in each group were administered 1 mg of AFS98, APB5, or isotype-matched irrelevant rat IgG (γ2A) once a day for 2 weeks after cuff placement.

Tissue Preparation

At euthanization, mice were anesthetized with barbiturate complex. Mouse thorax was opened, and physiological pressure-perfusion-fixation (100 mm Hg) was performed by cardiac puncture with 4% paraformaldehyde in PBS for 10 minutes. After the procedures, bilateral femoral arteries were harvested. The tissue was snap-frozen in OCT compound (Sakura Finetek). Serial cross sections (6 μm thick) were obtained throughout the entire length of the cuffed femoral artery or equivalent portion of the contralateral artery for histological analysis. Rat monoclonal antibody (mAb) BM8, labeled with biotin (BMA Biochemicals AG), was used as a specific marker for mouse macrophages. For macrophage staining, we used the Tyramide Signal Amplification system (NEN Life Science Products) to amplify the weak signal. For SMC staining, we used mouse monoclonal anti-human smooth muscle α-actin (SMA) antibody (clone 1A4), labeled with Cy3 (Sigma). For the staining of smooth muscle myosin heavy chain SM1,[11] we used rat anti-SM1 mAb (clone KM995) (kindly provided by the Kyowa Hakko Kogyo Co, Tokyo, Japan). Sections were secondarily incubated with rhodamine-labeled anti-rat IgG (Chemicon). ECs were identified by immunohistochemical staining with biotin-conjugated rat anti-mouse CD31 antibody (Southern Biotech) and rabbit anti–von Willebrand Factor (vWF) antibody (Sigma). For CD31 staining, the Tyramide Signal Amplification system was employed to augment antigenicity of ECs. For vWF staining, sections were secondarily incubated with rhodamine-labeled anti-rabbit IgG (Chemicon).

Image Analysis and Quantification

Eight equally crossed sections were used from each mouse to quantify the femoral artery lumen, BM-derived cell area, and vascular remodeling lesion size. Sections were evaluated by using Image-Pro Plus (Media Cybernetics). To estimate the effect of anti–c-*fms* or anti–PDGFR-β on vascular remodeling, we calculated the ratio of the number of SMCs or macrophages to the whole vascular remodeling lesion area. The area of the femoral artery lumen, BM-derived cells, and vascular remodeling lesion was calculated and expressed in square micrometers.

Statistical Analysis

Data are expressed as mean±SEM and were analyzed by ANOVA with Abacus Statview software (version 5.0). A value of $P<0.05$ was regarded as significant.

Results

Recruitment of Bone Marrow–Derived Progenitor Cells in Cuff-Induced Vascular Remodeling

To elucidate the involvement of BM-derived cells in cuff-induced vascular remodeling lesions, BM cells from GFP-transgenic mice were transplanted into lethally irradiated C57BL/6 mice before cuff placement. After 4 weeks of BMT, we confirmed the reconstitution of the hematopoietic system by checking the fluorescence of blood leukocytes by flow cytometry. We found that more than 85% of the cells were positive for GFP (data not shown); this finding indicates that most of the leukocytes were derived from the donor BM. One or two weeks after cuff placement, cuffed or sham-operated femoral arteries were examined under fluorescence microscopy. In the cuffed artery, the majority of the cells accumulating in the lesion were GFP-positive (Figure 1A and 1B), suggesting that those cells were derived from the donor BM. In contrast, in the sham-operated artery, GFP-positive cells were hardly detected (Figure 1C). We found that the accumulation of BM-derived cells in the vascular remodeling lesion was significantly increased from 1 week to 2 weeks after cuff placement (Figure 1A, 1B, and 1D). Although we did not find a visible change in intimal thickening after cuff placement, the lumen of the cuffed artery was more restricted than that of the sham-operated artery (Figure 1E).

Macrophages are the Major Component in the Cuff-Induced Vascular Remodeling Lesion

Next, to examine the recruitment of macrophages in the cuffed lesion, we stained the tissue with BM8. We found many cells recruited to the adventitia of the cuffed artery, most of which were positive for BM8 (Figure 2A), indicating the role of monocyte-macrophages in vascular remodeling

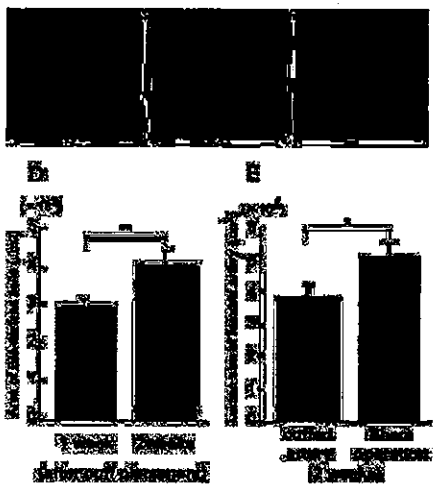

Figure 1. A through C, Representative microscopic photographs of BM-derived GFP-positive cells in C57BL/6 mouse vascular remodeling lesion. Four weeks after BMT, a nonconstrictive polyethylene cuff was placed around the right femoral artery in four mice in each group. The cuffed (A, 1 week after cuff placement; B, 2 weeks after cuff placement) or sham-operated (C) femoral arteries were examined under fluorescence microscopy. D and E, Quantitative analyses of BM-derived cell area (D) and femoral artery lumen area (E) after cuff placement showed a significant difference between 2 groups. Data from 20 slices per mouse artery are shown as mean±SEM. *P<0.05, **P<0.01. Scale bars: 100 μm

lesions. In the sham-operated femoral artery, we found few BM8-positive cells (Figure 2B).

BM Cells Can Differentiate into Vascular Smooth Muscle Cells

To examine whether BM-derived cells can differentiate into SMCs in the vascular remodeling lesion, we stained the tissue with Cy3-labeled anti-SMA (clone 1A4) and anti-SM1 (clone

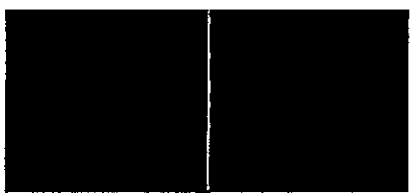

Figure 2. Numerous macrophage-like cells accumulating in the cuff-induced vascular remodeling lesion. After 2 weeks of cuff placement as described in Figure 1, tissues were subjected to immunohistochemistry with biotinylated anti-mouse macrophage antibody BM8. A number of cells were BM8-positive cells in cuffed femoral artery (A), but in the sham operated femoral artery, those cells could hardly be found (B). Scale bars: 100 μm

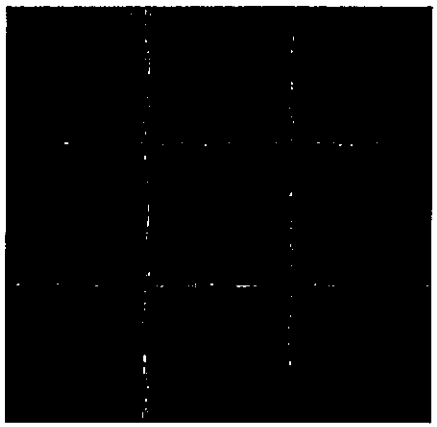

Figure 3. BM-derived SMCs in C57BL/6 mouse vascular remodeling lesion. After the same procedure in Figure 1, tissues were subjected to immunohistochemistry with antibodies to Cy3-labeled SMA (B, H) or SM1 (E). A, D, and G are fluorescent microscopic photographs for GFP. G, H, and I are fluorescent microscopic photographs from femoral artery of 1 week after cuff placement. All the others are samples at 2 weeks after cuff placement. C, F, and I are merged images of GFP and Cy3 signal from A and B, D and E, and G and H, respectively. Scale bars: 100 μm

KM995) antibodies. We found a number of 1A4- and KM995-positive cells in the adventitia of the lesion (Figure 3B and 3E). With the colorization of GFP signals, we observed that some of the 1A4- and KM995-positive cells were also positive for GFP (Figure 3C and 3F), indicating that BM-derived cells can also differentiate to SMCs in the cuff-induced vascular remodeling lesion. However, in the earlier time point at 1 week after cuff placement, we could find few SMCs in vascular remodeling lesion (Figure 3H).

Interference Exists Between Macrophages and Smooth Muscle Cells

To examine whether inhibiting the differentiation to macrophage or SMC by mAb could affect the manner of accumulation and differentiation of BM-derived cells in the vascular remodeling lesion, we administered an antagonistic rat mAb against murine *c-fms* (M-CSF receptor) (clone AFS98) or PDGFR-β (clone APB5) to C57BL/6 female mice which had undergone cuff placement. In comparison with the lesion from mice administered with control IgG (clone γ2A) (Figure 4C), we found that the treatment with AFS98 caused a marked decrease in macrophages in the lesion (Figure 4A and 4G). Interestingly, the density of SMCs was inversely increased (Figure 4D and 4H) in response to this treatment. In contrast, administration of APB5 resulted in a marked increase in macrophages (Figure 4B and 4G) with a concomitant decrease of SMCs (Figure 4E and 4H), suggesting that a certain interaction occurs between macrophages and SMCs during the vascular remodeling process.

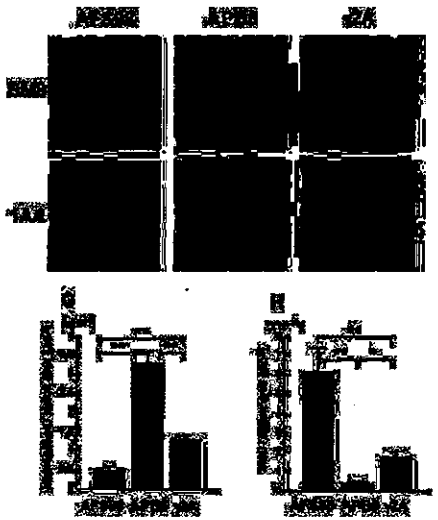

Figure 4. Progenitors of SMC and macrophage have opposite roles in the lesion formation. A total of 12 C57BL/6 mice (8 weeks of age) were injected for 2 weeks with 1 mg of AFS98 (n=4), APB5 (n=4), or γ2A (n=4) every day after cuff placement. Each mouse was euthanized and the femoral artery was subjected to immunohistochemistry with anti-macrophage antibody (A, B, and C) or anti-SMA antibody (D, E, and F). A and D are from mice injected with AFS98, B and E are from mice injected with APB5, and C and F are from mice given γ2A. Ratio of the number of macrophages (G) and SMCs (H) to whole vascular remodeling lesion area had a significant difference in each group. Data from 20 slices per mouse are shown as mean±SEM. *P<0.05, **P<0.01. Scale bars: 100 μm

To estimate the effects of anti–PDGFR-β or anti–*c-fms* mAb on vascular remodeling, we measured the lumen size of the artery treated with the two kinds of mAb and γ2A. We found no distinct difference in the lumen size of the femoral artery through administration of AFS98, APB5, or γ2A (data not shown).

We also examined whether each antibody administration had any effect on tissue formation after cuff placement. The calculated vascular remodeling lesion area of each mouse treated with AFS98, APB5, and γ2A was $1.18\times10^5\pm5.38\times10^3$ μm^2, $1.43\times10^5\pm7.27\times10^3$ μm^2, and $1.82\times10^5\pm1.11\times10^4$ μm^2, respectively (mean±SEM of 20 slices from each of 4 mice, P<0.05 versus γ2A). Less tissue formation was observed in the mice treated with AFS98 and APB5 than in mice treated with γ2A. This result indicates that AFS98 and APB5 administration could inhibit tissue formation after cuff placement. Further, to examine whether APB5 or AFS98 has an effect on BM-derived cell incorporation, we performed cuff placement and administered each antibody to mice that had been subjected to BMT. By measuring BM-derived cells accumulating in the cuff-induced lesion, we found a significant decrease of GFP-positive cells by mAb administration (data not shown), indicating that APB5 and AFS98 also affected the incorporation of BM-derived cells.

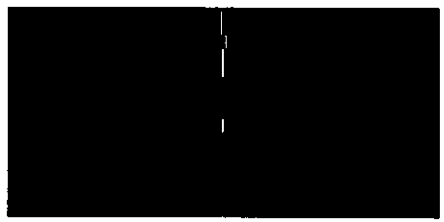

Figure 5. Representative microscopic photographs of BM-derived ECs in cuff-induced vascular remodeling lesion. After the same procedure in Figure 1, tissues were subjected to immunohistochemistry with biotin-conjugated rat anti-mouse CD31. The microscopic photograph of A is from cuffed right femoral artery, and B is from sham-operated left femoral artery. Scale bars: 100 μm

Endothelial Progenitor Cells Are Recruited to the Cuffed Vascular Remodeling Lesion

Because it is not known whether EPCs can contribute to cuff-induced vascular remodeling lesion formation in the injured femoral artery, we performed a series of endothelial staining. We found that the endothelial lining of the intima was clearly stained with anti-CD31 antibody, and that small vessels in the adventitia were also stained. There were also some CD31-positive cells clustered outside the small vessels in the adventitia in the cuffed lesions (Figure 5A), but not in the sham-operated lesions (Figure 5B). Because CD31 can also be expressed on monocyte-macrophages, we stained the tissue with anti-vWF antibody, another EC-specific marker, and compared the expression with GFP-positive cells. As shown in Figure 6E, the endothelial lining of the intima and small vessels in the adventitia were also positive for vWF. Some of the clustered cells in the adventitia were positive for

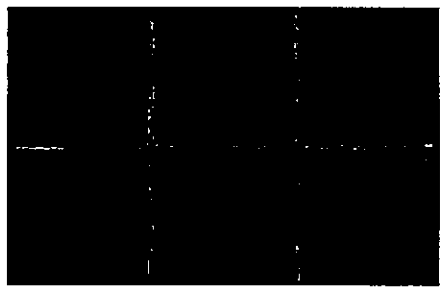

Figure 6. EPCs in cuff-induced vascular remodeling lesions. After the same procedure in Figure 1, tissues were subjected to immunostaining with anti-vWF antibody. A, B, and C are 1 week after cuff placement, and D, E, and F are 2 weeks after cuff placement. A and D indicate GFP signals, and B and E indicate vWF signals. C is a merged image of A and B, and F is a merged image of D and E. Scale bars: 100 μm

vWF and GFP, while the endothelial lining of the intima of the artery and small vessels in the adventitia were only positive for vWF (Figure 6F), indicating the involvement of angiogenesis from vasa vasorum. Notably, as we observed that significantly fewer SMCs could be found 1 week after cuffing (Figure 3B), EPCs could scarcely be found in the vascular remodeling lesion at this earlier phase (Figure 6C).

Discussion

In this study, we have clearly shown that BM-derived cells are critically involved in the lesion formation of cuff-induced vascular remodeling in mice. In this setting, BM-derived macrophages, SMCs, and ECs contributed to the lesion formation. However, not all of the SMCs or ECs in the lesion were derived from the BM. Interestingly, when anti-c-*fms* antibody was administered after cuff placement, the recruitment of macrophages was suppressed, but the density of SMCs was increased. On the other hand, administration of anti–PDGFR-β inhibited the recruitment of SMCs in the vascular remodeling lesion, but increased the number of macrophages. These results suggest an interaction between macrophages and SMCs during the lesion formation.

Although previous investigators have shown intimal thickening in the cuff-induced vascular injury model,[12,13] we have not been able to reproduce their results. This may be due to the technique of the cuff placement, because we were able to induce intimal thickening of the cuffed artery when we used apoE$^{-/-}$ mice fed with high-fat diet (data not shown). Indeed, we found a marked inflammatory change in the adventitial region around the cuffed artery. However, little is known about inflammatory responses in the adventitia after vascular injury, and adventitial and perivascular reactions are largely ignored. Recent clinical and experimental data by other investigators suggest that constrictive vascular remodeling is in large part responsible for lumen loss associated with restenosis.[14,15] Scott et al have indicated that the adventitia may be important in the first wave of growth after angioplasty of coronary arteries, with later growth of the lesion occurring in the neointima.[16] Therefore, studying the mechanism of cell recruitment to the adventitia in the vascular remodeling region is important for the understanding of the pathogenesis of restenosis.

Recent studies for transplant atherosclerosis have demonstrated that most of the neointimal α-actin–positive SMCs in recipient coronary arteries or aortas were from host origin,[4,5] suggesting that these SMCs might be at least in part from BM-derived smooth muscle progenitor cells. In this study, we have demonstrated that at least three types of cells, macrophage, SMC, and EC, are recruited from the BM to the adventitia of the cuff-induced vascular injury site. The characteristic feature of those cells is to form a cluster in the lesion. However, we have not determined when and how those cells migrate to the adventitia. Therefore, it is very important to understand the timing and pathway of cell migration in the pathogenesis of vascular injury. Elucidating the involvement of soluble factors in this model, such as chemokines and adhesion molecules, would also be intriguing.

In this study we have shown that administration of anti-c-*fms* antibody inhibited the recruitment of macrophages, and increased the recruitment of SMCs to the vascular injury lesion in wild-type mice. This finding is different from our report on apoE$^{-/-}$ mice, where we showed that the antibody inhibited the recruitment of SMCs as well as macrophages in early atherosclerotic lesion.[8] Thus, in hyperlipidemia-induced atherosclerosis, the recruitment of monocyte-macrophage is prerequisite for the migration of SMCs for the lesion formation; this paradigm was not applied to the current vascular injury model. If the common progenitors for macrophage and SMC exist, our data might indicate that BM-derived cells are playing an important role in vascular injury, but not in hyperlipidemia-induced atherosclerosis. The result with anti–PDGFR-β is also different from our previous observation in apoE$^{-/-}$ mice,[9] in which the antibody to apoE$^{-/-}$ mice failed to affect the density of macrophages in advanced atheromatous lesions. It was also notable that administration of anti–PDGFR-β increased the recruitment of macrophages in this study. Thus, in the vascular injury model, blocking the differentiation of one cell type can increase the recruitment or differentiation of the other cell type. Although we have not determined whether the progenitors of macrophages and SMCs are derived from the same precursor cell, anti-c-*fms* or anti–PDGFR-β might affect the differentiation of common precursor cells.

Schmeisser et al reported that BM-derived macrophages might contribute to neovascularization by in situ transdifferentiation to EC-like cells.[17] We found that in the vascular injury lesion there were many cells positive for CD31, which is an endothelial marker and is also positive for monocyte-lineage. However, vWF-positive cells were much smaller in number in this lesion. Furthermore, most of the cells forming a small vessel were positive for vWF, but negative for GFP, indicating that the source of the ECs forming a small vessel in the adventitia is from vasa vasorum, not from the BM.

Terada et al[18] and Ying et al[19] demonstrated that embryonic stem cells can spontaneously fuse with mononuclear BM cells[18] or brain cells[19] in vitro to form pluripotent tetraploid hybrids. In this study, there are a number of BM-derived cells stimulated after cuff placement in the cuff-induced vascular remodeling lesion. These BM-derived cells play an important role for lesion formation. Those two reports showed that the frequency of cell fusion was very low (2×10^{-4} to 10^{-4}), although it is difficult to directly correlate the in vitro findings of embryonic stem cells to our in vivo study. It is possible that some of the BM-derived cells in our experiments resulted from fusion between BM cells and vascular cells; however, this phenomenon would be an unlikely explanation for the extent of BM involvement seen in this study.

In summary, we have provided evidence that BM-derived cells are playing a critical role in cuff-induced vascular injury in mice. Understanding the interaction among the cells involved in the lesion formation will be important for regulating the accumulation of inflammatory cells in the vascular injury lesion.

Acknowledgments

This study was supported by Grants-in-Aid from the Ministry of Education, Science, Sports, and Culture of Japan (20045982, 12671111, 14571093, and 13307034) (to H.A., M.Y., T.K.); Center of Excellence grants (12CE2006) (to T.K.); a research grant for health sciences from the Japanese Ministry of Health and Welfare (to T.K.); and a grant from the Rotary Yoneyama Memorial Foundation (to Y.X.). T.M. is supported by Establishment of International COE for Integration of Transplantation Therapy and Regenerative Medicine (COE Program of the Ministry of Education, Culture, Sports, Science, and Technology, Japan). We thank Drs Hiroharu Kataoka and Masafumi Morimoto for their advice about cuff placement, and Akiko Kato for her excellent technical assistance.

References

1. Newby AC, Zaltsman AB. Molecular mechanisms in intimal hyperplasia. *J Pathol.* 2000;190:300–309.
2. Zalewski A, Shi Y. Vascular myofibroblasts. Lessons from coronary repair and remodeling. *Arterioscler Thromb Vasc Biol.* 1997;17:417–422.
3. Plissonnier D, Nochy D, Poncet P, Mandet C, Hinglais N, Bariety J, Michel JB. Sequential immunological targeting of chronic experimental arterial allograft. *Transplantation.* 1995;60:414–424.
4. Hillebrands JL, Klatter FA, van den Hurk BM, Popa ER, Nieuwenhuis P, Rozing J. Origin of neointimal endothelium and α-actin–positive smooth muscle cells in transplant arteriosclerosis. *J Clin Invest.* 2001;107:1411–1422.
5. Saiura A, Sata M, Hirata Y, Nagai R, Makuuchi M. Circulating smooth muscle progenitor cells contribute to atherosclerosis. *Nat Med.* 2001;7:382–383.
6. Pittenger MF, Mackay AM, Beck SC, Jaiswal RK, Douglas R, Mosca JD, Moorman MA, Simonetti DW, Craig S, Marshak DR. Multilineage potential of adult human mesenchymal stem cells. *Science.* 1999;284:143–147.
7. DeRuiter MC, Poelmann RE, VanMunsteren JC, Mironov V, Markwald RR, Gittenberger-de Groot AC. Embryonic endothelial cells transdifferentiate into mesenchymal cells expressing smooth muscle actins in vivo and in vitro. *Circ Res.* 1997;80:444–451.
8. Murayama T, Yokode M, Kataoka H, Imabayashi T, Yoshida H, Sano H, Nishikawa S, Kita T. Intraperitoneal administration of anti-c-*fms* monoclonal antibody prevents initial events of atherogenesis but does not reduce the size of advanced lesions in apolipoprotein E-deficient mice. *Circulation.* 1999;99:1740–1746.
9. Sano H, Sudo T, Yokode M, Murayama T, Kataoka H, Takakura N, Nishikawa S, Nishikawa SI, Kita T. Functional blockade of platelet-derived growth factor receptor-β but not of receptor-α prevents vascular smooth muscle cell accumulation in fibrous cap lesions in apolipoprotein E-deficient mice. *Circulation.* 2001;103:2955–2960.
10. Okabe M, Ikawa M, Kominami K, Nakanishi T, Nishimune Y. 'Green mice' as a source of ubiquitous green cells. *FEBS Lett.* 1997;407:313–319.
11. Nagai R, Kuro-o M, Babij P, Periasamy M. Identification of two types of smooth muscle myosin heavy chain isoforms by cDNA cloning and immunoblot analysis. *J Biol Chem.* 1989;264:9734–9737.
12. Liu HW, Iwai M, Takeda-Matsubara Y, Wu L, Li JM, Okumura M, Cui TX, Horiuchi M. Effect of estrogen and AT1 receptor blocker on neointima formation. *Hypertension.* 2002;40:451–457; discussion 448–450.
13. Suzuki J, Iwai M, Nakagami H, Wu L, Chen R, Sugaya T, Hamada M, Hiwada K, Horiuchi M. Role of angiotensin II-regulated apoptosis through distinct AT1 and AT2 receptors in neointimal formation. *Circulation.* 2002;106:847–853.
14. Mintz GS, Popma JJ, Pichard AD, Kent KM, Satler LF, Wong C, Hong MK, Kovach JA, Leon MB. Arterial remodeling after coronary angioplasty: a serial intravascular ultrasound study. *Circulation.* 1996;94:35–43.
15. Sangiorgi G, Taylor AJ, Farb A, Carter AJ, Edwards WD, Holmes DR, Schwartz RS, Virmani R. Histopathology of postpercutaneous transluminal coronary angioplasty remodeling in human coronary arteries. *Am Heart J.* 1999;138:681–687.
16. Scott NA, Cipolla GD, Ross CE, Dunn B, Martin FH, Simonet L, Wilcox JN. Identification of a potential role for the adventitia in vascular lesion formation after balloon overstretch injury of porcine coronary arteries. *Circulation.* 1996;93:2178–2187.
17. Schmeisser A, Garlichs CD, Zhang H, Eskafi S, Graffy C, Ludwig J, Strasser RH, Daniel WG. Monocytes coexpress endothelial and macrophagocytic lineage markers and form cord-like structures in Matrigel under angiogenic conditions. *Cardiovasc Res.* 2001;49:671–680.
18. Terada N, Hamazaki T, Oka M, Hoki M, Mastalerz DM, Nakano Y, Meyer EM, Morel L, Petersen BE, Scott EW. Bone marrow cells adopt the phenotype of other cells by spontaneous cell fusion. *Nature.* 2002;416:542–545.
19. Ying QL, Nichols J, Evans EP, Smith AG. Changing potency by spontaneous fusion. *Nature.* 2002;416:545–548.

Cell surface-anchored SR-PSOX/CXC chemokine ligand 16 mediates firm adhesion of CXC chemokine receptor 6-expressing cells

Takeshi Shimaoka,* Takashi Nakayama,† Noriko Fukumoto,* Noriaki Kume,‡ Shu Takahashi,§ Junko Yamaguchi,§ Manabu Minami,‡ Kazutaka Hayashida,‡ Toru Kita,‡ Jun Ohsumi,¶ Osamu Yoshie,† and Shin Yonehara*,1

*Graduate School of Biostudies and Institute for Virus Research and ‡Department of Cardiovascular Medicine, Graduate School of Medicine, Kyoto University, Sakyo-ku, Japan; †Department of Microbiology, Kinki University School of Medicine, Osaka-Sayama, Japan; and §Biomedical Research Laboratories and ¶Molecular Biology Research Laboratories, Sankyo Co. Ltd., Shinagawa-ku, Tokyo, Japan

Abstract: Direct contacts between dendritic cells (DCs) and T cells or natural killer T (NKT) cells play important roles in primary and secondary immune responses. SR-PSOX/CXC chemokine ligand 16 (CXCL16), which is selectively expressed on DCs and macrophages, is a scavenger receptor for oxidized low-density lipoprotein and also the chemokine ligand for a G protein-coupled receptor CXC chemokine receptor 6 (CXCR6), expressed on activated T cells and NKT cells. SR-PSOX/CXCL16 is the second transmembrane-type chemokine with a chemokine domain fused to a mucin-like stalk, a structure very similar to that of fractalkine (FNK). Here, we demonstrate that SR-PSOX/CXCL16 functions as a cell adhesion molecule for cells expressing CXCR6 in the same manner that FNK functions as a cell adhesion molecule for cells expressing CX_3C chemokine receptor 1 (CX_3CR1) without requiring CX_3CR1-mediated signal transduction or integrin activation. The chemokine domain of SR-PSOX/CXCL16 mediated the adhesion of CXCR6-expressing cells, which was not impaired by treatment with pertussis toxin, a Gαi protein blocker, which inhibited chemotaxis of CXCR6-expressing cells induced by SR-PSOX/CXCL16. Furthermore, the adhesion activity was up-regulated by treatment of SR-PSOX/CXCL16-expressing cells with a metalloprotease inhibitor, which increased surface expression levels of SR-PSOX/CXCL16. Thus, SR-PSOX/CXCL16 is a unique molecule that not only attracts T cells and NKT cells toward DCs but also supports their firm adhesion to DCs. *J. Leukoc. Biol.* 75: 267–274; 2004.

Key Words: *scavenger receptor · metalloprotease · T cells*

INTRODUCTION

The chemokine superfamily consists of small, heparin-binding cytokines that induce directed migration of various types of leukocytes through interactions with a group of seven-transmembrane G protein-coupled receptors [1]. More than 40 chemokines have been identified and classified into four subfamilies, C, CC, CXC, and CX_3C, based on the motif formed by the conserved cysteine residues in the amino-terminal region. In addition to migration-inducing activity, chemokines have been shown to induce signals that lead to cytoskeletal reorganization and integrin activation for cell adhesion [2–5]. Furthermore, fractalkine (FNK)/CX_3C chemokine ligand 1, the first reported transmembrane-type chemokine [6, 7], has been shown to function as a cell adhesion molecule under static and flow conditions without requiring CX_3C chemokine receptor 1 (CX_3CR1)-mediated signaling or integrin activation [8, 9].

Recently, we have identified and characterized SR-PSOX, a novel scavenger receptor for phosphatidylserine and oxidized low-density lipoprotein and bacteria [10, 11]. Separately, other groups have identified chemokine ligand 16 (CXCL16) [12, 13], the chemokine ligand for a G protein-coupled receptor CXC chemokine receptor 6 (CXCR6) [14, 15], and then SR-PSOX and CXCL16 turned out to be identical. Thus, SR-PSOX/CXCL16 is the second transmembrane-type chemokine with a chemokine domain fused to a mucin-like stalk, a structure very similar to that of FNK [6, 7]. SR-PSOX/CXCL16 is selectively expressed on antigen-presenting cells (APCs) such as dendritic cells (DCs) and macrophages, and its receptor CXCR6 is expressed on naive $CD8^+$ T cells, natural killer T (NKT) cells, and type 1-polarized, activated $CD4^+$ and $CD8^+$ T cells [12–16]. It has been proposed that CXCL16 promotes the movement of T cells toward DCs in the splenic red pulp [12]. Furthermore, CXCR6-expressing effector T cells were found to be abundant in type 1 inflammatory lesions such as rheumatoid joints and inflamed livers [16].

DCs, which capture and process antigens to form major histocompatibility complex peptide complexes, function as professional APCs to T cells. After up-taking antigen and migrating from the periphery to the T cell areas of secondary lymphoid organs, DC contact can initiate primary immune responses via activation of resting T cells. In addition, contacts between DCs and T cells are essential to maintain and restart immune responses of previously activated T cells [17, 18]. Adhesion molecules such as lymphocyte function-associated antigen-3 (LFA-3)/CD2, LFA-1/intercellular adhesion molecule-1 (ICAM-1) and DC-specific ICAM-3-grabbing nonintegrin/ICAM-3 are reported to mediate interactions between DCs and T cells and to provide activation signals via DC–T cell adhesion [19, 20]. Notably, the membrane-anchored chemokine, FNK, whose molecular structure is similar to that of SR-PSOX/CXCL16, can directly function as an adhesion molecule for cells expressing its receptor CX_3CR1 [8, 9]. Here, we demonstrate that in a manner very similar to that of FNK, SR-PSOX also functions as a direct adhesion cell molecule for cells expressing its receptor CXCR6. The chemokine domain of SR-PSOX primarily mediates the adhesion of CXCR6-expressing cells. The adhesion is not inhibited by pertussis toxin (PTX), the Gαi protein inhibitor, although it effectively suppresses chemotaxis of CXCR6-expressing cells induced by SR-PSOX/CXCL16. Furthermore, the adhesion of CXCR6-expressing cells can be enhanced by treatment of SR-PSOX/CXCL16-expressing cells with a metalloprotease inhibitor, which increases the surface expression of SR-PSOX/CXCL16. Thus, SR-PSOX/CXCL16 may play an important role in interactions between DCs and T cells or NKT cells as a chemoattractant as well as a cell adhesion molecule.

MATERIALS AND METHODS

Materials and cells

PTX, wortmannin, and PD098059 were purchased from Calbiochem-Novabiochem (La Jolla, CA). EGTA was purchased from Sigma Chemical Co. (St. Louis, MO). Mouse-activated T cells expressing CXCR6 were prepared as described previously [12] with minor modifications. In brief, T cells (2×10^5 cells/ml) isolated from splenocyte suspensions by magnetic cell sorter were activated by cultivation with RPMI-1640 medium containing 10% fetal bovine serum (FBS) and mouse interleukin (IL)-2 (4 ng/ml) for 5 days in plastic plates precoated with anti-CD3 (2C11) and anti-CD28 (37.51; PharMingen, San Diego, CA). The activated T cells were then left to rest in RPMI-1640 medium containing 10% FBS and IL-2 (2 ng/ml) for 4 days and were used as CXCR6-expressing cells. Transfection of COS-7 cells was performed as described previously [10]. L1.2 murine pre-B cells stably expressing CXCR6 (L-CXCR6) or CX_3CR1 (L-CX_3CR1) were generated as reported previously [8].

Monoclonal anti-human (h)- and mouse (m)SR-PSOX antibodies

Female Lewis rats were immunized with mSR-PSOX-Fc fusion protein, produced by COS-7 cells, transfected with a fusion construct consisting of the extracellular domain of mSR-PSOX (amino acids 1–198) fused at its C terminus with an Fc fragment of human immunoglobulin G (IgG)1. Three days after the last immunization, spleen cells were fused with NS-1 mouse myeloma cells as described previously [21]. Finally, we generated an anti-mSR-PSOX monoclonal antibody (mAb) 12-81. Anti-hSR-PSOX mAb 22-19-12, 49-36, and 28-12 were generated as described previously [11].

Preparation of polyclonal anti-hSR-PSOX antibody

Synthetic peptides corresponding to amino acid residues 42–61 of hSR-PSOX were conjugated to Imject Maleimide-Activated mcKLH (Pierce, Rockford, IL). After the immunization of a rabbit with the conjugates, polyclonal antiserum was collected and purified using a column packed with peptide corresponding to amino acid residues 42–61 of hSR-PSOX.

SR-PSOX-FNK hybrid protein

Plasmids encoding SR-PSOX-FNK hybrid molecules were generated by polymerase chain reaction (PCR) and subsequent ligation of DNA fragments into pME18S [22] as described previously [21]. In brief, the following fragments were amplified by PCR using primers as indicated: DNA encoding the chemokine domain of hSR-PSOX (amino acids 1–118) using primers 5′-TCACTCGAGATGGGACGGGACTTGCGGCC-3′ and 5′-TCAGAATTCAGGAAGTAAATGCTTCTGGTGGG-3′; DNA encoding the chemokine domain of hFNK (amino acids 1–206) using 5′-TCACTCGAGACGCTCTCCCCCCTGGCTCTA-3′ and 5′-TCACAATTCTAGGGCAGCAAGCCTGGCGGT-3′; DNA encoding the region containing the mucin, transmembrane, and cytoplasmic domains of hSR-PSOX (amino acids 120–254) using 5′-TCAGAATTCACCAGCCCCCCAATTTCTCA-3′ and 5′-TCACTGCAGTCAGGTATTAGAGTCAGGTC-3′; and DNA encoding the region containing the mucin, transmembrane, and cytoplasmic domains of hFNK (amino acids 97–397) using 5′-TCAGAATTCACTCGAAATGCCCGCACCTT-3′ and 5′-TCACTGCAGACTAGACACAGGCCAGAGCA-3′. PCR fragments of the chemokine domain were digested with *Xho*I and *Eco*RI, and PCR fragments of the other domains were digested with *Eco*RI and *Pst*I. These digested fragments were ligated together into pME18S digested with *Xho*I and *Pst*I, and expression vectors for four kinds of SR-PSOX-FNK hybrids (S-S, S-F, F-S, and F-F, see Fig. 4A) were prepared. DNA encoding hSR-PSOX without the mucin domain (amino acids 119–205; Δmucin) was generated by ligating DNA fragments encoding the chemokine domain of hSR-PSOX and the transmembrane and cytoplasmic domains of hSR-PSOX, which were prepared at once by PCR using 5′-GCACAGGACGGGCACAGGAAGTAAATGCTT-3′, 5′-TCACTCGAGATGGGACGGGACTTGCGCCC-3′, and 5′-GCAGTCGCTCGTTAGTCCTA-3′ as primers. These PCR fragments digested with *Xho*I and *Hin*dIII and with adaptor fragments generated by digestion of pME18S with *Xho*I and *Hin*dIII were ligated together into *Hin*dIII-digested pME18S-SR-PSOX.

Chemotaxis and calcium mobilization assays

Chemotaxis assays using transwell plates with 5 μm pore size membrane (Corning Costar, Corning, NY) and calcium mobilization assays were performed as described previously [8]. In some experiments, cells were preincubated with PTX (500 ng/ml), wortmannin (100 nM), or PD098059 (50 μM) for 30 min at 37°C.

Cell adhesion assays

Cell adhesion to immobilized SR-PSOX or FNK was measured essentially as described previously [8]. In adhesion assays with immobilized chemokines, enzyme-linked immunosorbent assay (ELISA) plates (Corning Costar) were precoated with 10 nM chemokines fused with a secreted form of placental alkaline phosphatase (SEAP). L-CXCR6 cells or mouse-activated T cells were transferred to each well (5×10^4 cells/well) and incubated for 30 min at room temperature (RT). After being washed, adherent cells were quantified using Picogreen double-strand DNA quantitation reagent (Molecular Probes, Eugene, OR). In adhesion assays with chemokine-expressing cells, L-CXCR6 or mouse-activated T cells labeled with calcein acetoxymethyl ester (calcein-AM; Molecular Probes) were transferred to 12-well plates (5×10^5 cells/well), where COS-7 cells expressing SR-PSOX (COS-SR-PSOX cells) were preseeded. After incubation for 60 min at 37°C, nonadherent cells were removed by washing, and fluorescence intensity was measured using Wallac 1420 ARVO fluoroscan (Wallac, Turku, Finland). To analyze effects of various inhibitors, COS-SR-PSOX cells and L-CXCR6 cells were preincubated with PTX (500 ng/ml), wortmannin (100 nM), PD098059 (50 μM), or soluble (s)SR-PSOX-SEAP (20 nM) for 30 min at 37°C.

Expression analysis of SR-PSOX and CXCR6

For flow cytometric analysis of cell surface-expressed hSR-PSOX, cells were detached from dishes with 5 mM EDTA and incubated for 1 h on ice with 20 μg/ml anti-hSR-PSOX mAb, clone 22-19-12, 49-36, or 28-12 or control mouse IgG. After being washed, cells were incubated with 20 μg/ml fluorescein isothiocyanate (FITC)-conjugated anti-mouse IgG antibody (Cappel, Aurora, OH) on ice for 1 h. After two-times washes, cells were analyzed on an EPICS

1 Correspondence: Graduate School of Biostudies and Institute for Virus Research, Kyoto University, Shogoin Kawahara-cho 53, Sakyo-ku, Kyoto 606-8507, Japan. E-mail: syonehar@virus.kyoto-u.ac.jp

Received October 9, 2003; accepted October 14, 2003; doi: 10.1189/jlb.1003465.

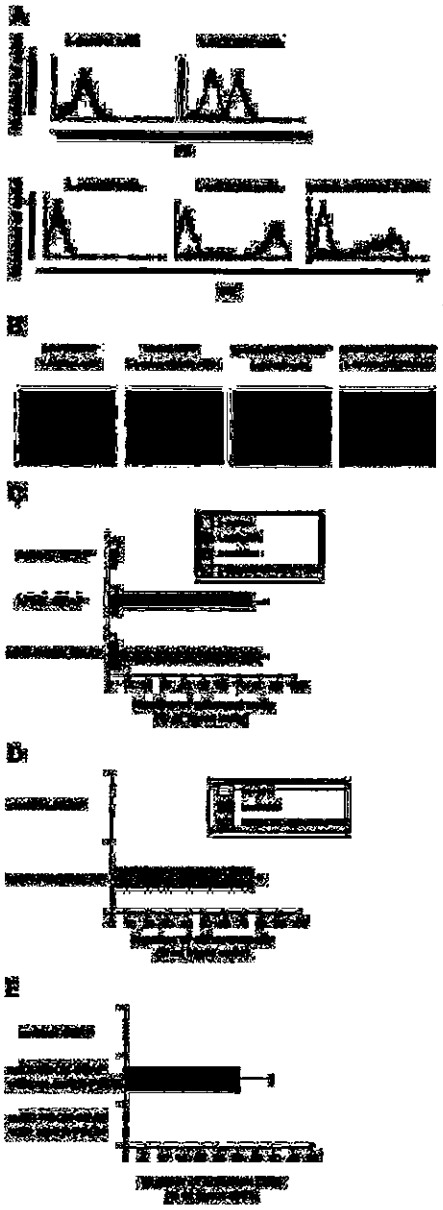

Fig. 1. Immobilized SR-PSOX/CXCL16 on plastic dish mediates cell adhesion of CXCR6-expressing cells. (A) Flow cytometric analysis. Surface expression of hCXCR6 on control murine L1.2 cells (L-control cells) and murine L-hCXCR6 cells was analyzed by flow cytometry after staining with anti-hCXCR6 mAb 56311 (bold line) or control IgG (dotted line). Surface expression of mCXCR6 on L-control cells, murine L-mCXCR6 cells, and mouse-activated T cells was analyzed by flow cytometry using SR-PSOX-Fc as described in Materials and Methods. Mouse-activated T cells were prepared by in vitro activation with CD3 and CD28 as described in Materials and Methods. (B–E) Assay of adhesion to immobilized SR-PSOX-SEAP on plastic culture dishes. L-control, L-hCXCR6, and L-hCX$_3$CR1 cells were transferred to plastic culture dishes precoated with control-SEAP, hSR-PSOX-SEAP, or hFNK-SEAP and were incubated for 30 min at RT (B and C). L-control and L-mCXCR6 cells (D) and mouse-activated T cells (E) were incubated in wells precoated with control SEAP or mSR-PSOX-SEAP and were incubated for 30 min at RT. After the washes of plates, adherent cells were observed under light microscopy (B) and quantified using Picogreen double-strand DNA quantitation reagent (C–E). In blocking experiments, shSR-PSOX and smSR-PSOX, respectively (20 nM), were preincubated with SR-PSOX-SEAP-coated plates, L-hCXCR6 or L-mCXCR6 cells, and mouse-activated T cells for 30 min. The data shown represent the mean ± SD from at least three independent experiments.

Elite (Coulter, Hialeah, FL). Flow cytometric analysis of cell surface-expressed mSR-PSOX was similarly performed using the anti-mSR-PSOX mAb 12-81. For flow cytometric analysis of cell surface-expressed hCXCR6, Fc receptors on cells were blocked by treatment with human IgG, and then cells were stained with phycoerythrin (PE)-labeled anti-hCXCR6 mAb (clone 56811). For flow cytometric analysis of mCXCR6, Fc receptors were blocked by FITC-labeled anti-CD16/CD32 (PharMingen), and then cells were stained with SR-PSOX-Fc and PE-labeled goat anti-human Fcγ as described previously [12].

Quantification of SR-PSOX by ELISA

ELISA plates were coated with the monoclonal anti-SR-PSOX antibody 28-12 (10 μg/ml, 50 μl/well) by incubating for 2 h at 37°C. After three-times washes with phosphate-buffered saline (PBS) containing 0.1% Tween 20, the plates were blocked with fourfold-diluted BlockAce (Dainippon Seiyaku, Osaka, Japan) for 1 h at RT. After three more washes, appropriately diluted samples or standards (50 μl/well) were loaded and incubated for 2 h at RT. After another three-times washes, rabbit polyclonal anti-SR-PSOX antibody (50 μl/well) against synthetic peptides corresponding to amino acid residues 42–61 of hSR-PSOX (10 μg/ml) was transferred to the plate and incubated for 1 h at RT. After three-times washes with PBS containing 0.1% Tween 20, anti-rabbit IgG–horseradish peroxidase (50 μl/well), which does not cross-react with mouse IgG (Amersham Biosciences, Little Chalfont, UK), was transferred and incubated for 30 min at RT. After another three washes with PBS containing 0.1% Tween 20, tetramethylbenzidine substrate buffer (100 μl/well; Dako, Carpinteria, CA) was transferred to each well. After incubation for 5–30 min at RT, stop solution (100 μl/well) was transferred to each well, and the optical density (O.D.) at 450 nm was determined using Wallac 1420 ARVO fluoroscan (Wallac).

Preparation of SR-PSOX-containing samples for ELISA

COS-SR-PSOX cells in 24-well tissue-culture plates were cultured for 24 h with serum-free medium in the presence or absence of the metalloproteinase inhibitor GM6001 (10 μM). Then, culture supernatants were collected for quantification of sSR-PSOX. After being washed with PBS, cells were lysed for 30 min with lysis buffer (PBS containing 1% Nonidet P-40, 0.5% sodium deoxycholate, 0.1% sodium dodecyl sulfate, 0.1 mM phenylmethylsulfonyl fluoride, and 1% protease inhibitor mixture). After clarification of the culture supernatants and cell lysates by centrifugation, ELISA quantified the SR-PSOX. The data shown represent the mean ± SD from at least three independent experiments.

Fig. 2. SR-PSOX/CXCL16-expressing cells mediate adhesion of CXCR6-expressing cells. (A) Flow cytometric analysis. COS-7 cells were transfected with control vector (COS-control cells) or hSR-PSOX (COS-hSR-PSOX cells) or mSR-PSOX (COS-mSR-PSOX) cells, respectively. The transient expression of hSR-PSOX or mSR-PSOX on these COS-7 cells was analyzed by flow cytometry after staining with anti-hSR-PSOX mAb 28-12 or anti-mSR-PSOX mAb 12-81 (bold lines) or with control antibody (dotted line) as described in Materials and Methods. (B–E) Adhesion assay with SR-PSOX-expressing COS-7 cells. L-control, L-hCXCR6, and L-hCX$_3$CR1, labeled with calcein-AM, were incubated with COS-control, COS-hSR-PSOX, or COS-hFNK cells for 60 min at 37°C (B and C). L-mCXCR6 (D) or mouse-activated T cells (E) were labeled with calcein-AM and then incubated with COS-control or COS-mSR-PSOX cells for 60 min at 37°C. After the washes of plates, adherent cells were observed under light microscopy (upper panels) and fluorescence microscopy (lower panels; B), and fluorescence intensity was quantified as described in Materials and Methods (C–E). In blocking experiments, shSR-PSOX or smSR-PSOX (20 nM) was preincubated with COS-SR-PSOX cells and L-CXCR6 or mouse-activated T cells for 30 min. The data shown represent the mean ± SD from at least three independent experiments.

RESULTS

Immobilized SR-PSOX/CXCL16 on plastic culture dish mediates adhesion of CXCR6-expressing cells

SR-PSOX/CXCL16 is a transmembrane protein with an N-terminal CXC chemokine domain fused to a mucin-like stalk [10–13]. This structure is very similar to that of another transmembrane-type chemokine, FNK [6, 7]. The membrane-anchored form of FNK has been demonstrated to induce firm adhesion of cells expressing its receptor CX$_3$CR1 in static and flow conditions [8, 9]. We, therefore, examined whether the membrane-anchored SR-PSOX/CXCL16 was also capable of mediating firm adhesion of CXCR6-expressing cells. First, we examined whether SR-PSOX-SEAP immobilized to plastic culture dishes was capable of trapping L-hCXCR6 cells, whose expression of CXCR6 was confirmed by flow cytometry (**Fig. 1A**). As shown in Figure 1, B and C, L-hCXCR6 cells indeed bound to immobilized hSR-PSOX-SEAP. Conversely, L-hCX$_3$CR1 cells did not bind to hSR-PSOX-SEAP but bound to hFNK-SEAP. Neither L-hCXCR6 cells nor L-hCX$_3$CR1 cells bound to control-immobilized SEAP. The adhesion of L-hCXCR6 cells was inhibited by shSR-PSOX. Similarly, L-mCXCR6 cells, whose expression of mCXCR6 was confirmed by flow cytometry (Fig. 1A) and reverse transcriptase-PCR (data not shown), selectively bound to immobilized mSR-PSOX-SEAP in a manner sensitive to smSR-PSOX (Fig. 1D). We further demonstrated specific adhesion of normal mouse T cells expressing CXCR6 (Fig. 1A), which were prepared by activation in vitro with anti-CD3 and anti-CD28, to immobilized mSR-PSOX-SEAP, again in a manner sensitive to smSR-PSOX (Fig. 1E).

Adhesion of CXCR6-expressing cells to SR-PSOX/CXCL16-expressing cells

We then examined adhesion of CXCR6-expressing cells to the membrane-anchored chemokines expressed on COS-7 cells. L-hCXCR6 cells selectively bound to COS-7 cells transfected with hSR-PSOX/CXCL16 (COS-hSR-PSOX cells), whose expression was confirmed by flow cytometry (**Fig. 2A**), and L-hCX$_3$CR1 cells selectively bound to those expressing FNK (COS-hFNK cells; Fig. 2, B and C). Adhesion of L-hCXCR6 cells to COS-hSR-PSOX cells was inhibited by shSR-PSOX. Neither L-CXCR6 nor L-CX$_3$CR1 bound to control COS-7 cells (COS-control cells). As shown in Figure 2, D and E, L-mCXCR6 cells and mouse-activated T cells selectively

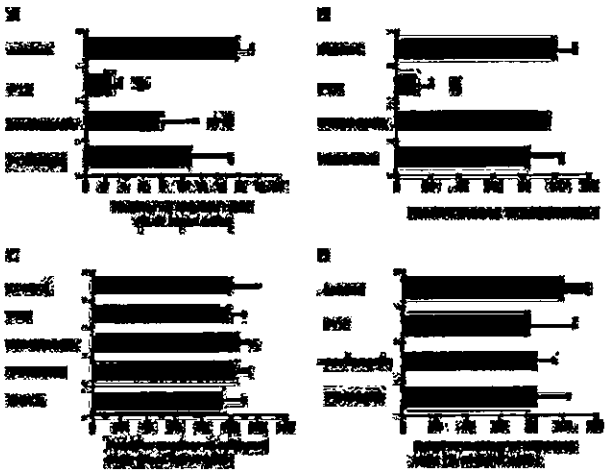

Fig. 3. Signal transduction through chemokine receptor is not required for SR-PSOX-CXCR6-induced cell adhesion. (A) Examination of chemotaxis by standard transwell assays. hSR-PSOX-SEAP (10 nM) was analyzed for its chemotactic activity against L-hCXCR6 cells preincubated with PTX (500 ng/ml), wortmannin (100 nM), or PD098059 (50 μM) for 30 min. (B) Calcium mobilization assay. L-hCXCR6 cells preincubated with or without the indicated inhibitors for 30 min, were loaded with fura-PE3-AM and stimulated with hSR-PSOX-SEAP (10 nM). The intracellular concentration of calcium was monitored using fluorescence ratio (F340/F380). Values in the absence of inhibitor were set as 100%. (C, D) Cell adhesion assays. Adhesion of L-hCXCR6 cells to hSR-PSOX-SEAP-coated plates (C) or COS-hSR-PSOX cells (D) was measured as described in Figures 1 and 2. Cells were preincubated with or without the indicated inhibitors for 30 min. Values in the absence of inhibitor were set as 100%. (A–D) The data shown represent the mean ± SD from at least three independent experiments. *, $P < 0.01$; **, $P < 0.05$.

bound to COS-mSR-PSOX/CXCL16, whose expression was confirmed by flow cytometry (Fig. 2A). Collectively, similar to the membrane-anchored FNK [8, 9], the membrane-anchored SR-PSOX/CXCL16 was indeed capable of mediating adhesion of cells expressing its receptor CXCR6.

CXCR6-mediated signal transduction is not required for adhesion induced by SR-PSOX/CXCL16

As shown in **Figure 3, A and B**, PTX, a potent inhibitor of the Gαi class of G proteins, effectively suppressed responses of L-hCXCR6 cells to hSR-PSOX-SEAP in chemotaxis and calcium-mobilization assays as described previously [12]. Chemotaxis but not calcium mobilization was also slightly inhibited by the phosphatidylinositol-3 kinase (PI-3K) inhibitor wortmannin, and the mitogen-activated protein kinase kinase inhibitor PD098059 did not show any significant inhibition of chemotaxis or calcium mobilization. The effects of wortmannin on chemotaxis and calcium mobilization are very similar to those shown in T lymphoblasts stimulated with another chemokine, stromal cell-derived factor 1/CXCL12 [23]. Conversely, the adhesion of L-hCXCR6 cells to immobilized hSR-PSOX-SEAP or COS-hSR-PSOX cells was not inhibited by PTX, wortmannin, or PD098059 (Fig. 3, C and D). We also confirmed that EGTA did not suppress the adhesion of L-hCXCR6 cells to hSR-PSOX-SEAP-coated plates (Fig. 3C). Therefore, the adhesion of CXCR6-expressing cells to SR-PSOX/CXCL16 did not require signaling via PTX-sensitive G proteins or PI-3K downstream of chemokine receptors or calcium-dependent activation of integrins. These data were very similar to those reported for adhesion of CX_3CR1-expressing cells mediated by membrane-anchored FNK [8]. In addition,

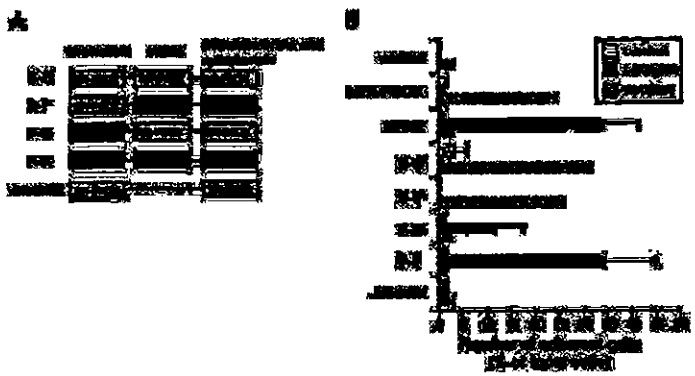

Fig. 4. Domain analyses of hSR-PSOX. (A) Schematic illustration of hSR-PSOX-FNK hybrids. The preparation of cDNA encoding these hybrid molecules was described in Materials and Methods. ΔMucin indicates hSR-PSOX without the mucin domain. (B) Adhesion assay. Adhesion of L-control, L-hCXCR6, and L-hCX$_3$CR1 cells to COS-7 cells transfected with the indicated hSR-PSOX-FNK hybrid was evaluated as in Figure 2. The data shown represent the mean ± SD from at least three independent experiments.

Fig. 5. Effects of metalloproteinase inhibitor GM6001 on expression and adhesion-inducing activity of SR-PSOX/CXCL16. (A) Standard curve for quantification of hSR-PSOX by ELISA. The standard curve was drawn by using hSR-PSOX-SEAP as described in Materials and Methods. The data shown represent the average of the duplicate. (B) Effect of metalloproteinase inhibitor on the release of shSR-PSOX. shSR-PSOX generated in the culture medium of COS-hSR-PSOX cells was quantified by ELISA after cultivation for 24 h with or without the metalloproteinase inhibitor GM6001 (10 μM). COS-control cells showed an undetectable level of shSR-PSOX (data not shown). The data represent the mean ± SD from at least three independent experiments. $P < 0.01$. (C) Effect of metalloproteinase inhibitor on the amount of cell-associated hSR-PSOX. ELISA determined the amounts of cell-associated hSR-PSOX in solubilized COS-hSR-PSOX cells after cultivation for 24 h with or without GM6001 (10 μM). COS-control cells showed an undetectable level of cell-associated hSR-PSOX (data not shown). The data shown represent the mean ± SD from at least three independent experiments. $P < 0.01$. (D) Effect of metalloproteinase inhibitor on the cell-surface expression of hSR-PSOX. Representative flow cytometric data of hSR-PSOX on COS-hSR-PSOX cells were shown after cultivation for 24 h with or without GM6001 (10 μM). The surface expression of hSR-PSOX on COS-hSR-PSOX cells was analyzed by flow cytometry after staining with anti-SR-PSOX mAb 22-19-12 (bold line) or control IgG (dotted line). (E) Adhesion assay for COS-7 cells. The adhesion of L-hCXCR6 cells to COS-hSR-PSOX cells after cultivation for 24 h with or without GM6001 (10 μM) was measured as in Figure 2. $P < 0.05$.

L-hCXCR6 cells were shown to bind not only to the immobilized extracellular domain of SR-PSOX on plastic culture dishes (Fig. 1) but also to the cytoplasmic domain-truncated SR-PSOX expressed on COS-7 cells (data not shown). These results indicate that the cytoplasmic domain of SR-PSOX is not required for adhesion between cells expressing SR-PSOX and those expressing CXCR6, although SR-PSOX has a predictable phosphorylation site in the cytoplasmic domain [12].

Domain analyses of SR-PSOX for adhesion of CXCR6-expressing cells

SR-PSOX/CXCL16 and FNK have two extracellular domains, namely a chemokine domain and a mucin-stalk domain. The chemokine domain of SR-PSOX without the mucin-stalk domain efficiently induced chemotaxis of CXCR6-expressing cells (data not shown). To clarify which domains of SR-PSOX were necessary for the adhesion of CXCR6-expressing cells, we generated SR-PSOX-FNK hybrids by shuffling the chemokine domains and mucin domains of hSR-PSOX and FNK, as described in Materials and Methods (**Fig. 4A**). COS-7 cells were transfected with the expression vectors for these hybrid proteins, and their similar levels of surface expression were confirmed by flow cytometry [11]. L-hCXCR6 cells but not L-hCX$_3$CR1 cells bound to COS-7 cells expressing the hybrid with the chemokine domain of hSR-PSOX and the mucin domain of FNK (Fig. 4B), and L-hCX$_3$CR1 cells but not L-hCXCR6 cells bound to COS-7 cells expressing the hybrid with the chemokine domain of FNK and the mucin domain of hSR-PSOX/CXCL16. It is interesting that COS-7 cells expressing SR-PSOX without its mucin domain had impaired adhesion activity (Fig. 4B), although its cell-surface expression was confirmed by flow cytometry [11]. These results are very similar to those reported for cell adhesion mediated by membrane-anchored FNK [8, 24, 25] and indicate that the specificity for CXCR6 is determined by the chemokine domain of SR-PSOX/CXCL16, and the mucin domain of SR-PSOX/CXCL16 is necessary for the effective presentation of the chemokine domain.

Enhancing effect of metalloproteinase inhibitor on cell adhesion mediated by SR-PSOX/CXCL16

FNK was reported to be prototypically released from the cell surface by the function of metalloproteinase, and the soluble form thus generated functions as a chemoattractant similar to other members of the chemokine family [26, 27]. Given the possibility of a similar processing of the membrane-anchored SR-PSOX/CXCL16, we examined the effect of metalloproteinase inhibitor on the ratio of soluble-to-membrane-bound forms of SR-PSOX/CXCL16. The release of sSR-PSOX from COS-hSR-PSOX cells was clearly inhibited by a metalloproteinase inhibitor GM6001, and cell-surface and cell-associated hSR-PSOX expression was increased by the treatment (**Fig. 5, A–D**). This prompted us to examine the effect of the metalloproteinase inhibitor on SR-PSOX/CXCL16-mediated adhesion activity. As expected from the increased cell-surface expression of SR-PSOX, more L-hCXCR6 cells were found to bind to GM6001-treated COS-hSR-PSOX cells than untreated COS-hSR-PSOX cells (Fig. 5E).

DISCUSSION

As FNK, the first reported transmembrane chemokine, mediates not only chemotaxis but also adhesion in CX_3CR1-expressing cells, SR-PSOX/CXCL16, the second reported transmembrane chemokine, can also be predicted to function as a

cell adhesion molecule for CXCR6-expressing cells. Recently, we reported in brief that immobilized SR-PSOX/CXCL16 induces direct adhesion of CXCR6-expressing plasma cells [28], although we did not examine the mechanism in detail. In the present study, we precisely showed the direct adhesion of CXCR6-expressing cells not only to immobilized SR-PSOX/CXCL16 on plastic culture dish (Fig. 1) but also to SR-PSOX/CXCL16-expressing cells (Fig. 2). In addition, the chemokine domain of SR-PSOX was proven to determine the specificity for CXCR6-expressing cells (Fig. 4). Furthermore, we demonstrated that metalloproteinase regulates the release of sSR-PSOX/CXCL16 from the membrane-anchored form and thus down-regulates the activity of SR-PSOX-expressing cells to bind CXCR6-expressing cells (Fig. 5).

SR-PSOX and CXCR6 regulate the processes of chemotaxis as well as direct adhesion. The Gαi protein blocker, PTX, can inhibit CXCR6-mediated migratory activity, however, by indicating that activation of Gαi protein is necessary for the induction of the chemotactic response. In contrast, adhesion occurs even in the presence of PTX (Fig. 3). These findings are similar to those reported for FNK [8]. Indeed, the adhesion between cells expressing SR-PSOX and those expressing CXCR6 can be induced, independent of the activation of G protein or the activation of integrins.

COS-7 cells expressing SR-PSOX without its mucin domain were shown to have impaired adhesion activity, although COS-7 cells expressing a hybrid with the chemokine domain of hSR-PSOX and the mucin domain of FNK efficiently bind L-hCXCR6 cells (Fig. 4). These results indicate that the chemokine domain of SR-PSOX/CXCL16 only determines specificity for CXCR6, and the mucin domain of SR-PSOX/CXCL16 is necessary for the efficient adhesion. The mucin domain of FNK was also shown to contribute to the efficient adhesion activity of CX_3CR1-expressing cells (Fig. 4B). However, the mucin domain is unlikely to determine the specificity of the cell adhesion directly, as the mucin domain of FNK when substituted for that of SR-PSOX is functional in terms of adhesion activity for CXCR6-expressing cells. Cell adhesion is mediated by direct protein–protein interactions, which may require some distance from the cell surface as discussed previously [8, 24, 25]. Thus, the mucin domain of SR-PSOX/CXCL16 may function as a necessary presenting structure of the chemokine domain, which provides some distance from the cell surface for the chemokine domain to interact with CXCR6 on the surface of target cells.

We have shown the multiple functions of SR-PSOX/CXCL16, which include the scavenger receptor activity, the chemotaxis-inducing activity, and the direct cell-adhesion activity. We therefore suggest that SR-PSOX/CXCL16 plays multifunctional roles in DCs. The soluble form of SR-PSOX/CXCL16 generated by metalloproteinase cleavage recruits CXCR6-expressing, activated T cells and NKT cells via its chemotactic activity in cooperation with other chemokines. Then, the membrane-anchored form of SR-PSOX/CXCL16 on DCs can function as a cell-surface adhesion molecule for CXCR6-expressing T and NKT cells in cooperation with other adhesion molecules. Such adhesion may lead to bidirectional stimulatory signals and may contribute to the formation of docking sites for the activation of antigen-specific, primary and secondary T cell responses. Thus, SR-PSOX/CXCL16 may play a role in DC functions for primary and secondary immune responses. These possibilities are currently under investigation.

ACKNOWLEDGMENTS

This work was supported in part by Grants-in-Aid from the Ministry of Education, Culture, Sports, Science and Technology of the Japanese Government. We thank Drs. K. Sakamaki and K. K. Lee for helpful comments.

REFERENCES

1. Zlotnik, A., Yoshie, O. (2000) Chemokines: a new classification system and their role in immunity. *Immunity* **12**, 121–127.
2. Goda, S., Imai, T., Yoshie, O., Yoneda, O., Inoue, H., Nagano, Y., Okazaki, T., Imai, H., Bloom, E. T., Domae, N., Umehara, H.. (2000) CX3C-chemokine, fractalkine-enhanced adhesion of THP-1 cells to endothelial cells through integrin-dependent and -independent mechanisms. *J. Immunol.* **164**, 4313–4320.
3. Campbell, J. J., Hedrick, J., Zlotnik, A., Siani, M. A., Thompson, D. A., Butcher, E. C. (1998) Chemokines and the arrest of lymphocytes rolling under flow conditions. *Science* **279**, 381–384.
4. Pachynski, R. K., Wu, S. W., Gunn, M. D., Erle, D. J. (1998) Secondary lymphoid-tissue chemokine (SLC) stimulates integrin α 4 β 7-mediated adhesion of lymphocytes to mucosal addressin cell adhesion molecule-1 (MAdCAM-1) under flow. *J. Immunol.* **161**, 952–956.
5. Campbell, J. J., Qin, S., Bacon, K. B., Mackay, C. R., Butcher, E. C. (1996) Biology of chemokine and classical chemoattractant receptors: differential requirements for adhesion-triggering versus chemotactic responses in lymphoid cells. *J. Cell Biol.* **134**, 255–266.
6. Pan, Y., Lloyd, C., Zhou, H., Dolich, S., Deeds, J., Gonzalo, J. A., Vath, J., Gosselin, M., Ma, J., Dussault, B., Woolf, E., Alperin, G., Culpepper, J., Gutierrez-Ramos, J. C., Gearing, D. (1997) Neurotactin, a membrane-anchored chemokine upregulated in brain inflammation. *Nature* **387**, 611–617.
7. Bazan, J. F., Bacon, K. B., Hardiman, G., Wang, W., Soo, K., Rossi, D., Greaves, D. R., Zlotnik, A., Schall, T. J. (1997) A new class of membrane-bound chemokine with a CX3C motif. *Nature* **385**, 640–644.
8. Imai, T., Hieshima, K., Haskell, C., Baba, M., Nagira, M., Nishimura, M., Kakizaki, M., Takagi, S., Nomiyama, H., Schall, T. J., Yoshi, O. (1997) Identification and molecular characterization of fractalkine receptor CX3CR1, which mediates both leukocyte migration and adhesion. *Cell* **91**, 521–530.
9. Fong, A. M., Robinson, L. A., Steeber, D. A., Tedder, T. F., Yoshie, O., Imai, T., Patel, D. D. (1998) Fractalkine and CX3CR1 mediate a novel mechanism of leukocyte capture, firm adhesion, and activation under physiologic flow. *J. Exp. Med.* **188**, 1413–1419.
10. Shimaoka, T., Kume, N., Minami, M., Hayashida, K., Kataoka, H., Kita, T., Yonehara, S. (2000) Molecular cloning of a novel scavenger receptor for oxidized low density lipoprotein, SR-PSOX, on macrophages. *J. Biol. Chem.* **275**, 40663–40666.
11. Shimaoka, T., Nakayama, T., Kume, N., Takahashi, S., Yamaguchi, J., Minami, M., Hayashida, K., Kita, T., Ohsumi, J., Yoshie, O., Yonehara, S. (2003) Cutting edge: SR-PSOX/CXC chemokine ligand 16 mediates bacterial phagocytosis by APCs through its chemokine domain. *J. Immunol.* **171**, 1647–1651.
12. Matloubian, M., David, A., Engel, S., Ryan, J. E., Cyster, J. G. (2000) A transmembrane CXC chemokine is a ligand for HIV-coreceptor Bonzo. *Nat. Immunol.* **1**, 298–304.
13. Wilbanks, A., Zondlo, S. C., Murphy, K., Mak, S., Soler, D., Langdon, P., Andrew, D. P., Wu, L., Briskin, M. (2001) Expression cloning of the STRL33/BONZO/TYMSTRligand reveals elements of CC, CXC, and CX3C chemokines. *J. Immunol.* **166**, 5145–5154.
14. Deng, H. K., Unutmaz, D., KewalRamani, V. N., Littman, D. R. (1997) Expression cloning of new receptors used by simian and human immunodeficiency viruses. *Nature* **388**, 296–300.
15. Liao, F., Alkhatib, G., Peden, K. W., Sharma, G., Berger, E. A., Farber, J. M. (1997) STRL33, a novel chemokine receptor-like protein, functions as a fusion cofactor for both macrophage-tropic and T cell line-tropic HIV-1. *J. Exp. Med.* **185**, 2015–2023.
16. Kim, C. H., Kunkel, E. J., Boisvert, J., Johnston, B., Campbell, J. J., Genovese, M. C., Greenberg, H. B., Butcher, E. C. (2001) Bonzo/CXCR6 expression defines type 1-polarized T-cell subsets with extralymphoid tissue homing potential. *J. Clin. Invest.* **107**, 595–601.
17. Banchereau, J., Steinman, R. M. (1998) Dendritic cells and the control of immunity. *Nature* **392**, 245–252.
18. Guermonprez, P., Valladeau, J., Zitvogel, L., Thery, C., Amigorena, S. (2002) Antigen presentation and T cell stimulation by dendritic cells. *Annu. Rev. Immunol.* **20**, 621–667.
19. Bleijs, D. A., Geijtenbeek, T. B., Figdor, C. G., van Kooyk, Y. (2001) DC-SIGN and LFA-1: a battle for ligand. *Trends Immunol.* **22**, 457–463.
20. Montoya, M. C., Sancho, D., Vicente-Manzanares, M., Sanchez-Madrid, F. (2002) Cell adhesion and polarity during immune interactions. *Immunol. Rev.* **186**, 68–82.
21. Yonehara, S., Ishii, A., Yonehara, M. (1989) A cell-killing monoclonal antibody (anti-Fas) to a cell surface antigen co-downregulated with the receptor of tumor necrosis factor. *J. Exp. Med.* **169**, 1747–1756.
22. Sakamaki, K., Miyajima, I., Kitamura, T., Miyajima, A. (1992) Critical cytoplasmic domains of the common β subunit of the human GM-CSF, IL-3 and IL-5 receptors for growth signal transduction and tyrosine phosphorylation. *EMBO J.* **11**, 3541–3549.
23. Sotsios, Y., Whittaker, G. C., Westwick, J., Ward, S. G. (1999) The CXC chemokine stromal cell-derived factor activates a Gi-coupled phosphoinositide 3-kinase in T lymphocytes. *J. Immunol.* **163**, 5954–5963.
24. Fong, A. M., Erickson, H. P., Zachariah, J. P., Poon, S., Schansberg, N. J., Imai, T., Patel, D. D. (2000) Ultrastructure and function of the fractalkine mucin domain in CX(3)C chemokine domain presentation. *J. Biol. Chem.* **275**, 3781–3786.
25. Haskell, C. A., Cleary, M. D., Charo, I. F. (2000) Unique role of the chemokine domain of fractalkine in cell capture. Kinetics of receptor dissociation correlate with cell adhesion. *J. Biol. Chem.* **275**, 34183–34189.
26. Tsou, C. L., Haskell, C. A., Charo, I. F. (2001) Tumor necrosis factor-α-converting enzyme mediates the inducible cleavage of fractalkine. *J. Biol. Chem.* **276**, 44622–44626.
27. Garton, K. J., Gough, P. J., Blobel, C. P., Murphy, G., Greaves, D. R., Dempsey, P. J., Raines, E. W. (2001) Tumor necrosis factor-α-converting enzyme (ADAM17) mediates the cleavage and shedding of fractalkine (CX3CL1). *J. Biol. Chem.* **276**, 37993–38001.
28. Nakayama, T., Hieshima, K., Izawa, D., Tatsumi, Y., Kanamaru, A., Yoshie, O. (2003) Cutting edge: profile of chemokine receptor expression on human plasma cells accounts for their efficient recruitment to target tissues. *J. Immunol.* **170**, 1136–1140.

THE JOURNAL OF BIOLOGICAL CHEMISTRY
© 2004 by The American Society for Biochemistry and Molecular Biology, Inc.

Vol. 279, No. 14, Issue of April 2, pp. 14201–14208, 2004
Printed in U.S.A.

Type IV Collagen Is Transcriptionally Regulated by Smad1 under Advanced Glycation End Product (AGE) Stimulation*

Received for publication, September 22, 2003, and in revised form, January 15, 2004
Published, JBC Papers in Press, January 19, 2004, DOI 10.1074/jbc.M310427200

Hideharu Abe‡, Takeshi Matsubara§, Noriyuki Iehara¶, Kojiro Nagai§, Toshikazu Takahashi‡, Hidenori Arai§, Toru Kita‖, Toshio Doi‡**

From the ‡Department of Clinical Biology and Medicine, Course of Biological Medicine, University of Tokushima, Tokushima 770-8503, Japan and the Departments of §Geriatric Medicine, ¶Artificial Kidney, and ‖Cardiovascular Medicine, Kyoto University Graduate School of Medicine, Kyoto 606-8507, Japan

Prolonged exposure to hyperglycemia is now recognized as the most significant causal factor of diabetic complications. Excessive advanced glycation end products (AGEs) as a result of hyperglycemia in tissues or in the circulation may critically affect the progression of diabetic nephropathy. In diabetic nephropathy, glomerulosclerosis is a typical pathologic feature characterized by the increase of the extracellular matrix (ECM). We have reported previously that α1 type IV collagen (Col4) is one of the major components of ECM, which is up-regulated by AGEs, and that the overexpression of Col4 is transcriptionally regulated by an unknown transcription factor binding to the promoter. Here we identified this protein as Smad1 by yeast one-hybrid screening. Using chromatin immunoprecipitation and reporter assay, we observed that Smad1 directly regulated transcription for Col4 through the binding of Smad1 to the promoter of Col4. Smad1 was significantly induced along with Col4 in AGE-treated mesangial cells. Moreover, suppression of Smad1 by antisense morpholino resulted in a decrease of AGE-induced Col4 overproduction. To elucidate the interaction between transforming growth factor-β and Smad1, we investigated whether activin receptor-liked kinase1 (ALK1) was involved in this regulation. AGE stimulation significantly increased the expression of the ALK1 mRNA in mesangial cells. We also demonstrated that Smad1 and ALK1 were highly expressed in human diabetic nephropathy. These results suggest that the modulation of Smad1 expression is responsible for the initiation and progression of diabetic nephropathy and that blocking Smad1 signaling may be beneficial in preventing diabetic nephropathy and other various diabetic complications.

Diabetic nephropathy is the leading cause of end-stage renal disease and a major contributing cause of morbidity and mortality in patients with diabetes throughout the world. There is accumulating evidence that AGEs[1] have a pathogenic role in the development of diabetic glomerulosclerosis. Excessive AGEs produced as the result of hyperglycemia are known to stimulate the production of the ECM and inhibits its degradation. AGEs have a wide range of chemical, cellular, and tissue effects through changes in charge, solubility, and conformation that characterize molecular senescence. AGEs induce a variety of cellular events in vascular cells and other cells, possibly through several functional AGE receptors, thereby modulating the disease processes (1–5). AGEs have recently been accepted as having an important role, not only in diabetic complications but also in aging and old age-related diseases, including atherosclerosis (6, 7). Moreover, a truncated, soluble form of the receptor for AGEs was reported to suppress the development of accelerated diabetic atherosclerosis (8). Exposure of cultured mesangial cells to AGEs results in a receptor-mediated up-regulation of mRNA and protein secretion of Col4 (5, 9). However, there is little information regarding the mechanisms that underlie this regulation.

It was recently shown that TGF-β plays an important role in the AGE response of the glomeruli (10). Transgenic mice overexpressing TGF-β develop severe glomerulosclerosis (11). Thus, TGF-β is a central mediator of the sclerosing process in diabetic nephropathy. Members of the TGF-β superfamily bind to two different types of serine/threonine kinase receptors, termed type I and type II receptors (12). Type II receptors activate type I receptors, and signals are mediated through the type I receptors. Ligand-specific Smads are direct substrates of type I receptor kinases. Thus, the specificity of the signals is determined by type I receptors. ALK1 is one of the type I receptor members for TGF-β family proteins and has been linked to the inherited multisystemic vascular disorder, hereditary hemorrhagic telangiectasia 2 (HHT2). Although ALK1 has been known as an orphan receptor, recent reports show that ALK1 transduces TGF-β signals via Smad1 (13, 14).

Morphologically, the development of diabetic nephropathy is characterized by progressive thickening of the glomerular basement membrane (GBM) and, by expansion, of the mesangial ECM. During the process of glomerular injuries, mesangial cells can overproduce Col4 and secrete type I collagen (Col1) and osteopontin (OPN), which are not normally present in the mesangial matrix (15). In particular, Col4 is a major component of the thickened GBM and expanded ECM, but no molecules that directly regulate the Col4 expression have been found. The 130-bp bidirectional promoter of Col4 contains a large stem-loop structure (CIV), which has been shown to interact with several DNA-binding proteins (16). Using a gel mobility shift assay, we reported previously that an unknown protein binding to the CIV site directly regulates Col4 expression only when exposed to AGEs (9). To identify the protein that binds to the CIV site in the promoter region of the mouse *Col4* gene, we constructed a cDNA library from mouse mesangial cells treated with AGEs. In this study, we used a yeast one-hybrid system to isolate a clone that encodes a specific transcription factor from the library, and we identified the clone as the cDNA that encodes Smad1.

* This work was supported by Grant-in Aid from the Ministry of Education, Science, Sports and Culture of Japan. The costs of publication of this article were defrayed in part by the payment of page charges. This article must therefore be hereby marked "*advertisement*" in accordance with 18 U.S.C. Section 1734 solely to indicate this fact.

** To whom correspondence should be addressed. Tel.: 81-88-633-7184; Fax: 81-88-633-9245; E-mail: doi@clin.med.tokushima-u.ac.jp.

[1] The abbreviations used are: AGE, advanced glycation end product; ALK1, activin receptor-liked kinase1; AS, antisense; BMP, bone morphogenetic protein; BSA, bovine serum albumin; Col1, type I collagen; Col4, α1 type IV collagen; ECM, extracellular matrix; GBM, glomerular basement membrane; OPN, osteopontin; pSmad1, phosphorylated Smad1; TGF, transforming growth factor

EXPERIMENTAL PROCEDURES

Cell Culture—A glomerular mesangial cell line was established from glomeruli isolated from normal, 4-week-old mice (C57BL/6JxSJL/J) and was identified according to the method described previously (17). The mesangial cells were maintained in B medium (a 3:1 mixture of minimal essential medium/F12 modified with trace elements) supplemented with 1 mM glutamine, penicillin at 100 units/ml, streptomycin at 100 mg/ml, and 20% fetal calf serum. The cultured cells fulfilled the criteria generally accepted for glomerular mesangial cells previously (17). AGE or bovine serum albumin (BSA) exposure was carried out as described previously (9).

Preparation of AGEs—AGE-BSA was prepared by incubating BSA in phosphate-buffered saline (10 mM, pH 7.4) with 50 mM glucose 6-phosphate for 8 weeks at 37 °C as described previously (5). Unmodified BSA was incubated under the same conditions without glucose 6-phosphate as control. Protein concentrations were measured by the Bradford method. All AGE-protein specific fluorescence intensities were measured at a protein concentration of 1 mg/ml. AGE-BSA and control BSA contained 61.8 and 8.31 units of AGE per milligram of protein, respectively.

cDNA Library Construction and Yeast One-hybrid Screening—We prepared cDNA from mouse mesangial cells exposed to AGEs and inserted it into the pGAD10 vector. Yeast one-hybrid screening was carried out according to the MATCHMAKER one-hybrid protocol (Clontech). Briefly, tandem repeats of the 27-bp sequence (5′-TTCCTCCCCTTGGAGGAGCGCCGCCCG-3′; CIV-1) from the mouse type IV collagen gene were ligated into the yeast integration and reporter vector pHISi or pLacZi to generate pHISi-CIV-1 or pLacZi-CIV-1, respectively (18). Each pHISi-CIV-1 and pLacZi-CIV-1 reporter construct was linearized and integrated into the genome of competent yeast YM4271, sequentially. The resulting yeast cells with the integrated pHISi-CIV-1 and pLacZi-CIV-1 were used for one-hybrid screening with the AGE-stimulated mouse mesangial cell library. Positive colonies were selected on synthetic dropout −His/−Leu plates with 45 mM 3-amino-1, 2, 4-triazole (3-AT). To exclude false positive clones, we performed a β-galactosidase filter lift assay according to manufacturer's instructions (Clontech). Plasmids were rescued from selected blue yeast colonies and retransformed into *E. coli* DH5α.

Chromatin Immunoprecipitation Assay—Chromatin immunoprecipitation assays were performed essentially as described previously by Luo *et al.* (19). We used anti-Smad1 antibody, anti-Smad4 antibody (Santa Cruz Biotechnology), or normal control IgG at 4 °C overnight. PCR was performed with primers to amplify the region containing the CIV-1 motif. The 5′-primer was 5′-GGAGCTCCCCAATTTGTTG-3′, and the 3′ primer was 5′-CAGCCTCCGCCTCTTACC-3′. The resulting product was ~100 bp by agarose gel electrophoresis.

Reporter Assay—1.3×10^6 COS7 cells in 10% fetal bovine serum/Dulbecco's modified Eagle's medium were seeded into 6-well plates. Eight hours later, the cells were transfected with 750 ng of CIV-1-LacZ reporter construct along with either 750 ng of vector encoding wild type Smad1 or the mock vector and 75 ng of CMV-LUC (Firefly luciferase under the control of cytomegalovirus promoter) as an internal control. Transfection was performed with FuGENE6 transfection reagent (Roche Molecular Biochemicals) according to the manufacturer's instructions. Forty-eight hours later, the cells were harvested in reporter lysis buffer, and β-galactosidase and luciferase activities were then measured using the Luminescent β-galactosidase reporter system (BD Biosciences) and the luciferase reporter assay system from Promega. β-galactosidase results were normalized for luciferase activity.

RNase Protection Assay—Total RNA was isolated from mesangial cells using the TRIsol reagent (Invitrogen), and an RNase protection assay was performed as described previously (20). Briefly, the RNA probes were prepared by linearizing the PvuII fragment of Col4 from p1234, the ApaI fragment of Col1 from pGM101, and the EcoRI fragment of glyceraldehyde-3-phosphate dehydrogenase (GAPDH) from pMGAP1. In addition, mouse riboprobe for Smad1 (5′-GCAAGTTTTTGCGATGTGAGA-3′ and 5′-GCATCTTCCAGAGTGAAGCC-3′), ALK1 (5′-GAGTGTGGCGGTCAAGATTT-3′ and 5′-GGAGCCGTGTTCATGGTAGT-3′), and osteopontin (5′-TGCACCCAGATCCTATAGCC-3′ and 5′-CCTCAGTCCATAAGCCAAGC-3′) were amplified by reverse transcription PCR. The PCR fragments were sequenced to confirm that they were the respective cDNAs and then were cloned into a pGEM-T plasmid. After digesting the plasmid with SacI, an antisense riboprobe was synthesized *in vitro* using T7 RNA polymerase. The RNA probes and the test RNA were hybridized overnight at 45 °C. RNase A (40 μg/ml) and RNase T1 (2 μg/ml) were added to each tube, and the tubes were incubated for 1 h at 30 °C. The RNase resistant fragments were analyzed by 5% polyacrylamide/8 M urea gel electrophoresis and autoradiography. The protected bands for each RNA probe had the same size as the coding sequence for the specific mRNA, thus providing evidence for their specificity, and were evaluated by densitometric analysis.

Western Blotting—Cultured mesangial cells were treated with AGEs or BSA for 72 h. Cells were harvested in sample buffer, resolved by SDS-polyacrylamide gel electrophoresis, transferred to nitro-cellulose membrane, subjected to Western blot using a 1:500 dilution of antibody for Smad1 and pSmad1 (Santa Cruz Biotechnology), and detected using an enhanced chemiluminescence detection system (Invitrogen).

Immunostaining of Cultured Cells—Cultured cells were fixed in 4% paraformaldehyde. The antibodies used were anti-Smad1 antibody, 1:100 (Santa Cruz Biotechnology), and anti-pSmad1, 1:100 (Calbiochem). An appropriate fluorescein isothiocyanate-conjugated secondary antibody was used for visualization, and imaging was done using a confocal laser microscope and a fluorescent microscope (Olympus).

Smad1 Morpholino Antisense Oligonucleotide—The antisense oligonucleotide used was a 25-nucleotide morpholino oligo (Genetools LLC) with the base composition 5′-CAAGCTGGTCACATTCATAGCGGCT-3′. A standard morpholino oligo with the base composition 5′-CAtGCTcGTCACATTCAaAGCcGCT-3′ (points of mismatch are shown by small letters) was used as a control. Microinjection of *in vitro* transcribed RNA was performed as described previously (21).

Histology—Histopathological studies were performed on human tissues. This study was in accordance with the Declaration of Helsinki, and we obtained approval from the institutional review board. All patients gave their informed written consent. Diabetic kidney specimens ($n = 5$) were obtained from renal biopsies. Control human tissue sections were obtained from normal renal cortex harvested from kidneys removed for renal malignancy. Tissues for analysis were sampled from the pole opposite the tumor. Cryopreserved kidney tissues were cut in 5-μm-thick sections and fixed in acetone for 5 min. Endogenous peroxidase activity was quenched by a 20-min incubation in the dark with 1% H_2O_2 in methanol. To eliminate nonspecific staining, sections were incubated with the appropriate preimmune serum for 20 min at room temperature, followed by incubation with primary antibodies anti-Smad1 (Santa Cruz Biotechnology) and anti-ALK1 (R&D Systems) antibodies.

RESULTS

Smad1 Is Identified as a Binding Protein to Col4—To identify the protein binds to the CIV site in the promoter region of the mouse *Col4* gene, we constructed a cDNA library from mouse mesangial cells treated with AGEs. We then used a yeast one-hybrid system to isolate a clone that encodes a specific transcription factor from the library. We identified this clone as the cDNA that encodes Smad1. Smad1 is well known for transducing the bone morphogenetic protein (BMP) signal (22) and is essentially important in the development of kidney (23). However, the expression of Smad1 is not detected in glomeruli in adult mouse (24).

To confirm the binding of Smad1 to the *Col4* promoter *in vivo*, we performed a chromatin immunoprecipitation assay. Precipitated DNA was purified, and the promoter of the *Col4* gene was detected by PCR. The anti-Smad1 antibody precipitated chromatin containing the CIV-1 site from cells stimulated with AGEs (Fig. 1). In contrast, considerably less binding was observed in BSA-exposed cells. We also detected Smad4 on the CIV-1 site (Fig. 1). These observations suggest that Smad1 and Smad4 can target the CIV motif in mesangial cells, especially when exposed to AGEs.

Smad1 Transcriptionally Regulates Col4 Expression—Next, we examined the transcriptional activity of the *Col4* gene by a reporter assay. We constructed a vector by fusing the *CIV-1* promoter in front of the LacZ reporter and then cotransfected

FIG. 1. **Binding of Smad1 to *Col4* promoter.** Chromatin immunoprecipitation was carried out with mesangial cells under treatment with AGEs (*A*) or BSA (*B*) using the indicated antibodies. PCR was performed using primers for the CIV-1 motif. After sonication, DNA from 10% of each sample was saved as input fraction (*Input*). One of three independent experiments is shown.

with a wild-type Smad1 vector in COS7 cells. First, we confirmed the expression of Smad1 by Western blot analysis (Fig. 2*a*). Phosphorylated Smad1 (pSmad1) was detected in cell lysates that had been tranfected with wild-type Smad1 vector. Cotransfection of the wild-type Smad1 resulted in an 18-fold increase in a relative β-galactosidase activity of Col4 compared with that of the vector alone (Fig. 2*b*, *mock*). The *CIV-1* promoter has a GC-rich sequence in its 3′ end, which has been identified as a binding site for Smad1 (25). We then constructed two mutant reporter plasmids, the deletion mutant of GC rich in CIV-1 (5′-TTCCTCCCCTTGGAGGA-3′; Mut1) and the trinucleotide substitution mutant of GC rich motif in CIV-1 (5′-TTCCTCCCCTTGGAGGAGCaCtGtCCG-3′; Mut2) (points of mutation are shown by small, underlined letters). The promoter activities of Mut1 and Mut2 were reduced to 4.9- and 4.3-fold increase, respectively (data not shown). β-galactosidase activity was normalized to luciferase activity and standardized as fold changes relative to cells cotransfected with the mock vector. In contrast, mock had no effect on the β-galactosidase activity in cotransfected cells. These results suggest that Smad1 is significantly involved in the induction of *Col4* gene transcription.

Activation and Translocation of Smad1 under AGE Exposure—To determine whether Smad1 is transcriptionally upregulated by AGEs, we examined the expression of Smad1 in mesangial cells with or without AGEs stimulation. The levels of Smad1 mRNA were proportionally increased in a time-dependent manner (Fig. 3*a*). Similarly, the levels of *Col4* mRNA increased in parallel with the up-regulation of Smad1 transcripts. After BSA treatment, however, no change in the mRNA expression of *Smad1* or *Col4* was detected. Smad1 is well known to be phosphorylated and translocated into the nucleus, where it participates in the transcriptional regulation of target genes (22, 26). Therefore, we next examined the issue of whether the phosphorylation and translocation of Smad1 is affected by AGE treatment in mesangial cells (Fig. 3*b*). Consistent with the RNase protection assay, Smad1 and pSmad1 were distributed throughout mesangial cells with a preferential cytoplasmic localization after a 72 h-incubation in the presence of AGEs. Furthermore, the nuclear accumulation of Smad1 and pSmad1 in response to AGEs was observed in the cells 120 h after AGE stimulation, whereas BSA treatment led to little expression of Smad1 and pSmad1. The cells were counterstained with DAPI, and the nuclei were identified (data not shown). Similarly, both the Smad1 and pSmad1 proteins were detected in extracts from AGE-treated, but not BSA-treated, cells (Fig. 3*c*). These findings indicate that the regulation of Col4 is correlated with the expression of Smad1 under AGE exposure.

The Blocking of Smad1 Attenuates ECM Protein Overproduction—To examine the importance of the Smad1 signaling pathway for the AGE-induced overexpression of Col4, we selectively inhibited this pathway by the antisense (AS) gene. The AGE-

FIG. 2. **Effects of Smad1 on Col4 transcriptional activity.** *a*, cells were cotransfected with CIV-1-lacZ reporter plasmid and with either the vector encoding wild-type Smad1 (*Smad1-Wt*) or the vector alone (*Mock*), along with CMV-LUC as an internal control. Whole cell lysates were analyzed by Western blot with the anti-Smad1 and anti-pSmad1 antibody. One of three independent experiments is shown. *b*, after 48 h, cells were lysed, and β-galactosidase (*β-gal*) and luciferase (*Luc*) activities were measured. Values are the averages of triplicate determinations ±S.D.

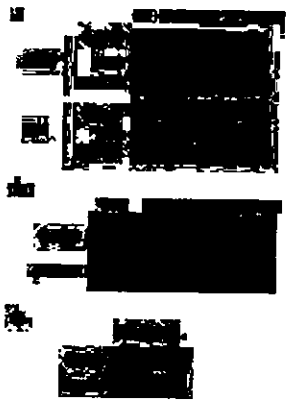

FIG. 3. **Exposure to AGEs causes dynamic changes in Smad1 expression.** *a*, RNase protection assay analysis of *Smad1* and *Col4* mRNA expression in total RNA lysates from mesangial cells treated with AGEs or BSA for the indicated time periods. Chronic stimulation of AGEs promotes *Smad1* continuous expression, paralleled with expression of *Col4*. One of three independent experiments is shown. Glyceraldehyde-3-phosphate dehydrogenase (*GAPDH*) was used as an internal control. *b*, immunofluorescence of mesangial cells after 72 or 120 h of treatment with AGEs or BSA. Data from one of three representative experiments is shown. *c*, Smad1 and pSmad1 were monitored by Western blot in response to a 72-h treatment with AGEs or BSA. One of three independent experiments is shown.

mediated induction of Smad1 was completely abolished in the presence of AS, but not in the presence of control oligos (4-mismatch) (Fig. 4, *a* and *b*). The overexpression of Col4 was strongly attenuated, consistent with the inhibition of Smad1. Similarly, both *Col1* and *OPN* mRNA levels were significantly

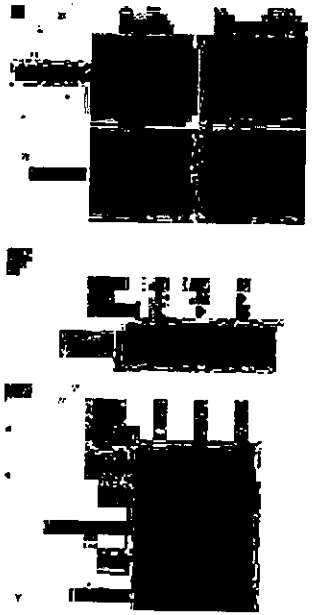

FIG. 4. **Effects of antisense oligo specific for Smad1 in mesangial cells.** *a*, immunofluorescence analysis of the antisense-treated mesangial cells, using the anti-Smad1 antibody (*green*) merged with DNA stained by DAPI (*blue*). After 72 h of incubation with AGEs, mesangial cells were incubated for 16 h in medium containing AS-Smad1 or 4-mismatch (*Control*). Data from one of three representative experiments is shown. *b*, Western blot analysis of Smad1 protein expression in mesangial cells treated with AGEs after transfection of AS or control. One of three independent experiments is shown. *c*, AS-Smad1 blocks the up-regulated mRNA levels of *Col4*, *osteopontin*, and *Col1* induced by AGEs treatment on mesangial cells. One of three independent experiments is shown.

decreased (Fig. 4*c*). Smad1 mismatch morpholino oligos (control) had no effect on the expression of these genes. These data indicate that Smad1 plays a critical role in the control of Col4 expression.

Smad1 and ALK1 Expression in Diabetic Conditions—To further elucidate the mechanism of Smad1 expression after AGE treatment, we investigated the expression of ALK1 in mesangial cells. ALK1 is a type I receptor for TGF-β family proteins and, specifically, phosphorylates Smad1 and Smad5. We were able to detect the significant increase in ALK1 mRNA expression in AGE-treated mesangial cells using an RNase protection assay (Fig. 5). In addition, at 10 μg/ml the TGF-β-neutralizing antibody significantly attenuated the up-regulated mRNA levels of *ALK1* and *Smad1* under AGE stimulation (data not shown). Furthermore, we examined whether high glucose exposure affected the expression of *ALK1*, *Smad1*, or *Col4*. In this condition, mRNA levels of these genes were increased, but they were weak and transient, compared with AGEs exposure (data not shown).

Finally, we investigated the glomerular expression of Smad1 and ALK1 in human diabetic nephropathy. We carried out indirect immunohistochemistry on renal biopsies (diabetic nephropathy) and on normal kidney tissue. Glomerular im-

FIG. 5. **Regulation of ALK1 mRNA expression by AGEs.** After treatment with AGEs, the specific mRNAs were determined by using the RNase protection assay. The amount of total RNA loaded (1 μg/lane) was checked by hybridization with a glyceraldehyde-3-phosphate dehydrogenase (*GAPDH*) probe. The data are representative of three independent experiments.

munoreactivity for Smad1 and ALK1 was correlated with the severity of sclerotic lesions in diabetic renal glomeruli; the immunoreactive signal was nearly absent in normal glomeruli (Fig. 6). These histological observations suggest that the ALK1/Smad1 signaling pathway is linked to the ECM expansion.

DISCUSSION

Changes in GBM structure occur very earlier in diabetic nephropathy, even before microalbuminuria is apparent. Although Col4 is the principal component of the GBM, the cellular and molecular mechanisms involved in the up-regulation of Col4 in diabetic conditions are, as yet, poorly understood. We have reported previously that an unknown protein binds to the Col4 promoter under AGE exposure (9). Here, we identified the protein as Smad1 using a yeast one-hybrid system. It is generally acknowledged that Smad1 transduces BMP signals, inducing formation of bone and cartilage (22). Moreover, signaling by Smad1 is modulated by various other proteins such as signal transducers and activators of transcription 3 (STAT3) (27) and Smurf1 (28), allowing the TGF-β superfumily ligands to elicit diverse effects on target cells. Recently, mesangial cells have been shown to produce TGF-β when exposed to AGEs (29). We observed that chronic exposure of AGEs, inducing the sustained increase in *Smad1* gene activation and expression, leads to Col4 overproduction, suggesting that Smad1 is a critical modulator in diabetic conditions.

Targeted gene disruption of the *Smad1* gene in mice results in embryonic lethality, suggesting that Smad1 plays critical roles in early embryogeneis (30). However, because of the early embryonic lethality, not much is known about the role of Smad1 *in vivo*, particularly in the adult. A recent study has shown that Smad1 is absent in renal glomeruli in normal adult mouse (24). We show for the first time that AGEs induce the expression of Smad1 in adult mouse glomeruli. Therefore, Smad1 may be the earliest indicator of renal dysfunction.

Development of diabetic kidney disease in diabetic patients is a huge clinical problem associated with increased morbidity and mortality. It is also clear that the current therapy, optimal glycemic control, can slow (1, 2) but not prevent the development or progression of diabetic nephropathy in most patients. Previous studies have shown that TGF-β is a key mediator of ECM accumulation in experimental and human kidney disease, leading to progressive glomerular scarring and renal failure (10, 11). Therapeutic approaches to down-regulate TGF-β signaling under diabetic conditions provide one strategy for inhibiting the progression of diabetic nephropathy. For example, the use of the endogenous proteoglycan decorin (natural inhibitor of TGF-β) (31) and the use of a neutralizing TGF-β antibody (32) have been shown to prevent the development of diabetic glomerulosclerosis. However, prolonged inhibition of TGF-β may lead to unwanted adverse effects, because TGF-β has anti-proliferative effect in some cancers and, in one report, Smad3-deficient animals found metastatic colon tumors (33). Therefore, inhibitors for specific responses of TGF-β will lead to

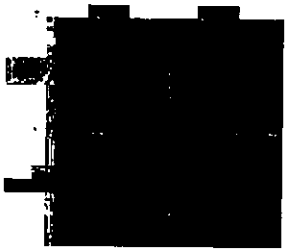

FIG. 6. **Detection of Smad1 and ALK1 in human diabetic kidney.** Immunohistochemical staining of glomeruli from kidneys of diabetic (*DM*; $n = 5$) or non-diabetic (*non-DM*; $n = 3$) patients stained with anti-Smad1 and anti-ALK1 antibodies. Glomerular positivity of Smad1 and ALK1 was prominently detectable in diabetic patients but not detectable in non-diabetic patients. All sections were counterstained with hematoxylin. Original magnification for all was ×400.

a novel therapeutic approach. We have demonstrated here that the morpholic antisense oligo specific for Smad1 strongly attenuated the overproduction of Col4 induced by AGEs. Similarly, Col1 and OPN mRNA expressions were partially inhibited. It is reported that Smad1 dissociates the repressor Hoxc-8 from the *OPN* promoter, thereby inducing *OPN* transcription (34). Thus, Smad1 may be a novel therapeutic target in diabetic complications and be useful in combination with the current therapy.

TGF-β evokes its biological effects by signaling through two different types of serine/threonine kinase receptors. Type II receptor activates type I receptors, which transduce various signals via the Smads (22, 26). Recent reports demonstrated that ALK1 has been thought of as a BMP signal transducer, mediating signals from TGF-β via Smad1 (13, 14). Therefore, we investigated the expression of ALK1 in mouse mesangial cells and human kidney tissues. We have also shown that ALK1 and Smad1 are expressed in renal glomeruli, corresponding to the progression of diabetic conditions. These results lead not only to a better understanding of the mechanisms responsible for the initiation and progression of diabetic conditions but also to the development of novel therapeutic strategies for the treatment of diabetic complications in various organs by suppressing the pathologically activated production of collagen. Both Smad1 and ALK1 are nearly absent in normal mesangial cells. In this study, we first demonstrated that ALK1 as well as Smad1 participate in the development of diabetic change in kidney, suggesting that ALK1 acts upstream of the excessive production of Col4.

AGEs are known to induce a variety of cellular events in vascular cells and other cells, possibly through the functional several AGEs receptors, thereby modulating the disease processes. AGEs have been recently accepted as having an important role, not only in diabetic complications but also in aging and old age-related diseases, including atherosclerosis (6, 7). Col4 is also a major component of the vascular basement membrane that lies beneath the endothelium, surrounds medial smooth muscle cells, and undergoes significant nonenzymatic glycosylation (glycation). Glycation leads ultimately to increased cross-linking of collagen, resulting in increased arterial stiffness (35). We report here that AGE-induced Col4 overproduction is mediated by Smad1 signaling. Recent reports show that Smad1 is expressed in endothelial cells of some blood vessels and is at the site of vasculogenesis in the developing yolk sac during blood island formation (36). Furthermore, ALK1 is highly expressed in vascular endothelial cells (22, 37) and may be essential for vascular maturation and stabilization (38, 39). Inactivating mutations of ALK1 result in human hereditary hemorrhagic telangiectasia 2, also known as Osler-Rendu-Weber syndrome (40). In addition, recent evidence indicates that Smad1 transcriptionally regulates the osteopontin gene (33), which is a key factor of the progression of renal injuries and atherosclerosis. Accordingly, we speculate that the ALK1/Smad1 signaling may mediate the development of atherosclerosis, both in diabetic patients and in the aged, by inducing an overproduction of ECM. Because diabetic renal disease in the human is a process that occurs slowly over many years, it is likely that a very detailed evaluation of this phenomenon will be required to determine the interaction of Smad1 and ALK1 in this condition. Further work is in progress to clarify the role of ALK1/Smad1 in diabetic kidney using animal models.

Acknowledgments—We thank Dr. K. Miyazono (The University of Tokyo, Japan) for providing a plasmid encoding Smad1 and Dr. Y. Takishita (Tokushima Prefectural Central Hospital, Japan) for his assistance with histological analysis. We also thank the members of our laboratory for discussions.

REFERENCES

1. The Diabetes Control and Complications Trial Research Group (1993) *N. Engl. J. Med.* **329**, 977–986
2. United Kingdom Prospective Diabetes Study (UKPDS) Group (1998) *Lancet* **352**, 837–853
3. Vlassara, H., Striker, L. J., Teichberg, S., Fuh, H., Li, Y. M., and Steffes, M. (1994) *Proc. Natl. Acad. Sci. U. S. A.* **91**, 11704–11708
4. Brownlee, M., Cerami, A., and Vlassara, H. (1988) *N. Engl. J. Med.* **318**, 1315–1321
5. Doi, T., Vlassara, H., Kirstein, M., Yamada, Y., Striker, G. E., and Striker, L. J. (1992) *Proc. Natl. Acad. Sci. U. S. A.* **89**, 2873–2877
6. Vlassara, H., Fuh, H., Makita, Z., Krungkrai, S., Cerami, A., and Bucala, R. (1992) *Proc. Natl. Acad. Sci. U. S. A.* **89**, 12043–12047
7. Huijberts, M. S., Wolffenbuttel, B. H., Boudier, H. A., Crijns, F. R., Kruseman, A. C., Poitevin, P., and Levy, B. I. (1993) *J. Clin. Investig.* **92**, 1407–1411
8. Park, L., Raman, K. G., Lee, K. J., Lu, Y., Ferran, L. J., Jr., Chow, W. S., Stern, D., and Schmidt, A. M. (1998) *Nat. Med.* **4**, 1025–1031
9. Iehara, N., Takeoka, H., Yamada, Y., Kita, T., and Doi, T. (1996) *Kidney Int.* **50**, 1166–1172
10. Yang, C. W., Vlassara, H., Peten, E. P., He, C. J., Striker, G. E., and Striker, L. J. (1994) *Proc. Natl. Acad. Sci. U. S. A.* **91**, 9436–9440
11. Sanderson, N., Factor, V., Nagy, P., Kopp, J., Kondaiah, P., Wakefield, L., Roberts, A. B., Sporn, M. B., and Thorgeirsson, S. S. (1995) *Proc. Natl. Acad. Sci. U. S. A.* **92**, 2572–2576
12. ten Dijke, P., Miyazono, K., and Heldin, C. H. (1996) *Curr. Opin. Cell Biol.* **8**, 139–145
13. Oh, S. P., Seki, T., Goss, K. A., Imamura, T., Yi, Y., Donahoe, P. K., Li, L., Miyazono, K., ten Dijke, P., Kim, S., and Li, E. (2000) *Proc. Natl. Acad. Sci. U. S. A.* **97**, 2626–2631
14. Chen, Y. G., and Massague, J. (1999) *J. Biol. Chem.* **274**, 3672–3677
15. Ploeg, J., Johnson, R. J., Gordon, K., Iida, H., Pritzl, P., Yoshimura, A., Campbell, C., Alpers, C. E., and Couser, W. G. (1991) *Kidney Int.* **40**, 477–488
16. Bruggeman, L. A., Burbelo, P. D., Yamada, Y., and Klotman, P. E. (1992) *Oncogene* **7**, 1497–1502
17. Davies, M. (1994) *Kidney Int.* **45**, 320–327
18. Burbelo, P. D., Utani, A., Pan, Z. Q., and Yamada, Y. (1993) *Proc. Natl. Acad. Sci. U. S. A.* **90**, 11543–11547
19. Lan, R. X., Postigo, A. A., and Dean, D. C. (1998) *Cell* **92**, 463–473
20. Abe, H., Iehara, N., Utsumoniya, K., Kita, T., and Doi, T. (1999) *J. Biol. Chem.* **274**, 20874–20878
21. Ahn, D. G., Kourakis, M. J., Rohde, L. A., Silver, L. M., and Ho, R. K. (2002) *Nature* **417**, 754–758
22. Massague, J., and Wotton, D. (2000) *EMBO J.* **19**, 1745–1754
23. Roelen, B. A., van Rooijen, M. A., and Mummery, C. L. (1997) *Dev. Dyn.* **209**, 418–430
24. Huang, S., Flanders, K. C., and Roberts, A. B. (2000) *Gene* **258**, 43–53
25. Kusanagi, K., Inoue, H., Ishidou, Y., Mishima, H. K., Kawabata, M., and Miyazono, K. (2000) *Mol. Biol. Cell* **11**, 555–565
26. Heldin, C. H., Miyazono, K., and ten Dijke, P. (1997) *Nature* **390**, 465–471
27. Nakashima, K., Yanagisawa, M., Arakawa, H., Kimura, N., Hisatsune, T., Kawabata, M., Miyazono, K., and Taga, T. (1999) *Science* **284**, 479–482
28. Zhu, H., Kavsak, P., Abdollah, S., Wrana, J. L., and Thomsen, G. H. (1999) *Nature* **400**, 687–693
29. Throckmorton, D. C., Brogden, A. P., Min, B., Rasmussen, H., and Kashgarian, M. (1995) *Kidney Int.* **48**, 111–117
30. Tremblay, K. D., Dunn, N. R., and Robertson, E. J. (2001) *Development* **128**, 3609–3621
31. Isaka, Y., Brees, D. K., Ikegaya, K., Kaneda, Y., Imai, E., Noble, N. A., and Border, W. A. (1996) *Nat. Med.* **2**, 418–423
32. Chen, S., Carmen, Iglesias-de la Cruz, M., Jim, B., Hong, S. W., Isono, M., and Ziyadeh, F. N. (2003) *Biochem. Biophys. Res. Commun.* **300**, 16–22
33. Zhu, Y., Richardson, J. A., Parada, L. F., and Graff, J. M. (1998) *Cell* **94**, 703–714
34. Shi, X., Yang, X., Chen, D., Chang, Z., and Cao, X. (1999) *J. Biol. Chem.* **274**, 13711–13717
35. Chappey, O., Dosquet, C., Wautier, M. P., and Wautier, J. L. (1997) *Eur. J. Clin. Investig.* **27**, 97–106
36. Dick, A., Risau, W., and Drexler, H. (1996) *Dev. Dyn.* **211**, 293–305
37. Attisano, L., Carcamo, J., Ventura, F., Weis, F. M., Massague, J., and Wrana, J. L. (1993) *Cell* **75**, 671–680
38. Urness, L. D., Sorensen, L. K., and Li, D. Y. (2000) *Nat. Genet.* **26**, 328–331
39. Larsson, J., Goumans, M. J., Sjostrand, L. J., van Rooijen, M. A., Ward, D., Leveen, P., Xu, X., ten Dijke, P., Mummery, C. L., and Karlsson, S. (2001) *EMBO J.* **20**, 1663–1673
40. Johnson, D. W., Berg, J. N., Baldwin, M. A., Gallione, C. J., Marondel, I., Yoon, S. J., Stenzel, T. T., Speer, M., Pericak-Vance, M. A., Diamond, A., Guttmacher, A. E., Jackson, C. E., Attisano, L., Kucherlapati, R., Porteous, M. E., and Marchuk, D. A. (1996) *Nat. Genet.* **13**, 189–195

THE JOURNAL OF BIOLOGICAL CHEMISTRY
© 2004 by The American Society for Biochemistry and Molecular Biology, Inc.

Vol. 279, No. 19, Issue of May 7, pp. 19816–19823, 2004
Printed in U.S.A.

Advanced Glycation End Products Increase Collagen-specific Chaperone Protein in Mouse Diabetic Nephropathy*

Received for publication, September 22, 2003, and in revised form, February 24, 2004
Published, JBC Papers in Press, March 5, 2004, DOI 10.1074/jbc.M310428200

Seiji Ohashi‡, Hideharu Abe‡, Toshikazu Takahashi‡, Yasuhiko Yamamoto§, Masayoshi Takeuchi¶, Hidenori Arai‖, Kazuhiro Nagata, Toru Kita‡‡, Hiroshi Okamoto§§, Hiroshi Yamamoto§, and Toshio Doi‡¶¶**

*From the ‡Department of Clinical Biology and Medicine, Course of Biological Medicine, School of Medicine, The University of Tokushima, Tokushima 770-8503, Japan, §Department of Biochemistry and Molecular Vascular Biology, Kanazawa University Graduate School of Medical Science, Kanazawa 920-8640, Japan, ¶Department of Biochemistry, Faculty of Pharmaceutical Science, Hokuriku University, Kanazawa 920-1181, Japan, ‖Department of Geriatric Medicine, **Department of Molecular and Cellular Biology, Institute for Frontier Medical Sciences, ‡‡Department of Cardiovascular Medicine, Kyoto University, Kyoto 606-8575, Japan, and §§Department of Biochemistry, Tohoku University Graduate School of Medicine, Sendai 980-8575, Japan*

Advanced glycation end products (AGEs) appear to contribute to the diabetic complications. This study reports the inhibitory effect of OPB-9195 (OPB), an inhibitor of AGEs formation, and the role of a collagen-specific molecular chaperone, a 47-kDa heat shock protein (HSP47) in diabetic nephropathy. Transgenic mice carrying nitric-oxide synthase cDNA fused with insulin promoter (iNOSTg) leads to diabetes mellitus. The iNOSTg mice at 6 months of age represented diffuse glomerulosclerosis, and the expression of HSP47 was markedly increased in the mesangial area in parallel with increased expression of types I and IV collagens. OPB treatment ameliorated glomerulosclerosis in the iNOSTg mice associated with the decreased expression of HSP47 and types I and IV collagens. The expression of transforming growth factor-β (TGF-β) was increased in glomeruli of iNOSTg mice and decreased after treatment with OPB. To confirm these mechanisms, cultured mesangial cells were stimulated with AGEs. AGEs significantly increased the expression of HSP47, type IV collagen, and TGF-β mRNA. Neutralizing antibody for TGF-β inhibited the overexpression of both HSP47 and type IV collagen *in vitro*. In conclusion, AGEs increase the expression of HSP47 in association with collagens, both *in vivo* and *in vitro*. The processes may be mediated by TGF-β.

Nephropathy is a morbid complication associated with diabetes mellitus and is the leading cause of end-stage renal disease (1). Diabetic nephropathy is characterized by a mesangial expansion followed by glomerulosclerosis. The mechanism of these processes remains unknown. Advanced glycation end products (AGEs)[1] have been recently reported to play an important role in the pathogenesis of diabetic complications, particularly in the progression of retinopathy and nephropathy (2). AGEs, late compounds formed from early Amadori compounds produced during the Maillard reaction, slowly accumulate in various tissues. Direct evidence indicating the importance of AGEs in the progression of diabetic nephropathy has been reported previously (3–5). The administration of exogenous AGEs to normal rats induces glomerular hypertrophy and mesangial sclerosis, gene expression of matrix proteins, and production of various growth factors. An inhibitor of AGEs formation, aminoguanidine, ameliorates the mild glomerular changes and functional changes found in streptozocin-induced diabetic rats (6). Recently, a synthetic thiazolidine derivative, OPB-9195, was shown to have a strong inhibitory effect of AGE formation (7).

The 47-kDa heat shock protein (HSP47) has been identified as a collagen-binding stress protein and plays a role in the intracellular processing of procollagen molecules as a collagen-specific molecular chaperone. We recently reported that the expression of HSP47 was markedly increased in parallel with the development of glomerulosclerosis in a rat renal ablation model (8). We also found that the inhibition of HSP47 ameliorated glomerulosclerosis (9). Despite a possible pathophysiological role of collagen-binding HSP47 in the fibrotic process in various organs, factors that modulate its expression remain undefined.

To understand the pathogenesis of diabetic nephropathy and to develop prophylactic and therapeutic measures against it, suitable animal models are needed. However, no single animal model that develops the renal changes seen in humans is available. Spontaneously diabetic animals such as the non-obese diabetic mouse develop only limited lesions, at most mild mesangial sclerosis (10). The same is the case with chemically induced diabetic rodents. In this study, we analyzed transgenic mice carrying the mouse, type 2-inducible nitric-oxide synthase (iNOS) cDNA under the control of an insulin promoter (iNOSTg) (11). The nitric oxide-mediated destruction of β cells results in a markedly reduced pancreatic islet mass and in the development of type 1 diabetes mellitus. These characteristics were followed by glomerulosclerosis that resembled human diabetic nephropathy (3).

Transforming growth factor (TGF)-β was originally identified in neoplastic cells and subsequently reported to be present in most cells in which it exerts a variety of effects on cell proliferation, cell differentiation, and embryogenesis. It has also been shown to stimulate the production of extracellular matrix components including collagens and fibronectin and to play a pivotal role in fibrogenesis (12). Thus, TGF-β is considered to be a mediator of collagen production in the models of fibrogenesis. Significant progress has recently been made in our understanding of the expression of the collagen genes and their transcriptional regulation by TGF-β (8, 9). A recent report has shown that high glucose transiently induces a transcriptional activity of *c-fos* responsible for stimulation of the TGF-β (13). However, there is little information regarding the interaction between AGE and c-*Fos*. We investigated here the expression of c-*Fos* in cultured mesangial cells treated with AGE and examined whether c-*Fos* affected the expression of TGF-β.

Furthermore, our recent report demonstrates that type IV collagen is up-regulated by AGE and its overexpression is transcriptionally regulated by Smad1 (14). Smad1 also enhances the levels of expression of type I collagen and osteopontin and plays a critical role in TGF-β-mediated overexpression of extracellular matrix in diabetic nephropathy (14). Therefore, we examined the role of Smad1 for regulating HSP47 expression by AGE stimulation in mesangial cells.

In this study, we reported on a study of the inhibitory effect of OPB-9195 (OPB), a novel inhibitor of AGEs formation, in a model of diabetic nephropathy. The pathogenic role of HSP47 in the development of the glomerulosclerotic lesions in diabetes was examined. We also confirmed the mechanism of these processes with the use of cultured mesangial cells.

* This work was supported in part by the "Research for the Future" Program for the Promotion of Science (Grant 97L00305). The costs of publication of this article were defrayed in part by the payment of page charges. This article must therefore be hereby marked "*advertisement*" in accordance with 18 U.S.C. Section 1734 solely to indicate this fact.

¶¶ To whom correspondence should be addressed: Dept. of Clinical Biology and Medicine, Course of Biological Medicine, School of Medicine, The University of Tokushima, 3-18-15 Kuramoto-cho, Tokushima 770-8503, Japan. Tel.: 81-88-633-7184; Fax: 81-88-633-9245; E-mail: doi@clin.med.tokushima-u.ac.jp.

[1] The abbreviations used are: AGEs, advanced glycation end-products; HSP47, 47-kDa heat shock protein; iNOS, inducible nitric-oxide synthase; OPB, OPB-9195; TGF, transforming growth factor; CML, carboxymethyllysine; BSA, bovine serum albumin; GAPDH, glyceraldehyde-3-phosphate dehydrogenase; siRNA, small interfering RNA.

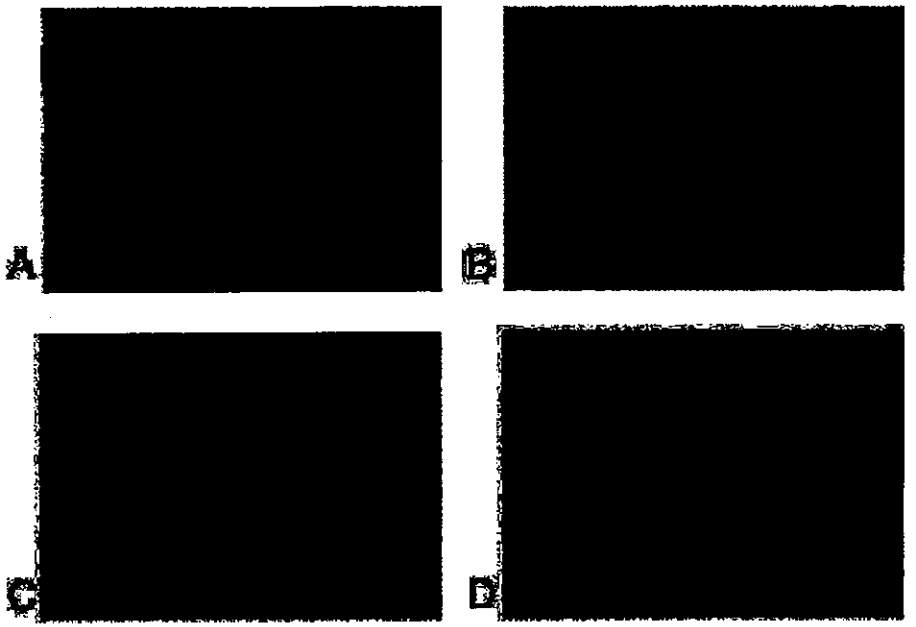

FIG. 1. **Light microscopy examination.** The microscopic lesions in iNOSTg mice took the form of diffuse proliferation of mesangial matrix and an expansion of the mesangial area. These lesions were ameliorated by treatment with OPB. *A*, control. *B*, iNOSTg. *C*, control + OPB. *D*, iNOSTg + OPB.

MATERIALS AND METHODS

Experimental Animals—iNOSTg were maintained on CD-1 mouse background (11). Male littermates were screened for the transgenes by the PCR amplification and used for analysis. The primers used for the detection of iNOSTg were as follows: forward primer, 5′-GTGGGCTATGGGTTTGTGGAAGGAGA-3′, and reverse primer 5′-CGATGTCACATGCAGCTTGT-3′.

No expression of iNOS protein, whose synthesis is directed only in pancreatic islets, was detected in the kidney. The mice were divided into four groups: CD-1 as control mice (Control); control mice treated with OPB (Control + OPB); iNOSTg; and iNOSTg treated with OPB (iNOSTg + OPB). Each group was fed either normal chow or the chow containing 0.28% OPB (provided by Fujii Memorial Research Institute, Otsuka Pharmaceutical, Tokushima, Japan) from 1 to 6 months after birth.

Blood Glucose and HbA1c Concentration—The levels of blood glucose and HbA1c were measured from the tail vein blood using Dexter Z sensor (Bayer-Medical, Tokyo, Japan) and DCA2000 analyzer (Bayer-Medical), respectively.

Determination of AGEs Concentration—Levels of serum carboxymethyllysine (CML) and non-CML AGEs were determined using a competitive enzyme-linked immunosorbent assay as described previously (15). 1 unit/ml CML or non-CML AGEs corresponded to a protein concentration of 1 μg/ml CML-bovine serum albumin (BSA) or non-CML AGE-BSA, respectively.

Renal Histology and Morphometric Analysis—Kidneys were processed for light microscopy examination, and the severity of the renal sclerosis was scored on an arbitrary scale from 0 to 4. The mean glomerular volume was determined as described previously (3, 16).

Immunofluorescence Analysis for HSP47, Types I and IV Collagens, and TGF-β—Immunofluorescence analysis was carried out as described previously using an affinity-purified polyclonal antibody specific to HSP47, types I and IV collagens, and TGF-β (8, 9).

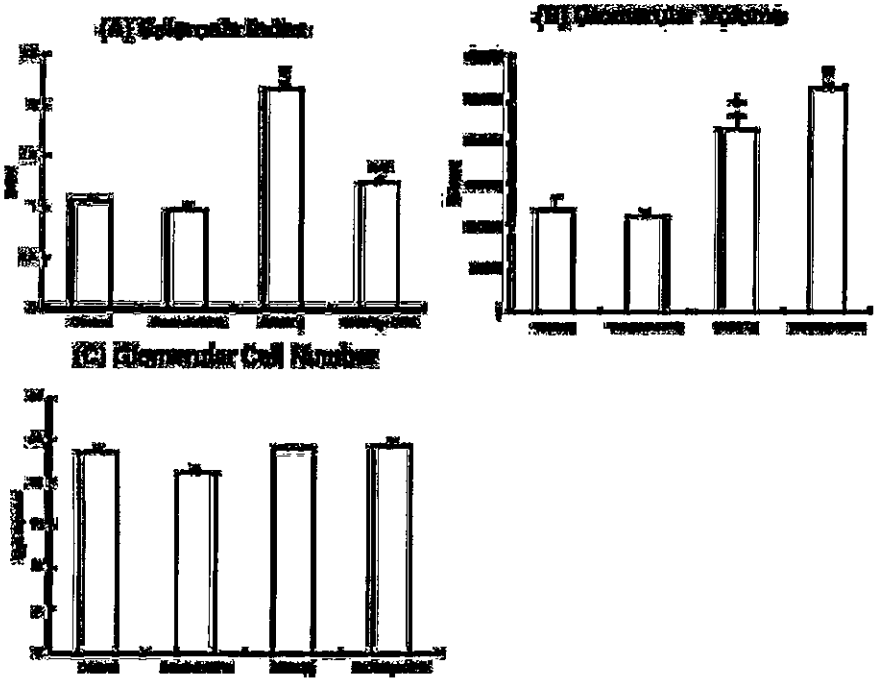

FIG. 2. **Effects of OPB in diabetic glomerulosclerosis.** OPB markedly improved glomerulosclerosis in iNOSTg mice (*A*) with no decrease in of glomerular volume (*B*). *C*, no significant differences in glomerular cell number were found. Number of experiments: Control, 11; OPB(−), 9; and OPB(+), 10. *, $p < 0.05$ *versus* Control; **, $p < 0.05$, OPB(+) *versus* OPB(−).

Laser-manipulated Microdissection and Laser Pressure Catapulating—Laser-manipulated microdissection is a method to cut out a small region from a specimen under microscope observation by means of laser beam. Laser pressure catapulating is a method to push up and collect samples that have been microdissected using laser-manipulated microdissection by means of a strong laser. These methods were performed using the Robot-Microbeam (P.A.L.M) and an inverted microscope (Carl Zeiss, Oberkochem, Germany) (17). By tracing around the glomeruli shown on the monitor, the targeted glomeruli were cut out by the laser. For laser pressure catapulating, the setting for the laser energy should be sufficiently high to catapult the microdissected glomeruli of the histologic specimen into the microcentrifuge cap, which was held in place by the micromanipulator. When the laser pressure catapulating was performed, the microdissected glomeruli "jumped up" and were attached to the cap. 60–80 glomeruli for each experiment were collected from this procedure. Glomeruli were obtained from those of control, iNOSTg, and iNOSTg-OPB mice at 24 weeks of age.

Quantitative PCR—Total RNA was prepared from isolated glomeruli, and a cDNA synthesis was performed with reverse transcription. Real-time PCR was performed by using the ABI Prism 7700 sequence detection system (PerkinElmer Life Sciences). Primers for mouse glyceraldehyde-3-phosphate dehydrogenase (*GAPDH*) (PerkinElmer Life Sciences) were used for internal control. The primers for HSP47, type IV collagen, and TGF-β were as follows: HSP47 (forward primer, 5′-GCGAGATAATCAGAGCGGCT-3′; reverse primer, 5′-CCACGCCCACTCTTGGACT-3′; and *Taq*Man Probe, 5′-CTTGCTCTTCATTGGCCGCCTGG-3′); type IV collagen (forward primer, 5′-GACCCCGAGGTTAGGAAGG-3′; reverse primer, 5′-CACTCGGTCCATGATCCCA-3′; and *Taq*Man Probe, 5′-ATCGAGCCGAGCCTAGAGCTGAAAGA-3′); and TGF-β (forward primer, 5′-AAGTCACCCGCGTGCTAATG-3′; reverse primer, 5′-CCCGAATGTCTGACGTATTGAA-3′; and *Taq*Man Probe, 5′-TGGACCGCAACAACGCAATCTATG-3′).

The cleavage of the sequence-specific probe (*Taq*Man Probe) by 5′-nuclease activity of the *Taq*DNA polymerase releases the reporter dye, resulting in an emission increase. With each cycle, the fluorescence intensity of additional reporter dye molecules is monitored by the system. The threshold cycles were selected in the line in which all of the samples were in the logarithmic phase. The quantity of PCR products was calculated from the threshold cycle value. This real-time detection generates quantitative data based on PCR at early cycles when PCR fidelity is highest (18, 19).

Cell Culture—A glomerular mesangial cell line was established from glomeruli isolated from normal 4-week-old mice (C57BL/6JxSJL/J) and was identified according to a method described previously (4, 5). The mesangial cells were plated on 100-mm plastic dishes (Nunc) that were maintained in B medium (a 3:1 mixture of minimal essential medium/F12 modified with trace elements) supplemented with 1 mM glutamine, penicillin at 100 units/ml, streptomycin at 100 μg/ml, and 20% fetal calf serum (Irvine Scientific). The cells were passaged weekly with trypsin-EDTA. The cultured cells fulfilled the previously described criteria generally accepted for glomerular mesangial cells (20).

AGE-BSA—AGE-BSA was prepared by the method described previously (5, 21). BSA was incubated with glucose 6-phosphate for >60 days at 37 °C. AGE content was measured by the fluorescence intensity at a protein concentration of 1 mg/ml. Control BSA was prepared by incubating BSA without glucose 6-phosphate under the same conditions as those for AGE-BSA. AGE-BSA and control BSA contained 61.3 and 8.31 AGE units/mg protein, respectively. Protein concentrations were determined by the method of Bradford using BSA as the standard.

Mesangial cells were plated in the B medium, 20% fetal bovine serum at 5×10^5/well in six-well dishes, that had been coated with AGE-BSA or control BSA at 50 μg/cm^2 for 72 h. After the treatment, the cells were washed with phosphate-buffered saline and total RNA was isolated using TRIzol reagent (Invitrogen).

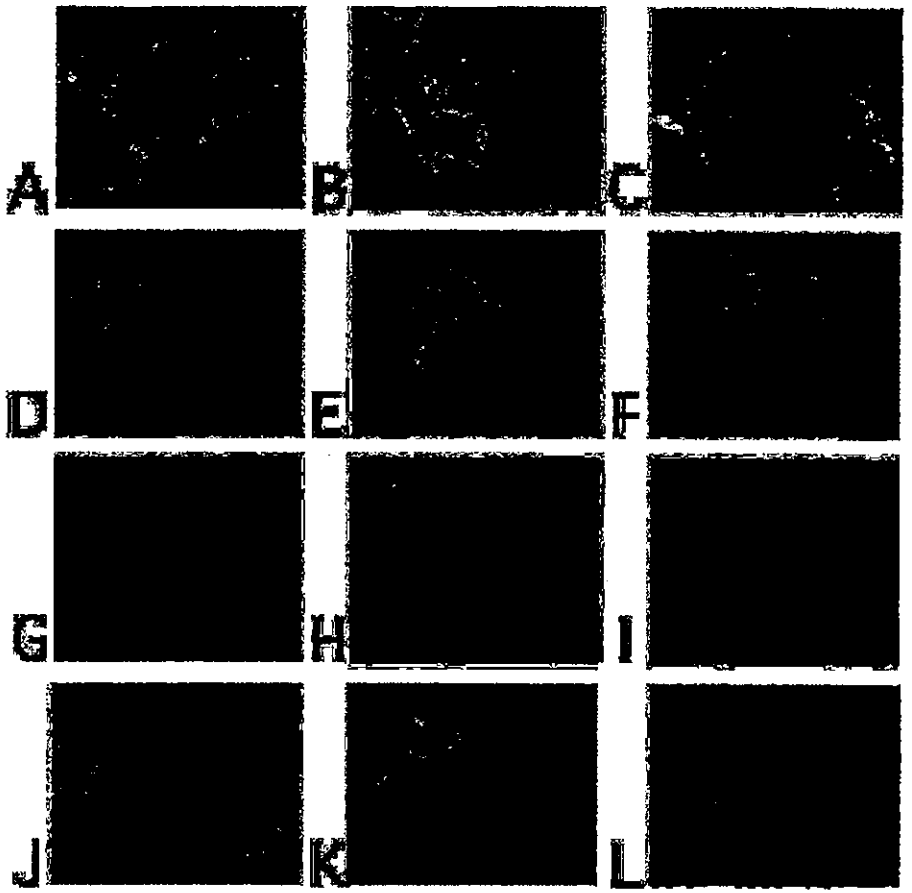

FIG. 3. **Immunofluorescence analysis of HSP47, collagens, and TGF-β.** A remarkable increase in the expression of HSP47, types I and IV collagens, and TGF-β was seen. OPB treatment led to show a significant decrease. *A–C*, type I collagen; *D–F*, type IV collagen. *G–I*, HSP47. *J–L*, TGF-β. *A*, *D*, *G*, and *J*, control. *B*, *E*, *H*, and *K*, iNOSTg. *C*, *F*, *I*, and *L*, iNOSTg + OPB.

TGF-β-neutralizing Antibody Assay—The cells were resuspended at a concentration of 1×10^6 cells/ml and plated onto 100-mm dish either in the presence of 10 μg/ml TGF-β1-neutralizing antibody (R&D Systems) or a control normal IgG (22). After 24 h of incubation, the cells were harvested and underwent RNA isolation on real-time reverse transcription-PCR.

Smad1 Morpholino Antisense Oligonucleotide—The antisense oligonucleotide for *Smad1* was a 25-nucleotide morpholino oligomer (Genetools LLC) with the base composition of 5′-CAAGCTGGTCACATTCATAGCGGCT-3′. A standard morpholino oligomer with the base composition of 5′-CAtGCTcGTCACATTCAaAGCcGCT-3′ (points of mismatch are shown by *small letters*) was used as a control. Microinjection of *in vitro* transcribed RNA was performed as described previously (14).

Western Blotting—Cultured mesangial cells were harvested in sample buffer, resolved by SDS-polyacrylamide gel electrophoresis, transferred to nitrocellulose membrane, subjected to Western blot using a 1:500 dilution of antibody for HSP47, type IV collagen, and TGF-β (8, 9), and detected using an enhanced chemiluminescence detection system (Invitrogen).

RNase Protection Assay—Total RNA was isolated from mesangial cells using the TRIzol reagent, and an RNase protection assay was performed as described previously (14, 22). The RNA probes were prepared by linearizing the PvuII fragment of type IV collagen from p1234, the SacI fragment of *Smad1* from pGEM-T, and the EcoRI fragment of *GAPDH* from pMGAP1. In addition, mouse riboprobe for HSP47 (5′-TCCTATACTGTGGGTGTTACGATGA-3′ and 5′-TACAACTCATCTCGCATCTTGTCTC-3′), *c-fos* (5′-TATCTCCTGAAGAGGAAGAGAAACG-3′ and 5′-AACAAGAAGTCATCAAAGGGTTCTG-3′), and TGF-β (5′-ATACCAACTATTGCTTCAGCTCCAC-3′ and 5′CACGTAGTAGACGATGGGCAGT-3′) was amplified by reverse transcription-PCR. The PCR fragments were sequenced to confirm to be cDNAs, respectively, and

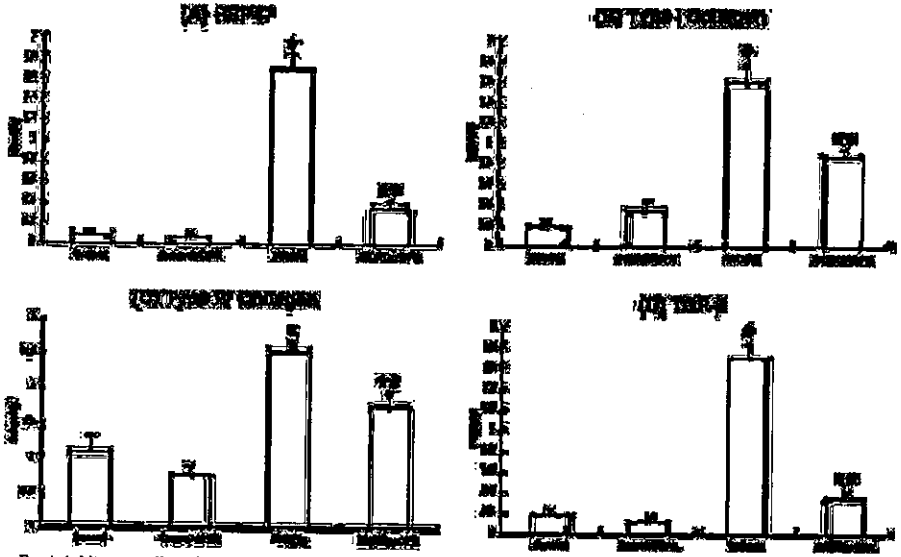

FIG. 4. **Arbitrary scaling of expressions of HSP47, collagens, and TGF-β.** A remarkable increase in the expression of HSP47 (*A*), types I (*B*) and IV (*C*) collagens, and TGF-β (*D*) was seen. OPB treatment showed a significant decrease. *, $p < 0.05$; *versus* Control; **, $p < 0.05$, OPB(+) *versus* OPB(−).

were cloned into a pGEM-T plasmid. After digesting the plasmid with SacI, an antisense riboprobe was synthesized *in vitro* using T7 RNA polymerase. The RNA probes and the test RNA were hybridized overnight at 45 °C. RNase A (40 μg/ml) and RNase T1 (2 μg/ml) were added to each tube, and the tubes were incubated for 1 h at 30 °C. The RNase resistant fragments were analyzed by 5% polyacrylamide, 8 M urea gel electrophoresis. The protected bands for each RNA probe had the same size as the coding sequence for the specific mRNA.

Small Interfering RNA (siRNA) and Transfections—The siRNA sequence targeting c-*fos* (5′-CCAATCTGCTGAAGAGAAGGAAAA-3′) was purchased from Hokkaido Science (Sapporo, Japan). Cells were transfected with LipofectAMINE 2000 (Invitrogen) according to the manufacturer's protocol in the presence of siRNA. siRNA against *Luciferase GL2* (5′-CGTACGCGGAATACTTCGA-3′) (Dharmacon) was used as a control.

RESULTS

Blood Glucose, HbA1c, and AGE Concentration—Blood glucose levels of iNOSTg mice were >500 mg/dl (503 ± 19 mg/dl, $n = 9$), and OPB had no effect on this parameter (586 ± 74 mg/dl, $n = 5$). HbA1c levels were over 7% in iNOSTg mice (7.5 ± 0.8%), whereas that of controls was below the detection limit. Both serum levels of CML and non-CML AGEs were significantly higher in iNOSTg mice (7.3 ± 0.6 and 20.7 ± 2.5 units/ml, respectively) than controls (6.2 ± 0.4 and 12.6 ± 1.0 units/ml, respectively), whereas OPB treatment of iNOSTg mice led to a decrease to the control levels (4.3 ± 1.0 and 10.2 ± 2.6 units/ml, respectively).

Response of Matrix Expansion to Treatment with OPB—The microscopic lesions in iNOSTg mice were observed as a diffuse proliferation of the mesangial matrix and the expansion of the mesangial area (Fig. 1). These lesions were ameliorated by treatment with OPB. OPB markedly improved the glomerulosclerosis of iNOSTg mice with no decrease in glomerular volume. No significant differences in glomerular cell number were detected among these groups (Fig. 2).

Response of Expressions of Collagens and HSP47 to Treatment with OPB—Although only traces of type I collagen could be detected in control glomeruli, it was strongly expressed in the mesangial area of glomeruli in iNOSTg mice. OPB treatment decreased this expression. Type IV collagen was expressed in both the glomerular basement membrane and the mesangium in control mice. Mesangial expression was increased in iNOSTg mice, which decreased after treatment with OPB. Immunofluorescent staining also revealed a remarkable increase in the expression of HSP47, which paralleled the expression of type I and type IV collagen and TGF-β in iNOSTg mice. These expressions were decreased as the result of OPB treatment (Figs. 3 and 4).

Quantitation of the Expression Ratio of HSP47/GAPDH mRNA and Type IV Collagen/GAPDH mRNA in Glomeruli by Real-time RT-PCR—Isolated mRNA of 50 glomeruli randomly selected from 5-μm frozen sections by laser-manipulated microdissection and laser pressure catapulating was used to quantitate the expression of HSP47 and type IV collagen mRNA in this diabetic nephropathy model. A remarkable increase in the expression of HSP47, type IV collagen, and TFG-β was seen in iNOSTg mice, and OPB treatment showed a significant decrease (Fig. 5).

Stimulation by AGEs in Cultured Mesangial Cells—To confirm the mechanism, cultured mesangial cells were stimulated with AGEs. AGEs significantly increased both HSP47 and type IV collagen expressions. In addition, AGEs were found to enhance the expression of TGF-β in cultured mesangial cells (Fig. 6*a*). Similarly, the levels of both HSP47 and type IV collagen proteins increased in accordance with the elevation of TGF-β protein (Fig. 6*b*). Neutralizing antibody for TGF-β inhibited overexpression of both HSP47 and type IV collagen (Fig. 7, *a* and *b*).

FIG. 5. **Glomerular mRNA expression.** Number of experiments: Control, 4; OPB(−), 5; and OPB(+), 6. *, $p < 0.05$ *versus* Control; **, $p < 0.05$, OPB(+) *versus* OPB(−).

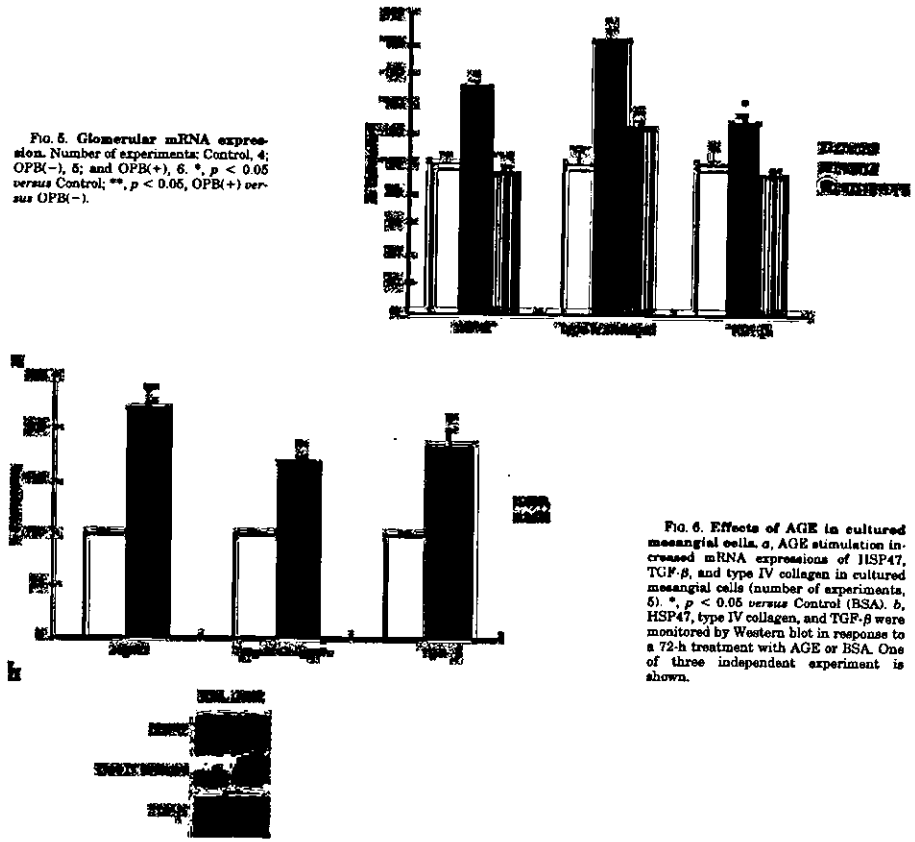

FIG. 6. **Effects of AGE in cultured mesangial cells.** *a*, AGE stimulation increased mRNA expressions of HSP47, TGF-β, and type IV collagen in cultured mesangial cells (number of experiments, 5). *, $p < 0.05$ *versus* Control (BSA). *b*, HSP47, type IV collagen, and TGF-β were monitored by Western blot in response to a 72-h treatment with AGE or BSA. One of three independent experiment is shown.

To further elucidate the mechanism for AGE-mediated induction of TGF-β, we investigated the expression of c-*fos* in mesangial cells. We found that AGE treatment caused a significant increase of c-*fos* mRNA by RNase protection assay. The AGE-mediated induction of c-*fos* was completely abolished in the presence of the specific siRNA but not in the presence of control siRNA. Consistent with the inhibition of c-*fos*, the induction of TGF-β was strongly attenuated (Fig. 8).

We next examined the involvement of Smad1 in TGF-β-mediated induction of HSP47 and type IV collagen expression. We transfected antisense morpholino oligomers to block Smad1-mediated effect in mesangial cells. Mesangial cells transfected with Smad1-antisense oligomers showed much less expression of HSP47 and type IV collagen transcripts after AGE stimulation than those with control oligomers (Fig. 9).

DISCUSSION

This study shows that the collagen-specific chaperone protein, HSP47, is strongly expressed in glomerulosclerotic lesions in parallel with increased expression of collagens I and IV in diabetic nephropathy. The findings of the study also suggest that AGEs are a key factor in the synthesis of increased expression of both HSP47 and collagens *in vitro* and *in vivo*. Our *in vitro* study indicates that AGEs-mediated induction of HSP47 and collagens may be through TGF-β.

Collagen is synthesized in the form of pro-α chains, and three pro-α chains form procollagen with a triple-helical structure in the endoplasmic reticulum. HSP47 is a collagen-binding stress protein and has been shown to be localized exclusively in the endoplasmic reticulum. Procollagen polypeptides form a complex with HSP47 in the endoplasmic reticulum, which plays an important role as a collagen-specific molecular chaperone in the intracellular processing/folding of procollagen molecules (23, 24). The crucial role of HSP47 in regulating biosynthesis of collagen molecules has been reported previously (25), and transcriptional regulation for HSP47 expression was clarified (26, 27). However, its role in kidney diseases in relation to sclerosis/fibrosis in diabetic nephropathy and IgA nephropathy is completely unknown. We and others (8, 28) have demonstrated that HSP47 in glomerulosclerosis is associated with collagen staining. Furthermore, the blocking of HSP47 with antisense

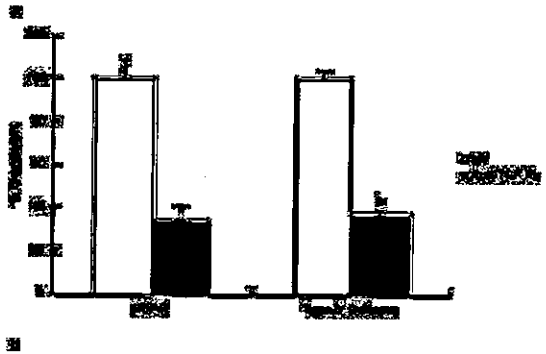

FIG. 7. **Inhibition of HSP47 and type IV collagen by TGF-β-neutralizing antibody.** *a*, neutralizing antibody for TGF-β inhibited both HSP47 and type IV collagen mRNA expressions in cultured mesangial cells (number of experiments, 5; *, $p < 0.05$ *versus* Control (IgY)). *b*, Western blot analysis of HSP47 and type IV collagen protein expression in cultured mesangial cells treated with AGE in the presence of neutralizing antibody for TGF-β or control (IgY).

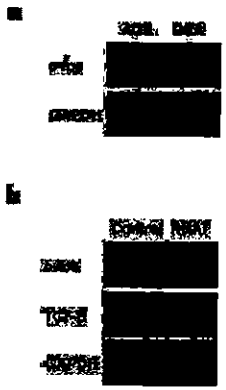

FIG. 8. **Regulation of c-*fos* mRNA expression by AGE.** *a*, RNase protection assay analysis of c-*fos* mRNA expression in total RNA lysates from cultured mesangial cells treated with AGE. One of three independent experiments is shown. *GAPDH* was used as an internal control. *b*, RNA interference (*RNAi*) against c-*fos* blocked the up-regulated mRNA level of *TGF-β* induced by AGE treatment. One of three independent experiments is shown.

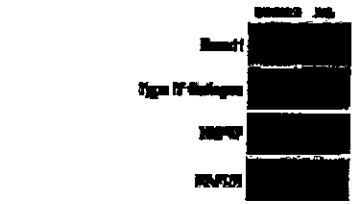

FIG. 9. **Effects of antisense oligomer specific for Smad1 in mesangial cells.** Antisense for *Smad1 (AS)* blocked the up-regulated mRNA levels of *type IV collagen* and *HSP47* induced by AGE treatment on cultured mesangial cells. *Smad1* mismatch morpholino oligomer (*Control*) had no effect on the expression of these genes. One of three independent experiments is shown.

oligonucleotides caused a dramatic amelioration of glomerular lesions in the rat glomerulonephritis model (9). These findings suggest that HSP47 is a key factor in the development of various glomerular injuries. In this study, a close relationship of HSP47 to glomerulosclerosis in diabetic nephropathy was found.

The blocking of AGEs formation inhibited the overreproduction of HSP47 and collagens, thereby suppressing the gene expression of type IV collagen, extracellular matrix accumulation, and glomerulosclerosis in diabetic nephropathy *in vivo*. AGEs also increased mRNA expression of both HSP47 and type IV collagen *in vitro*. Thus, our study implicates that AGEs are a key factor in the synthesis of both HSP47 and collagens in diabetic nephropathy *in vivo* and *in vitro*. The mechanism of these processes remains unclarified, but we demonstrated that AGEs stimulate several novel transcription factors in gene expression for glomerulosclerosis (5). We have recently reported that Smad1 transcriptionally regulates of type IV collagen under AGE stimulation (14). Here, we also observed that the expression of HSP47 was regulated by Smad1 under AGE exposure. Yamamura *et al.* (29) has reported that TGF-β transcriptionally activates *HSP47* gene expression. Thus, Smad1 may partially participate in the TGF-β-mediated up-regulation of HSP47.

It has been shown that TGF-β stimulates the production of extracellular matrix components including collagens and fibronectin and that it plays a key role in glomerulosclerosis (12). TGF-β regulates the expression of the collagen genes and their transcriptional activities. In particular, the promoter analysis of the collagen genes revealed that TGF-β1 regulates the transcription of collagen genes via several *cis*-elements of their promoters (13). TGF-β also increases HSP47 gene expression in other cell types (29). We first demonstrated that TGF-β stimulates not only collagen but also HSP47 in mesangial cells. In addition, we showed that c-*Fos* participates in the induction of TGF-β under AGE exposure. These data suggest that TGF-β and its signaling pathway are important targets for treating diabetic nephropathy.

Most experimental models of diabetic nephropathy are different from human pathological lesions (10, 30). On the other hand, the iNOSTg mice showed remarkably advanced glomerular lesions that resemble human diabetic glomerulosclerosis. From the analysis of this model, we confirmed that glomerular hypertrophy is important in the development of diabetic nephropathy because the iNOSTg mice showed glomerular hypertrophy in association with typical glomerulosclerosis. However, the intervention of AGE formation showed a decreased level of glomerulosclerosis with no evidence for diminished glomerular hypertrophy. The mechanism for this is unclear, but the regulation of HSP47 and collagens seemed to be independent of the control of glomerular hemodynamics. Further investigation will be needed to clarify the mechanism of these findings.

REFERENCES

1. Bojestig, M., Arnqvist, H. J., Hermansson, G., Karlberg, B. E., and Ludvigsson, J. (1994) *N. Engl. J. Med.* **330**, 15–18
2. Vlassara, H., Bucala, R., and Striker, L. (1994) *Lab. Investig.* **70**, 138–151
3. Yamamoto, Y., Kato, I., Doi, T., Yonekura, H., Ohashi, S., Takeuchi, M., Watanabe, T., Yamagishi, S., Sakurai, S., Takasawa, S., Okamoto, H., and Yamamoto, H. (2001) *J. Clin. Investig.* **108**, 261–268
4. Doi, T., Vlassara, H., Kirstein, M., Yamada, Y., Striker, G. E., and Striker, L. J. (1992) *Proc. Natl. Acad. Sci. U. S. A.* **89**, 2873–2877
5. Ishara, N., Takeoka, H., Yamada, Y., Kita, T., and Doi, T. (1996) *Kidney Int.* **50**, 1166–1172
6. Soulis-Liparota, T., Cooper, M., Papazoglou, D., Clarke, B., and Jerums, G. (1991) *Diabetes* **40**, 1328–1334
7. Nakamura, S., Makita, Z., Ishikawa, S., Yasumura, K., Fujii, W., Yanagisawa, K., Kawata, T., and Koike, T. (1997) *Diabetes* **46**, 895–899
8. Sumamoto, M., Kuze, K., Ishara, N., Takeoka, H., Nagata, K., Kita, T., and Doi, T. (1996) *Int. J. Exp. Pathol.* **79**, 133–140
9. Sumamoto, M., Kuze, K., Tsuji, H., Ohishi, N., Yagi, K., Nagata, K., Kita, T., and Doi, T. (1998) *Lab. Investig.* **78**, 967–972
10. Doi, T., Hattori, M., Agodoa, L. Y., Sato, T., Yoshida, H., Striker, L. J., and Striker, G. E. (1990) *Lab. Investig.* **63**, 204–212
11. Takamura, T., Kato, I., Kimura, N., Nakazawa, T., Yonekura, H., Takasawa, S., and Okamoto, H. (1998) *J. Biol. Chem.* **273**, 2493–2496
12. Border, W. A., and Ruoslahti, E. (1992) *J. Clin. Investig.* **90**, 1–7
13. Weigert, C., Brodbeck, K., Bierhaus, A., Haring, H. U., and Schleicher, E. D. (2003) *Biochem. Biophys. Res. Commun.* **304**, 301–307
14. Abe, H., Matsubara, T., Ishara, N., Nagai, K., Takahashi, T., Arai, H., Kita, T., and Doi, T. (2004) *J. Biol. Chem.* **279**, 14201–14206
15. Takeuchi, M., Makita, Z., Yanagisawa, K., Kameda, Y., and Koike, T. (1999) *Mol. Med.* **5**, 393–405
16. Doi, T., Striker, L. J., Gibson, C. C., Agodoa, L. Y., Brinster, R. L., and Striker, G. E. (1990) *Am. J. Pathol.* **137**, 541–552
17. Schutze, K., and Lahr, G. (1998) *Nat. Biotechnol.* **16**, 737–742
18. Fink, L., Seeger, W., Ermert, L., Hanze, J., Stahl, U., Grimminger, F., Kummer, W., and Bohle, R. M. (1998) *Nat. Med.* **4**, 1329–1333
19. Makibayashi, K., Tatematsu, M., Hirata, M., Fukushima, N., Kusano, K., Ohashi, S., Abe, H., Kuze, K., Fukatsu, A., Kita, T., and Doi, T. (2001) *Am. J. Pathol.* **158**, 1733–1741
20. MacKay, K., Striker, L. J., Elliot, S., Pinkert, C. A., Brinster, R. L., and Striker, G. E. (1988) *Kidney Int.* **33**, 677–684
21. Tsuji, H., Ishara, N., Masegi, T., Imura, M., Ohkawa, J., Arai, H., Ishii, K., Kita, T., and Doi, T. (1998) *Biochem. Biophys. Res. Commun.* **245**, 583–588
22. Abe, H., Ishara, N., Uetsunomiya, K., Kita, T., and Doi, T. (1999) *J. Biol. Chem.* **274**, 20874–20878
23. Nagata, K., Saga, S., and Yamada, K. M. (1988) *Biochem. Biophys. Res. Commun.* **153**, 428–434
24. Nakai, A., Satoh, M., Hirayoshi, K., and Nagata, K. (1992) *J. Cell Biol.* **117**, 903–914
25. Nagai, N., Hosokawa, M., Itohara, S., Adachi, E., Matsushita, T., Hosokawa, N., and Nagata, K. (2000) *J. Cell Biol.* **150**, 1499–1506
26. Hirata, H., Yamamura, I., Yasuda, K., Kobayashi, A., Tada, N., Suzuki, M., Hirayoshi, K., Hosokawa, N., and Nagata, K. (1999) *J. Biol. Chem.* **274**, 35703–35710
27. Yasuda, K., Hirayoshi, K., Hirata, H., Kubota, H., Hosokawa, N., and Nagata, K. (2002) *J. Biol. Chem.* **277**, 44613–44622
28. Razzaque, M. S., Kumatori, A., Harada, T., and Taguchi, T. (1998) *Nephron* **80**, 434–443
29. Yamamura, I., Hirata, H., Hosokawa, N., and Nagata, K. (1998) *Biochem. Biophys. Res. Commun.* **244**, 68–74
30. Velasques, M. T, Kimmel, P. L., and Michaelis, O. E., IV (1990) *FASEB J.* **4**, 2850–2859

MOLECULAR AND CELLULAR BIOLOGY, June 2004, p. 4627–4635 Vol. 24, No. 11
0270-7306/04/$08.00+0 DOI: 10.1128/MCB.24.11.4627–4635.2004

Role of *Hand1/eHAND* in the Dorso-Ventral Patterning and Interventricular Septum Formation in the Embryonic Heart

Kiyonori Togi,[1] Takahiro Kawamoto,[1] Ryoko Yamauchi,[2] Yoshinori Yoshida,[2] Toru Kita,[2] and Makoto Tanaka[1,3]*

Department of Geriatric Medicine[1] and Department of Cardiovascular Medicine,[2] Graduate School of Medicine, Kyoto University, and Department of Social Service, Kyoto University Hospital,[3] Kyoto, Japan

Received 18 November 2003/Returned for modification 17 December 2003/Accepted 25 February 2004

Molecular mechanisms for the dorso-ventral patterning and interventricular septum formation in the embryonic heart are unknown. To investigate a role of *Hand1/eHAND* in cardiac chamber formation, we generated *Hand1/eHAND* knock-in mice where *Hand1/eHAND* cDNA was placed under the control of the *MLC2V* promoter. In *Hand1/eHAND* knock-in mice, the outer curvature of the right and left ventricles expanded more markedly. Moreover, there was no interventricular groove or septum formation, although molecularly, *Hand1/eHAND* knock-in hearts had two ventricles. However, the morphology of the inner curvature of the ventricles, the atrioventricular canal, and the outflow tract was not affected by *Hand1/eHAND* expression. Furthermore, expression of *Hand1/eHAND* in the whole ventricles altered the expression patterns of *Chisel*, *ANF*, and *Hand2/dHAND* but did not affect *Tbx5* expression. In contrast, the interventricular septum formed normally in transgenic embryos overexpressing *Hand1/eHAND* in the right ventricle but not in the boundary region. These results suggested that *Hand1/eHAND* is involved in expansion of the ventricular walls and that absence of *Hand1/eHAND* expression in the boundary region between the right and left ventricles may be critical in the proper formation of the interventricular groove and septum. Furthermore, *Hand1/eHAND* is not a master regulatory gene that specifies the left ventricle myocyte lineage but may control the dorso-ventral patterning in concert with additional genes.

In vertebrate cardiac development, dorso-ventral (DV) patterning, as well as antero-posterior (AP) patterning, plays an essential role in the transformation of the linear heart tube into the four-chambered heart (7, 9). The linear heart tube is polarized along the AP axis, composed of five primordial segments: inflow tract (IFT), common atrium, atrioventricular canal (AVC), primitive ventricle, and outflow tract (OFT). Each segment is controlled by different developmental programs, characterized by specific gene expression profiles (2, 9, 20). In addition to the AP polarity, DV patterning has recently received attention. During cardiac looping, the ventricular chambers expand from the ventral surface of the heart tube (8). Trabeculae form only at the outer curvature of the heart tube, whereas the inner curvature remains smooth walled (7). Christoffels et al. and Lamers and Moorman proposed a two-step model for chamber formation in the embryonic heart (7, 13). First, the primary myocardium is induced, which makes up the linear heart tube. Second, the chamber myocardium is specified on the ventral side of the heart tube, acquiring an additional and presumably more advanced transcriptional program. In the looping heart, the specified chamber myocardium located at the outer curvature expands rapidly while the myocardium of the inner curvature, as well as the IFT, AVC, and OFT, retains the functional and molecular properties of the primary myocardium that has a limited proliferative capacity (7, 13). As a result, the atrial and ventricular chambers balloon out along the outer curvature (9). This ballooning model provides a view that DV, as well as AP, patterning information is critical for chamber specification. However, molecular mechanisms for the expansion of the chamber walls and the DV patterning of the embryonic heart are unknown.

Hand1/eHAND is a potential candidate gene. *Hand1/eHAND* is expressed on the ventral surface in the caudal half of the linear heart tube and predominantly at the outer curvature of the left ventricle (LV) in the looping heart while the gene is absent at the inner curvature (1, 21, 24). Therefore, its expression is highly restricted along the DV as well as the AP axis. Tetraploid-rescued *Hand1/eHAND* null embryos displayed a single ventricle, suggesting that the gene may play a critical role in specification or proliferation of LV myocytes during ballooning (17).

Moreover, the ballooning of chamber walls may be closely related to the formation of the interventricular septum (IVS). In the ballooning model, the structures flanking the atrial and ventricular chambers do not expand and retain the tubular shape, contributing to the proper AV septation and alignment of the IFT and OFT (7, 13). However, in this model, it is not clear what determines the boundary between the right ventricle (RV) and LV. The myocardium at the interventricular groove (IVG) is not the primary but working myocardium according to this model, but this region does not expand. It is totally unknown what molecular mechanisms determine the location of the IVS and IVG.

In this study, we examined a role of *Hand1/eHAND* in the DV patterning of the embryonic heart and the IVS formation. For this purpose, we knocked in the *Hand1/eHAND* gene to the mouse myosin light chain 2V (*MLC2V*) locus. We demonstrated that *Hand1/eHAND* enhanced expansion of chamber walls and that absence of *Hand1/eHAND* expression in the IVG may be critical in the proper formation of the IVS.

* Corresponding author. Mailing address: Department of Social Service, Kyoto University Hospital, 54 Shogoin-Kawahara-cho, Sakyo-ku, Kyoto 606-8507, Japan. Phone: 81-75-751-3465. Fax: 81-75-751-3574. E-mail: makoto@kuhp.kyoto-u.ac.jp.

MATERIALS AND METHODS

Gene targeting. From a 129SvJ bacterial artificial chromosome library, 3-kb upstream and 6-kb downstream fragments of the coding region of the *MLC2V* gene were isolated. The upstream 3-kb fragment, FLAG-tagged mouse *Hand1/eHAND* cDNA, the human growth hormone poly(A) signal, and the 6-kb downstream fragment were ligated into pPNTloxPneo (15). The targeting vector was linearized with NotI for transfection.

RW4 embryonic stem (ES) cells (Incyte Genomics, St. Louis, Mo.) isolated from the 129SvJ strain were cultured on mouse embryonic fibroblast feeder layers in high-glucose Dulbecco's modified Eagle medium containing 20% fetal calf serum and 10^3 U of leukemia inhibitory factor/ml. ES cells (1.0×10^7) were electroporated with 30 μg of the linearized targeting vector. Electroporated ES cells were cultured on neomycin-resistant feeder cells with 300 μg of G418/ml and 2 μM ganciclovir for 8 days. Two hundred eight drug-resistant colonies were isolated, and Southern hybridization demonstrated that four clones contained the correctly targeted allele at the *MLC2V* locus.

These clones were electroporated with 5 μg of the Cre-expressing vector pCre-Pac (KURABO, Osaka, Japan). After electroporation, cells were cultured on feeder cells with 1.7 μg of puromycin/ml for 2 days. Single colonies were picked up in duplicate, and neomycin-sensitive colonies were amplified and genotyped by Southern blotting. Two correctly targeted clones were injected into blastocysts from C57BL/6J mice. Male chimeras were bred with female C57BL/6J mice to test for germ line transmission. All animal procedures were approved by the Animal Research Committee, Graduate School of Medicine, Kyoto University.

Genotyping of progeny. DNA was isolated from tail biopsy specimens of weaned mice, yolk sacs, or placentas. PCR and Southern hybridization were performed to genotype embryos and mice. The primers used for detection of the targeted allele were 5′-TCCGCCTCACCTACAACTGC-3′ and 5′-ACAGAAG GGGGTCACCGTGG-3′.

Generation of transgenic mice. The 250-bp rat MLC2V promoter (10) was synthesized by PCR and was ligated to FLAG-tagged mouse *Hand1/eHAND* cDNA with the human growth hormone poly(A) signal. The identity of the synthesized promoter was confirmed by DNA sequencing. The creation of transgenic mice was done in a standard manner. F_0 embryos were dissected at embryonic day 11.5 (E11.5), and genotyping was performed by PCR on DNA isolated from the yolk sacs. PCR primer pairs used for detection of the transgenes were 5′-TGCTGTCAGCCCAATTAG-3′ and 5′-GGCTGCAGTCCTC CTCTTCCTCCCCCTC-3′.

In situ hybridization. In situ hybridization was performed as described previously (23). Briefly, embryos were fixed in 4% paraformaldehyde at 4°C overnight, dehydrated through graded ethanol and xylene, and embedded in paraffin wax. Sections of 6-μm thickness were hybridized with [^{35}S]CTP-labeled riboprobe at 55°C overnight. After hybridization, they were treated with RNase A, washed, and dehydrated through graded ethanol, and emulsion autoradiography was performed. Probes for α-cardiac actin, atrial natriuretic factor (*ANF*), *Hand1/eHAND*, *Hand2/dHAND*, *MEF2C*, *TEF-1*, *Nkx2.5*, and N-*myc* were described previously (23). An EagI-EcoRI fragment of the 3′ untranslated region (3′ UTR) of *Hand1/eHAND* was used to detect endogenous *Hand1/eHAND* expression. A probe for *Tbx5* (3) was kindly provided by Benoit G. Bruneau (University of Toronto, Toronto, Canada). A probe for *Chisel* (16) was synthesized by reverse transcription-PCR. The identity of the probe was confirmed by DNA sequencing.

Immunohistochemistry. After rehydration, paraffin sections of embryos were autoclaved in 10 mM EDTA (pH 8.0) at 121°C for 10 min, blocked with an avidin-biotin blocking kit (Vector, Burlingame, Calif.), and incubated with biotinylated mouse anti-FLAG M2 monoclonal antibody (Sigma, St. Louis, Mo.) (1:200) overnight at 4°C. After incubation, sections were washed and incubated with streptavidin-horseradish peroxidase (Nichirei, Tokyo, Japan), and peroxidase activity was detected with 3,3′-diaminobenzidine.

RESULTS

Generation of *Hand1/eHAND* KI mice. To investigate a role of *Hand1/eHAND* in the DV patterning of the embryonic heart, we generated mice expressing *Hand1/eHAND* in the whole ventricles. For this purpose, we employed a knock-in (KI) strategy to place *Hand1/eHAND* cDNA into the genomic locus of *MLC2V*, since this gene is expressed in ventricular myocytes throughout development, and heterozygous knockout mice for *MLC2V* were reported to display no obvious phenotype (5). After the first round of homologous recombination, the FLAG-tagged *Hand1/eHAND* cDNA and the *pgk-neo* cassette flanked by two *loxP* sites were inserted into the *MLC2V* locus (Fig. 1A). Four correctly targeted clones were identified (Fig. 1B). We then removed the *pgk-neo* cassette by transiently expressing the Cre recombinase (Fig. 1C). After the second round of recombination, two ES clones were injected into C57BL/6 blastocysts. We crossed male chimeras with female C57BL/6 to check for germ line contribution of ES cells by screening for the presence of agouti offspring. Two germ line chimeras were obtained, but none of their offspring carried the KI allele (0 of 20 agouti offspring), indicating that *Hand1/eHAND* KI mice were embryonically lethal.

Morphological and histological analysis of *Hand1/eHAND* KI embryos. To investigate the timing of lethality, we examined litters from a germ line chimera, all of whose offspring had agouti coat color. At E9.5 and E10.5, *Hand1/eHAND* KI embryos were indistinguishable from wild-type littermates. However, *Hand1/eHAND* KI embryos showed slight growth retardation at E11.5 and were severely retarded at E12.5, and PCR analysis of the placenta of absorbed embryos at E14.5 revealed that all absorbed embryos carried the KI allele. Viable embryos at E14.5 were all wild type. These results indicated that *Hand1/eHAND* KI embryos died between E12.5 and E14.5.

Histological examination at E9.5 revealed that trabeculation and endocardial cushion formation occurred normally in the hearts of *Hand1/eHAND* KI embryos. *Hand1/eHAND* KI and wild-type embryos were indistinguishable except that there was no IVG in *Hand1/eHAND* KI hearts (Fig. 2A and B). At E10.5, ventricular chambers, particularly the RVs, balloon out more markedly in *Hand1/eHAND* KI embryos, although their ventricles were single chambers, lacking the IVG and IVS (Fig. 2D and F). In contrast, IVS formation was clearly observed in wild-type littermates (Fig. 2C and E). The morphology of the inner curvature, AVC, and OFT was comparable between *Hand1/eHAND* KI and wild-type embryos (Fig. C, D, G, and H). At E11.5, no IVG or IVS formation was observed in *Hand1/eHAND* KI embryos (Fig. 2J and L), whereas the IVS was well developed in wild-type hearts (Fig. 2I and K). The compact zone myocardium was thinner in *Hand1/eHAND* KI embryos, suggesting that the embryonic lethality may be due to heart failure caused by poor development of the compact zone myocardium.

Gene expression in *Hand1/eHAND* KI heart. We first examined expression of *Hand1/eHAND* in *Hand1/eHAND* KI and wild-type embryos. In wild types, *Hand1/eHAND* was expressed in the outer curvature of the LV and the OFT at E9.5 and E10.5 (Fig. 3A and C). Weak expression of *Hand1/eHAND* was also observed in the outer curvature of the RV. At E11.5, *Hand1/eHAND* expression was down-regulated (Fig. 3E). Notably, *Hand1/eHAND* expression was absent at the IVG and IVS throughout development in wild-type embryos (Fig. 3A, C, and E). In contrast, *Hand1/eHAND* was expressed in the whole ventricle as well as in the AVC and OFT in *Hand1/eHAND* KI embryos (Fig. 3B, D, F, and H). The expression level was still

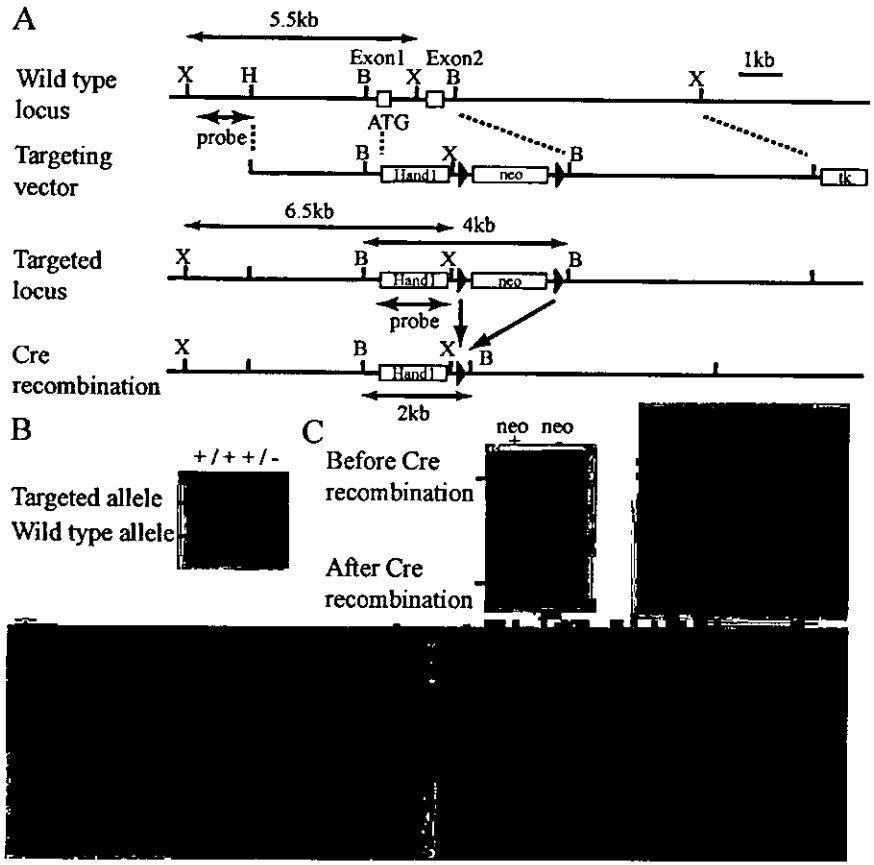

FIG. 1. (A) Targeting strategy. The structure of the *MLC2V* locus and the targeting vector are shown first and second, respectively. The mutated locus after homologous recombination is shown third, and the modified locus by Cre recombination is shown at the bottom. ATG is the transcriptional start site. The closed arrowheads represent the *loxP* sites. B, BamHI; H, HindIII; X, XbaI. (B) Genotyping of ES cell clones after homologous recombination. Genomic DNA was digested with XbaI and analyzed by Southern blotting. The 5′ probe (a BamHI-HindIII fragment) was used. Hybridization with the 5′ probe revealed the expected 5.5- and 6.5-kb fragments from the wild-type and targeted alleles, respectively. (C) Genotyping of ES clones after Cre recombination. Genomic DNA was digested with BamHI and analyzed by Southern blotting. *Hand1/eHAND* cDNA was used as a probe. The expected 4-kb fragment from the original targeted allele and the 2-kb fragment from the Cre mutated allele were revealed. Fragments from the wild-type allele for *Hand1/eHAND* were also detected (not shown on this figure). (D, E, and F) Immunohistochemistry with an anti-FLAG antibody. FLAG-tagged Hand1/eHAND protein was expressed in the nuclei of ventricular cells, whereas the expression was not detected in atrial cells in *Hand1/eHAND* KI embryos (E). FLAG-tagged Hand1/eHAND protein was expressed in the whole ventricle (F). A, atrium; V, ventricle. Bars, 100 μm.

high at E11.5 (Fig. 3F). To confirm the expression of the FLAG-tagged Hand1/eHAND protein, we also performed immunohistochemistry with an anti-FLAG antibody. The FLAG-tagged Hand1/eHAND protein was detected in cardiac myocytes of the whole ventricle in *Hand1/eHAND* KI embryos (Fig. 1D, E, and F) but not in wild types (data not shown).

We next examined endogenous *Hand1/eHAND* expression using the 3′ UTR of *Hand1/eHAND* as a probe, since the 3′ UTR is not included in the FLAG-tagged *Hand1/eHAND* cDNA. Endogenous *Hand1/eHAND* expression was confined to the left side of the single ventricle in *Hand1/eHAND* KI embryos, and the expression level was comparable to that in

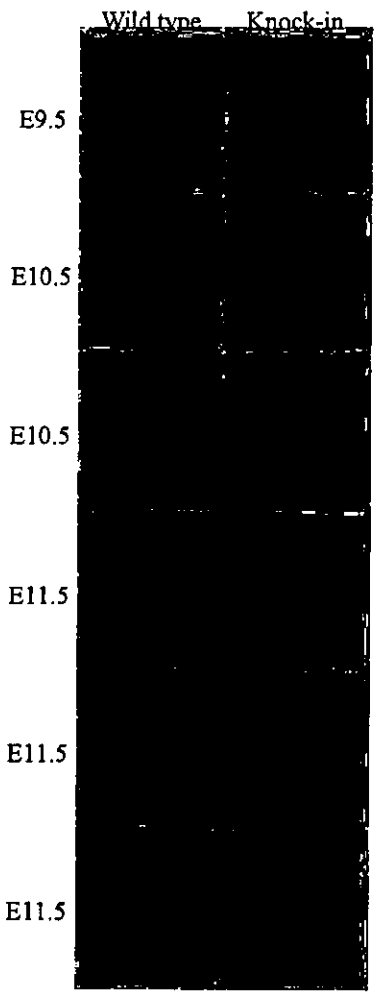

FIG. 2. Histological analysis of wild-type and *Hand1/eHAND* KI embryos from E9.5 to E11.5. Hematoxylin- and eosin-stained sections of wild-type (A, C, E, G, I, and K) and *Hand1/eHAND* KI (B, D, F, H, J, and L) embryos are shown. At E9.5, trabeculation, endocardial cushion formation, and looping normally occurred in *Hand1/eHAND* KI embryos (B). Note the absence of the IVG in *Hand1/eHAND* KI embryos. The IVG can be observed in wild-type embryos (arrowhead in panel A). At E10.5, the outer curvature expanded more markedly in *Hand1/eHAND* KI embryos (C and D). The difference was more evident in the RV. There was no IVG or IVS formation in *Hand1/eHAND* KI embryos (D and F). At E11.5, *Hand1/eHAND* KI embryos exhibited a single ventricle with complete absence of the IVS and IVG (J and L). Endocardial cushion formation in the OFT was comparable between wild-type (G) and *Hand1/eHAND* KI (H) embryos. In KI embryos, the development of the AVC was disturbed (J and L). The arrowheads in panels A, C, and E indicate the IVG. Bars, 200 μm.

wild-type embryos (Fig. 4A and B), indicating that there was a clear distinction between the left and right sides of the ventricle at the molecular level, although there was no IVG or IVS formation. Moreover, the left-side expression of *Tbx5* was not disturbed in *Hand1/eHAND* KI embryos (Fig. 4C and D), further supporting the observation that the right and left sides of the ventricle were molecularly distinctive in *Hand1/eHAND* KI embryos. Furthermore, endogenous *Hand1/eHAND* expression was detected in the AVC in *Hand1/eHAND* KI embryos (Fig. 4B), suggesting that a positive feedback regulation of *Hand1/eHAND* may exist in the AVC.

Chisel and *ANF* are regarded as molecular markers for the working myocardium (7). *Chisel* was expressed in the atrium and the outer curvature of the ventricle but was absent in the inner curvature and the AVC in wild-type embryos (Fig. 4I) (7, 16). Interestingly, in *Hand1/eHAND* KI embryos, *Chisel* was also expressed in the inner curvature and AVC, suggesting that *Chisel* expression was dependent on *Hand1/eHAND* (Fig. 4J). In wild-type embryos, *ANF* was strongly expressed in the trabecular layer of the LV and weaker expression was observed in the atrium and the trabecular layer of the RV. *ANF* expression was not observed in the inner curvature, the AVC, or the IVG in wild-type embryos (Fig. 4K). In *Hand1/eHAND* KI embryos, *ANF* expression in the RV was up-regulated and the expression was also detected in the inner curvature but not in the AVC, indicating that *ANF* expression in the RV and the inner curvature was regulated by *Hand1/eHAND* (Fig. 4L).

We further examined expression of transcription factors known to play critical roles in cardiac development. While expression of *Nkx2.5* (Fig. 4G and H) and *MEF2C* (data not shown) was comparable, *Hand2/dHAND* expression in the RV was down-regulated in *Hand1/eHAND* KI embryos (Fig. 4E and F), suggesting that *Hand1/eHAND* may suppress *Hand2/dHAND* expression. What is the molecular mechanism for thin myocardium in *Hand1/eHAND* KI embryos? Inactivation of *N-myc* or *TEF-1* in mice resulted in thin myocardium (4, 6, 14), but these genes were normally expressed in *Hand1/eHAND* KI embryos (data not shown). Homozygous Splotch mutant mice that lack the transcription factor *Pax3* also showed thin myocardium. *p57*, a cyclin-dependent kinase inhibitor normally expressed in the trabecular layer, was also expressed in the compact zone layer in the mutant embryos, suggesting precocious cardiomyocyte differentiation in Splotch mutants (11). We thus investigated expression of *p57* in *Hand1/eHAND* KI embryos, but *p57* expression was detected only in the trabecular layer both in *Hand1/eHAND* KI and wild-type embryos (Fig. 4M and N).

Normal IVS formation in transgenic embryos overexpressing *Hand1/eHAND* in the RV. The defect in the IVS formation in *Hand1/eHAND* KI embryos may be due to nonspecific effects of *Hand1/eHAND* overexpression. To further examine the significance of the absence of *Hand1/eHAND* expression in the boundary region, we generated and analyzed transgenic em-